

UNIVERSITÉ DU QUÉBEC À MONTRÉAL

THÈSE PRÉSENTÉE À  
L'UNIVERSITÉ DU QUÉBEC À CHICOUTIMI  
COMME EXIGENCE PARTIELLE  
DU DOCTORAT EN RESSOURCES MINÉRALES  
OFFERT À  
L'UNIVERSITÉ DU QUÉBEC À MONTRÉAL  
EN VERTU D'UN PROTOCOLE D'ENTENTE  
AVEC L'UNIVERSITÉ DU QUÉBEC À CHICOUTIMI

PAR

GEMA RIBEIRO OLIVO

LES GÎTES D'OR PALLADIFÈRES DES MINES DE CAUÊ ET DE CONCEIÇAO,  
DANS LES FORMATIONS DE FER DU TYPE LAC SUPÉRIEUR  
DU DISTRICT D'ITABIRA, CRATON SAO FRANCISCO, BRÉSIL:  
STRUCTURE, MINÉRALOGIE, GÉOCHRONOLOGIE ET MÉTALLOGÉNIE.

(PALLADIUM-BEARING GOLD DEPOSITS OF THE CAUÊ AND CONCEIÇAO  
MINES, HOSTED BY LAKE SUPERIOR-TYPE IRON-FORMATIONS  
OF THE ITABIRA DISTRICT, SAO FRANCISCO CRATON, BRAZIL:  
STRUCTURE, MINERALOGY, GEOCHRONOLOGY AND METALLOGENY)

SEPTEMBRE 1994



### **Mise en garde/Advice**

Afin de rendre accessible au plus grand nombre le résultat des travaux de recherche menés par ses étudiants gradués et dans l'esprit des règles qui régissent le dépôt et la diffusion des mémoires et thèses produits dans cette Institution, **l'Université du Québec à Chicoutimi (UQAC)** est fière de rendre accessible une version complète et gratuite de cette œuvre.

Motivated by a desire to make the results of its graduate students' research accessible to all, and in accordance with the rules governing the acceptance and diffusion of dissertations and theses in this Institution, the **Université du Québec à Chicoutimi (UQAC)** is proud to make a complete version of this work available at no cost to the reader.

L'auteur conserve néanmoins la propriété du droit d'auteur qui protège ce mémoire ou cette thèse. Ni le mémoire ou la thèse ni des extraits substantiels de ceux-ci ne peuvent être imprimés ou autrement reproduits sans son autorisation.

The author retains ownership of the copyright of this dissertation or thesis. Neither the dissertation or thesis, nor substantial extracts from it, may be printed or otherwise reproduced without the author's permission.

## ABSTRACT

The Cauê and Conceição iron mines are located in the Itabira District in the Southern São Francisco Craton, Brazil. Three geologic units metamorphosed to amphibolite facies have been identified in both mines: (1) an Archean volcano-sedimentary sequence; (2) a Proterozoic iron-formation unit; and (3) a Proterozoic quartzite unit. The iron-formation unit is cut by amphibolite dykes and tectonically imbricated with talc schists and amphibolites of the volcano-sedimentary sequence. All the rocks were affected by three phases of folding and associated thrusting and boudinage. In the iron-formation unit, the D1 and D2 structures have been generated by a progressive simple shear regime with a transport direction consistently east-over-west. D3-structures are characterized by open folds with an associated crenulation cleavage.

The Cauê and Conceição palladium-bearing deposits are hosted by jacutinga in the iron-formation unit. Jacutinga is a highly-sheared, metamorphosed, hydrothermally-altered Lake Superior-type iron-formation composed of hematite, quartz, talc, and phlogopite, with minor amounts of tourmaline, apatite, and monazite.

The Cauê gold deposit consists of five gold orebodies: Corpo Y, Corpo X, Central, Aba Leste and Aba Norte. In the Corpo Y orebody, the highest gold concentrations occur in quartz veins, whereas in the other four, the highest gold grades occur in hematite veins containing local quartz concentrations. The gold-rich veins are parallel to S1-foliation in all orebodies except Aba Norte, where the gold-rich boudinaged hematite vein is parallel to S2. The ore minerals are gold, palladian gold, palladium, palladium-oxide, palladseite and arsenopalladinite. Palladium content of the gold grains varies from 1% to 20%. The highest values are from the Corpo X and Corpo Y orebodies, where the gold grains contain palladium-copper-oxide inclusions showing island-mainland and replacement (relict) textures. In the Aba Leste orebody, palladium is homogeneously distributed throughout the gold grains. In the Aba Norte, gold grains are not palladium-bearing; instead, they have rhodium contents of up to 1.5 %.

The single Conceição palladium-bearing gold orebody is parallel to S1 mylonitic foliation in the limb of macroscopic D1 and D2 folds and was dismembered by the progressive shear deformation. Gold grains occur as free platy grains, parallel to mylonitic foliation, as inclusions in specular hematite, tourmaline and quartz grains. Fine gold grains ( $< 3.0 \mu$ ) are common in goethitic bands which resulted from the weathering of carbonates. Palladium contents in bent grains are up to 0.8 %.

The main mineralizing event was synchronous with the peak of thermal metamorphism ( $T = 600^\circ \text{C}$ ) and with D1-shearing and thrusting. The age of the mineralizing event was estimated by Pb-Pb isotope dating at  $1.9 +/ - 0.2 \text{ G.a}$ . This age

is in agreement with the metamorphic age of the Minas Supergroup and corresponds with the age of the Transamazonian orogenesis in the southern part of the São Francisco craton.

The hydrothermal alteration associated with this event is characterized by the formation of talc, phlogopite, and tourmaline, as well as vein of hematite and quartz, resulting in the jacutinga rock-type. The weathering of the jacutinga resulted in the alteration of silicates to kaolin and oxides to goethite.

At high temperatures and oxygen fugacities, Pd and Au may have been transported as chloride complexes, their deposition occurring mainly in response to an increase in pH. It is proposed that this increase was caused by reactions between the mineralizing fluids and the jacutinga precursor: a dolomitic itabirite. The most probable source of these precious metals is the Archean volcano-sedimentary sequence.

The characteristics of the Cauê and Conceição deposits warrant a new type of gold deposit, entitled here "Palladium-bearing gold deposit hosted by highly sheared, metamorphosed Lake Superior-type iron-formation". Along the eastern border of the southern São Francisco Craton, other palladium-bearing gold occurrences are also hosted by jacutinga, suggesting that this geological environment is exceptionally favourable for this type of deposit.

## RÉSUMÉ

Les mines de fer de Cauê et de Conceição sont situées dans le District d'Itabira, dans la partie sud du Craton São Francisco, au Brésil. Trois unités géologiques, métamorphosées au faciès amphibolite, sont présentes aux deux mines: (1) une séquence volcano-sédimentaire Archéenne; (2) une formation de fer Protérozoïque et; (3) une unité de quartzite Protérozoïque. La formation de fer est recoupée par des dykes d'amphibolite et est tectoniquement imbriquée avec des schistes à talc et des amphibolites de la séquence volcano-sédimentaire. Les roches des trois unités ont été affectées par trois phases de déformation, subissant les chevauchements et boudinages associés. Dans la formation de fer, les structures associées à D1 et à D2 ont été générées par un cisaillement simple progressif dont la direction de transport est de l'Est vers l'Ouest. La structure D3 est caractérisée par des plis ouverts auxquels sont associés des clivages de crénulation.

*La jacutinga est la roche hôte des minéralisations d'or palladifère exploitées dans les formations de fer des mines de Cauê et de Conceição. La jacutinga est un faciès fortement cisaillé, métamorphosé et hydrothermalement altéré de la formation de fer de type Lac Supérieur, et est composée d'hématite, de quartz, de talc, de phlogopite, et de quantités mineures de tourmaline, d'apatite et de monazite.*

Le gisement aurifère de Cauê est composé de cinq corps minéralisés: Corpo Y, Corpo X, Central, Aba Leste et Aba Norte. Dans le corps minéralisé Corpo Y, les plus fortes concentrations d'or sont rencontrées dans les veines de quartz, alors que dans les quatre autres corps minéralisés les plus fortes concentrations d'or sont dans les veines d'hématite localement enrichies en quartz. Les veines riches en or sont parallèles à la foliation S1 dans tous les corps minéralisés, sauf pour Aba Norte où les veines d'hématite boudinées enrichies en or sont parallèles à S2. L'or et le palladium du mineraï se trouvent dans les minéraux suivants: l'or, l'or palladifère, le palladium, l'oxyde de palladium, la palladséite et l'arsénopalladinite. La teneur en palladium dans les grains d'or varie de 1 à 20 %. Les plus hautes teneurs de palladium sont rencontrées dans les corps minéralisés Corpo X et Corpo Y, là où les grains d'or contiennent des inclusions d'oxyde cuivre-palladium se présentant sous forme d'îlots et sous forme de reliques en texture de remplacement. Dans le corps minéralisé Aba Leste, le palladium forme un alliage homogène avec l'or. Dans le corps Aba Norte, les grains d'or ne contiennent pas de palladium mais sont plutôt porteurs de rhodium à des teneurs jusqu'à 1,5 %.

L'unique corps minéralisé en or et palladium de la mine de Conceição est parallèle à la foliation mylonitique. Cette minéralisation se retrouve dans le flanc des plis macroscopiques associés à D1 et à D2 et a été démembrée par la déformation de cisaillement progressif. L'or se trouve sous forme de grains aplatis, parallèles à la foliation mylonitique, et sous forme d'inclusions dans les grains d'hématite

commune dans les horizons de goethite résultant de l'altération des carbonates. Une teneur en palladium jusqu'à 0,8 % est rencontrée dans les grains d'or en plaquettes recourbées.

Le principal événement minéralisateur est contemporain au maximum du métamorphisme thermique ( $T=600^{\circ}\text{C}$ ), durant les cisaillements et chevauchements associés à D1. L'âge de l'événement minéralisateur a été estimé à  $1,9 +/ - 0,2 \text{ Ga}$  par datation isotopique Pb/Pb. Cet âge est en accord avec l'âge métamorphique du Supergroupe du Minas, et correspond à l'âge de l'Orogène Transamazonien dans la partie sud du Craton Sao Francisco.

L'altération hydrothermale associée à cet événement tectonique, caractérisée par la formation de talc, de phlogopite et de tourmaline, et par la formation de veines d'hématite et de quartz, a engendré la roche de type jacutinga. L'altération superficielle de la jacutinga a résulté en l'altération des silicates en kaolins et des oxydes en goethite.

Aux hautes températures et hautes fugacités d'oxygène, le palladium et l'or ont pu être transportés sous forme de complexes chlorures; leur déposition serait reliée à une augmentation du pH. Il est proposé que cette augmentation du pH ait été causée par la réaction entre le fluide minéralisateur et la roche précurseur de la jacutinga, une itabirite dolomitique. La source la plus probable des métaux précieux est la séquence volcano-sédimentaire Archéenne.

Les caractéristiques des minéralisations de Cauê et de Conceição amènent la définition d'un nouveau type de gisement aurifère, que nous nommons "Gisement d'or palladifère associé aux formations de fer de type Lac Supérieur fortement cisaiillées et métamorphisées". D'autres occurrences d'or palladifère sont aussi rencontrées dans la jacutinga, le long de la frontière est de la partie sud du Craton Sao Francisco, suggérant que cet environnement géologique est exceptionnellement favorable pour le type de minéralisation décrit.

## RESUMO

As minas de ferro de Cauê e Conceição localizam-se no Distrito de Itabira, na parte sul do Craton São Francisco, Brasil. Três unidades geológicas metamorfisadas no facies anfibolito foram identificadas em ambas as minas: (A) sequência volcano-sedimentar Arqueana; (2) formação de ferro Proterozóica; e (3) quartzito Proterozóico. A formação de ferro é cortada por diques de anfibolitos e está imbricada tectônica com talco xistos e anfibolitos da sequência volcano-sedimentar. Todas as rochas foram submetidas a três fases de dobramentos, assim como falhamentos de empurrao e "boudinage". Na formação de ferro, as estruturas D1 e D2 foram geradas num regime de cisalhamento simples progressivo, com o transporte tectônico de este em direção à oeste. As estruturas D3 são caracterizadas por dobras abertas com clivagem de crenulação associada.

Os depósitos de ouro paladiado são hospedados pela jacutinga na formação de ferro. Jacutinga é uma formação de ferro do tipo Lago Superior intensamente cisalhada, metamorfizada e alterada hidrotermalmente. Ela é composta de hematita, quartzo, talco, flogopita, com quantidades secundárias de turmalina, apatita e monazita.

O depósito de Cauê consiste de 5 corpos de minério: Corpo X, Corpo Y, Central, Aba Leste e Aba Norte. No Corpo Y, os teores mais elevados de ouro ocorrem nos veios de quartzo; entretanto nos outros corpos de minério os teores mais elevados ocorrem nos veios de hematita com concentrações locais de quartzo. Os veios auríferos são paralelos à xistosidade S1 em todos os corpos de minério, com exceção do Corpo Aba Norte. Neste, o veio de hematita aurífero é paralelo à xistosidade S2. Os minerais de minério são: ouro, ouro paladiado, paládio, óxidos de paládio, "paladseite" e arsenopaladinita. Nos Corpo Y e Corpo X, os teores de paládio nos grãos de ouro variam de 1% à 20%. Os valores mais elevados estão associados à inclusões de óxidos de paládio, que exibem texturas de substituição. No Corpo Aba Leste, o paládio apresenta-se distribuído homogeneous nos grãos de ouro. No Corpo Aba Norte os grãos de ouro apresentam teores em Rh de até 1.5% e não são paladiados.

O Corpo aurífero paladiado de Conceição é paralelo à xistosidade milonítica S1 nos flancos de dobras D1 e D2. Ele foi dismembrado pelo cisalhamento progressivo. O ouro ocorre em grãos placoides livres paralelos à S1, ou como inclusões nos grãos de hematita espelhada, tourmalina e quartzo. Finos grãos de ouro (< 3,0 µm) são comuns nas bandas de goetita, que resultaram da alteração dos carbonatos. Os teores em paládio nos grãos placoides são inferiores a 0.8 %.

O principal evento de mineralização foi contemporâneo com o pico do metamorfismo termal ( $T = 600^\circ C$ ), e com o cisalhamento e cavagamento D1. A idade

desse evento foi estimada a partir de datações Pb-Pb em 1.9 +/- 0.2 G.a. Esta idade concorda com a idade do metamorfismo do Supergrupo Minas e corresponde à idade da Orogênese Tranzamazônica na parte sul do Craton São Francisco.

A alteração hidrotermal associada com esse evento é caracterizada pela formação de talco, flogopita, e turmalina, assim como formação de veios de quartzo e hematita, resultando no tipo de rocha conhecido como jacutinga. Em consequência do intemperismo da jacutinga, os silicatos alteraram para caolin e os óxidos para goetita.

À elevadas temperaturas e alta fugacidade de oxigênio, Pd e Au devem ter sido transportados com complexos clorados e sua deposição deve ter ocorrido em consequência do aumento do pH. Esse aumento do pH deve ter sido causado pelas reações entre os fluidos mineralizados e o precursor da jacutinga, possivelmente um itabirito dolomítico. A fonte mais provável dos metais preciosos é a sequência volcano-sedimentar Arqueana.

As características peculiares dos depósitos de Cauê e Conceição permitem a definição de um novo tipo de depósito de ouro intitulado nesse trabalho como "Depósito de ouro paladiado hospedado em formação de ferro do tipo Lago Superior metamórfica e intensamente cisalhada". Na borda este do Craton São Francisco, outros depósitos de ouro são também associados à jacutinga, sugerindo que este ambiente geológico foi excepcionalmente favorável à esse tipo de depósito.

## ACKNOWLEDGEMENTS

I wish to thank Michel Gauthier, my advisor, for inviting me to take place in his research group at the Université du Québec à Montréal (UQAM) and who payed for research costs. His confidence in me are greatly appreciated.

I am gratefully to the Conselho Nacional de Desenvolvimento Científico e Tecnológico Regional (CNPq) of Brazil, for awarding me a four-year graduate scholarship, without which this project would not have materialized, and to the Companhia Vale do Rio Doce (CVRD; Itabira and Belo Horizonte Districts) for field work support, access to their properties and documents, sample preparations and the opportunity to consult their geological staff.

Special thanks go to:

Marc Bardoux (UQAM) and François Robert (Geological Survey of Canada) for their constructive discussion and for their extensive review of the structural data and for Marc's assistance in the field;

Glenn Poirier (McGill), Raymond Mineau, Michel Preda, and Raynald Lapointe (UQAM) for assistance during electron-microprobe, scanning electronic microscope, X-ray diffractometry analyses and sample preparations;

Clément Gariépy, Jean Carignan, and Francine Robert (all of UQAM) who performed the chemical and mass spectrometric analyses, and who helped me with both sample preparation and data interpretation for the Pb-Pb isotope work;

Luc Harnois and Ross Stevenson of UQAM for helpful evaluation of the mineralogical data;

James Bourne (UQAM) for his helpful discussion of the metamorphic data and for his confidence in me as a teaching assistant for Metamorphic Petrology and Field School III.

The Economic Geology and Mineralogical Magazine reviewers for their constructive criticism on the earlier draft manuscript of Chapter I and Chapter II and III, respectively;

The Minnesota Department of Natural Resources which payed for some of the major and trace element analyses;

Cecilia L. Jenkins and Venetia Bodycomb for improving the English manuscripts;

**Michelle Laithier for carefully drafting the figures;**

**Gaston Gelinas and Guy Robert for the preparation of thin sections;**

**Marie Auclair and the Earth Science department's secretarial staff who helped me with many day to day problems;**

**All my friends, especially Christine Giguère, who helped me enormously in my adaptation to Québec life;**

**Onildo Joao Marini who believed in my potential as a researcher and who suggested I go to Quebec for my Ph.D. studies;**

**And, last, but certainly not least, to my dear Alain, for his continuous assistance during my Ph.D. studies and for his help in editing French texts.**

## TABLE OF CONTENTS

<b>ABSTRACT</b>	ii
<b>RÉSUMÉ</b>	iv
<b>RESUMO</b>	vi
<b>ACKNOWLEDGEMENTS</b>	viii
<b>TABLE OF CONTENTS</b>	x
<b>LIST OF FIGURES</b>	xv
<b>LIST OF TABLES</b>	xxiii
 <b>INTRODUCTION</b>	 1
 <b>REFERENCES</b>	 9
 <b>CHAPTER I</b>	
 <b>PALLADIUM-BEARING GOLD DEPOSIT HOSTED BY PROTEROZOIC LAKE SUPERIOR-TYPE IRON-FORMATION AT CAUÊ IRON MINE, ITABIRA DISTRICT, SOUTHERN SAO FRANCISCO CRATON, BRAZIL: GEOLOGIC AND STRUCTURAL CONTROLS</b>	 13
1.1 INTRODUCTION	14
1.2 REGIONAL GEOLOGIC SETTING	17
1.3 CAUÊ MINE GEOLOGY	20
1.3.1 Geologic Units	20
1.3.2 Structure and Metamorphism	25
1.4 NATURE OF D1-D2 DEFORMATION IN THE CAUÊ MINE	32
1.4.1 Progressive Simple Shear Regime	32
1.4.2 Shear Sense	33
1.4.3 Bulk Shear Strain	33

1.4.4 Décollement Surfaces . . . . .	34
<b>1.5 PALLADIUM-BEARING GOLD OREBODIES OF THE CAUÊ MINE . . . . .</b>	<b>35</b>
1.5.1 Structural Controls and Geometry . . . . .	35
1.5.2 Hydrothermal Alteration and Effects of Weathering in Jacutinga . . . . .	41
1.5.3 Ore Mineralogy . . . . .	46
1.5.4 Whole Rock Geochemical Investigations . . . . .	51
<b>1.6 DEFORMATION HISTORY OF PALLADIUM-BEARING GOLD MINERALIZATION . . . . .</b>	<b>57</b>
<b>1.7 PROBABLE SOURCE, TRANSPORT AND MECHANISMS OF PALLADIUM AND GOLD DEPOSITION IN JACUTINGA . . . . .</b>	<b>60</b>
<b>1.8 COMPARISON OF THE CAUÊ GOLD DEPOSIT WITH ARCHEAN-IRON-FORMATION-HOSTED GOLD DEPOSITS . . . . .</b>	<b>61</b>
<b>1.9 REGIONAL IMPLICATIONS . . . . .</b>	<b>63</b>
<b>1.10 CONCLUSIONS . . . . .</b>	<b>64</b>
<b>REFERENCES . . . . .</b>	<b>66</b>

## CHAPTER II

<b>PALLADIAN GOLD FROM THE CAUÊ IRON MINE, ITABIRA DISTRICT, MINAS GERAIS - BRAZIL . . . . .</b>	<b>73</b>
<b>1.1 INTRODUCTION . . . . .</b>	<b>74</b>
<b>1.2 CAUÊ IRON MINE . . . . .</b>	<b>75</b>
1.2.1 Geologic Units . . . . .	75
2.2.2 Structure . . . . .	77
2.2.3 Gold Orebodies . . . . .	77
<b>2.3 ELECTRON-MICROPROBE (EMP) AND SCANNING ELECTRON MICROSCOPE (SEM) ANALYTICAL TECHNIQUES . . . . .</b>	<b>78</b>
<b>2.4 OCCURRENCES OF PALLADIAN GOLD . . . . .</b>	<b>79</b>
2.4.1 Corpo Y . . . . .	79
2.4.2 Corpo X . . . . .	84
2.4.3 Aba Leste . . . . .	90

<b>2.5 DISCUSSION .....</b>	<b>90</b>
2.5.1 Timing of Palladium-Gold Mineralization .....	90
2.5.2 Temperature and oxygen fugacity conditions .....	94
2.5.3 Transport and probable mechanisms of deposition of palladium and gold in jacutinga .....	94
<b>2.6 CONCLUSIONS .....</b>	<b>96</b>
<b>REFERENCES .....</b>	<b>98</b>

### **CHAPTER III**

<b>PALLADIUM MINERALS FROM THE CAUÊ IRON MINE, ITABIRA DISTRICT, MINAS GERAIS - BRAZIL .....</b>	<b>101</b>
<b>3.1 INTRODUCTION .....</b>	<b>102</b>
<b>3.2 GEOLOGICAL SETTING .....</b>	<b>103</b>
<b>3.3. ELECTRON-MICROSCOPE (EMP) AND SCANNING ELECTRON         MICROSCOPE (SEM) ANALYTICAL TECHNIQUES .....</b>	<b>106</b>
<b>3.4. PALLADIUM MINERALS: OCCURRENCES AND CHEMICAL         COMPOSITIONS .....</b>	<b>107</b>
3.4.1 Palladium and palladseite .....	108
3.4.2 Palladium-copper oxide .....	112
3.4.3 Arsenopalladinite .....	117
<b>3.5 DISCUSSION .....</b>	<b>121</b>
<b>3.6 CONCLUSIONS .....</b>	<b>123</b>
<b>REFERENCES .....</b>	<b>125</b>

**CHAPTER IV**

<b>LEAD ISOTOPE DETERMINATIONS IN THE IRON-FORMATION AND AMPHIBOLITE OF THE CAUÊ MINE, ITABIRA DISTRICT, BRAZIL: TECTONIC AND METALLOGENIC IMPLICATIONS . . . . .</b>	127
4.1 INTRODUCTION . . . . .	128
4.2 REGIONAL GEOLOGIC SETTING . . . . .	129
4.3 CAUÊ MINE GEOLOGY AND SAMPLING . . . . .	132
4.3.1 Geologic Units . . . . .	132
4.3.2 Structure . . . . .	134
4.3.3 Metamorphism . . . . .	135
4.3.4 Palladium-bearing Gold Orebodies . . . . .	136
4.4 TECTONIC REGIME AND RELATIVE TIMING OF PALLADIUM-GOLD MINERALIZATION . . . . .	137
4.5 ANALYTICAL TECHNIQUES FOR PB ISOTOPE DETERMINATIONS . . . . .	138
4.6 RESULTS . . . . .	140
4.6.1 Amphibolite . . . . .	140
4.6.2 Iron-formation . . . . .	141
4.7 DISCUSSION AND CONCLUSIONS . . . . .	143
4.7.1 Amphibolite . . . . .	143
4.7.2 Iron-formation and associated palladium-bearing mineralization . . . . .	145
REFERENCES . . . . .	147

**CHAPTER V**

<b>PALLADIUM-BEARING GOLD DEPOSIT HOSTED BY LAKE SUPERIOR-TYPE IRON-FORMATION AT CONCEICAO IRON MINE, ITABIRA DISTRICT, SOUTHERN SAO FRANCISCO CRATON, BRAZIL . . . . .</b>	150
5.1 INTRODUCTION . . . . .	151
5.2 REGIONAL GEOLOGIC SETTING . . . . .	154

5.3 CONCEIÇAO MINE GEOLOGY .....	157
5.3.1 Geological units .....	157
5.3.2 Structure .....	162
5.3.3 Metamorphism .....	166
5.4 PALLADIUM-BEARING OREBODY OF THE CONCEIÇAO MINE .....	166
5.4.1 Geometry and structural controls .....	167
5.4.2 Hydrothermal alteration and effects of weathering in jacutinga ..	171
5.4.3 Ore mineralogy .....	171
5.4.4 Whole rock geochemical investigations .....	174
5.5 COMPARISON OF THE CONCEIÇAO GOLD DEPOSIT WITH THE CAUÊ DEPOSITS .....	180
5.6 CONCLUSIONS .....	182
REFERENCES .....	183
 <b>CONCLUSIONS AND RECOMMENDATIONS .....</b>	 186
<b>REFERENCES .....</b>	 195
 <b>APPENDIX 1</b>	
 <b>SAO FRANCISCO CRATON: TECTONIC EVOLUTION AND ORE DEPOSITS .....</b>	 196
SAO FRANCISCO CRATON .....	197
Tectonic Evolution .....	197
Ore Deposits .....	204
REFERENCES .....	208

## LIST OF FIGURES

### INTRODUCTION

Figure 1. Alternative models for Archean iron-formation-hosted gold deposits: A: Syngenetic seawater-leaching model adapted from Frip's (1976) model; B: Syngenetic metamorphic model (adapted from Kerrich and Fryer, 1979); and C: Epigenetic metamorphic fluid model (Phillips et al., 1984).  
 After Groves et al., 1987. .... 4

### CHAPTER I

Figure 1.1.. Schematic geologic map of the southern part of the Sao Francisco Craton (modified after Dorr and Barbosa, 1963; Schorscher et al., 1982; Dorr, 1969; Ladeira, 1991), showing the main gold mines and occurrences hosted by:  
 (a) Archean banded-iron-formation: 1= Morro Velho, 2= Raposos, 3=Cuiabá; 4= Sao Bento; (b) mylonitic Archean volcano-sedimentary rocks: 5= Bela Fama, 6= Juca Vieira, 7= Paciência; (c) Early Proterozoic Witwatersrand-type conglomerates: 8= Cata Branca, 9= Serra do Gandarela; (d) Early Proterozoic graphitic phyllite: 10= Passagem de Mariana; and (e) Lake Superior-type iron-formation: 11= Congo Soco, 12= Maquiné, 13= Pitangui, 14= Cauê, 15= Conceição. Dashed line= staurolite in isograd (modified after Hoefs et al., 1982). .... 15

Figure 1.2. Simplified map of the Itabira District Map (modified after Dorr and Barbosa, 1963; Schorscher et al., 1982; Chemale and Quade, 1986). The iron mine open pits correspond to the northern and western sectors of the iron-formation unit which is complete outcrop. .... 21

Figure 1.3. Simplified geologic map of the Cauê mine (modified after Leao de Sá and Borges, 1991). The open pit of the Cauê iron mine corresponds to itabirite and hematite (iron-formation unit; IFU) outcrop. (AN=Aba Norte; AL= Aba Leste; C= Central; X=Corpo X; Y=Corpo Y gold orebodies). .... 22

Figure 1.4. Lower hemisphere, equal-area, stereographic projections of structural data from the Cauê mine structural domains outlined in the inset. Open circles: poles to the S1 foliation; filled circles: poles to the S2 foliation; open boxes: fold axis of D1-folds; filled boxes: fold axis of D2-folds; great circle girdle: best-fit plane to S1 foliation poles with eigenvectors (stippled boxes); stars: mean elongation lineation. ....	26
Figure 1.5. Block diagram of the core of the macroscopic sheath fold in the central-west area of the Cauê mine based on open pit mapping and drill log information of CVRD. ....	27
Figure 1.6 A. Sheath fold with a compact hematite core (He); from the east structural domain. B. Stretched quartz bands parallel to the long axes of sheath folds, observed in the XZ plane of a finite strain ellipsoid (from Corpo Y gold orebody, central structural domain). C. A complex F1-F2 fold pattern from Corpo Y gold orebody, central structural domain. D. Mesoscopic duplex structures in the iron-formation unit showing the shear sense (arrows= shear sense). ....	28
Figure 1.7. A. Map of level 868 of the Corpo Y gold orebody and the (modified after Leao de Sá and Borges, 1991). B. Schematic geological section of the Corpo Y gold orebody based on drill core data (modified after Leao de Sá and Borges, 1991). ....	38
Figure 1.8. A. Map of level 856 of the Corpo X palladium-bearing gold orebody located in Figure 1.3. B. Map of level 847 of the Corpo X palladium-bearing gold orebody located in Figure 1.3. ....	39
Figure 1.9. Map of level 840 of the Central palladium-bearing gold orebody located in Figure 1.3. ....	40
Figure 1.10. Map of level 865 of the Aba Leste palladium-bearing gold orebody located in Figure 1.3. ....	42
Figure 1.11. Map of level 880 of the Aba Norte gold orebody located in Figure 1.3. ....	43

Figure 1.12 A. Back-scattered electron image showing gold (Gd) as free grains or as inclusions in tourmaline (To) in the core of a dismembered D1-sheath fold of the Corpo Y orebody. He=hematite. B. Back-scattered electron image showing stretched gold grains (Gd) parallel to the elongation lineation (Le) in the Corpo Y orebody. He=hematite. C. Photomicrograph of gold (Gd) grain in boudinaged quartz (Qz) veins parallel to S1 in the Corpo Y orebody. He=hematite. D. Photomicrograph of gold (Gd) grains in the S2 transposition foliation plane from the Corpo Y orebody. He=hematite. .... 47

Figure 1.13 A. Secondary electron image of gold (Gd) coating around a zoned palladium-copper-oxide grain (PdO) from hematite-rich band parallel to elongation lineation (Le). From the Corpo Y orebody. Zoning is characterized by dark coloured zones with the highest Pd/Cu ratios alternating with and light zones. He=hematite. B. Back-scattered electron image of gold (Gd) coating around palladium (Pd) with a core of palladseite (Ps) from a phyllosilicate-rich boudin parallel to the elongation lineation (Le). From the Corpo Y orebody. .... 50

Figure 1.14. Passive model for development of sheath folds in a ductile, non-coaxial, and progressive tectonic regime with high bulk shear strain :  $\sigma$  greater than 10 (adapted from Cobbold and Quinquis, 1980). See text for explanation. .... 59

## CHAPTER II

Figure 2.1. Simplified geologic map of the Cauê iron mine, Itabira District, Minas Gerais State, Brazil, showing the gold orebodies (C= Central; L= Aba Leste; N= Aba Norte; X= Corpo X; Y= Corpo Y). Modified after Leao de Sá and Borges (1991). .... 76

Figure 2.2. Back-scattered electron image showing gold (Au) as free grains or inclusions in rotated tourmaline (To) in the core of a dismembered sheath fold. He=hematite. .... 80

Figure 2.3. Back-scattered electron image showing gold (Au) in hematite (He) bands parallel to the S1 mylonitic foliation (from Corpo Y). .... 81

Figure 2.4. Gold grains form the Corpo Y stretched parallel to the elongation lineation .....	82
Figure 2.5. Back-scattered electron image of gold with small inclusions of Pd-Cu oxides, showing island-mainland and replacement (relict) textures (from Corpo Y). ....	85
Figure 2.6. Enlargement of area outlined in Figure 2.5 showing Pd-Cu-oxide inclusions in the gold grain. ....	86
Figure 2.7. Single-element scans for Pd, Cu, and Au in the area analyzed (enclosed in box) in Figure 2.6. ....	87
Figure 2.8. Scanning electron micrograph of gold grain from Corpo X orebody with a Pd-Cu-oxide inclusion. ....	88
Figure 2.9. Single-element scans for Au, Pd, and Cu of the gold grain close to the Pd-Cu- oxide inclusion in Figure 2.8. ....	89
Figure 2.10. Scanning electron micrograph of a palladian gold grain from Aba Leste .....	91
Figure 2.11. Single-element scans for Au and Pd of the gold grain in Figure 2.10. ....	92

### CHAPTER III

Figure 3.1. Simplified map of the Itabira District (after Olivo et. al., in press). .	104
Figure 3.2. Simplified geologic map of the Cauê iron mine, Itabira District, Minas Gerais State, Brazil, showing the palladian gold orebodies (C= Central; L= Aba Leste; N= Aba Norte; X= Corpo X; Y= Corpo Y). Modified after Leao de Sá and Borges (1991) .....	105
Figure 3.3. Photomicrograph of two palladium grains (Pd) coated with gold (Au) in a phyllosilicate-rich boudin parallel to S1; The large grain has a core of palladseite (Ps), and in the small grain, only the rim is preserved. He= hematite. ....	110
Figure 3.4. Single-element scans of Pd, Cu, Au, and Se for the large palladium grain of Figure 3.3 showing a core of palladseite. ....	111

- Figure 3.5. Photomicrograph of palladium-copper oxide (PdO) coated with gold (Au) in a hematite (He) band parallel to the S1 mylonitic foliation and stretched parallel to the elongation lineation. Zoning is characterized by the alternation of dark colored zones (high Pd/Cu ratios) with light zones (low Pd/Cu ratios). Arabic numbers correspond to analyzed points referred to in Table 3.2. .... 113
- Figure 3.6 Back-scattered electron image showing finely zoned palladium-copper oxide (PdO) coated with gold occurring in white phyllosilicate band parallel to the S1 mylonitic foliation. Arabic numbers correspond to analyzed points referred to in Table 3.2. .... 114
- Figure. 3.7. Back-scattered electron image showing a finely zoned palladium-copper-oxide grain (PdO) in a white phyllosilicate band parallel to the S1 mylonitic foliation. The oxide grain was coated with gold which was removed by repeated polishing, and contains fine inclusions of gold oblique to the compositional bands (Au). Arabic numbers correspond to the analyzed points referred to in Table 3.2. .... 115
- Figure 3.8. Back-scattered electron image of stretched gold with small inclusions of Pd-Cu oxides (PdO), showing island-mainland and replacement (relict) textures (from Corpo Y). He= hematite .... 118
- Figure 3.9. Back-scattered electron image of arsenopalladinite (Aspd) with inclusions of palladium-copper oxide (PdO) .... 119
- Figure 3.10. Single-element scans of Pd, As, Sb, and O for the area shown in Figure 3.9. .... 120
- CHAPTER IV**
- Figure 4.1. Schematic geologic map of the southern part of the Sao Francisco Craton (modified after Dorr and Barbosa, 1963; Schorscher et al., 1982; Dorr, 1969; Ladeira, 1991) showing the gold mines hosted by Lake Superior-type iron-formation in the Itabira District: 1= Cauê, 2= Conceição, 3= Congo Soco, 4= Maquiné, 5= Pitangui .... 130

**Figure 4.2 . Simplified geologic map of the Cauê mine (modified after Leao de Sá and Borges, 1991), showing the palladium-bearing gold ore bodies (Y= Corpo Y, X= Corpo X, C= Central, L= Aba Leste, and N= Aba Norte) with locations of samples analyzed in this paper. The open pit of the Cauê iron mine corresponds to itabirite and hematite (iron-formation unit) outcrop. .... 133**

**Figure 4.3.  $^{207}\text{Pb}/^{204}\text{Pb}$  vs  $^{206}\text{Pb}/^{204}\text{Pb}$  diagram showing data on minerals from amphibolite of the Cauê mine. Hornblende and ilmenite yield an age of  $2.7 +/- 0.6$  Ga. .... 142**

**Figure 4.4.  $^{207}\text{Pb}/^{204}\text{Pb}$  vs  $^{206}\text{Pb}/^{204}\text{Pb}$  diagram showing data on minerals from the iron-formation of the Cauê mine. An age of  $1.9 +/- 0.2$  Ga is obtained for hematite, quartz and gold, when the most radiogenic residues and bulk analysis of samples with relict of magnetite are omitted from the regression. .... 144**

## CHAPTER V

**Figure 5.1 . Schematic geologic map of the southern part of the São Francisco Craton (modified after Dorr and Barbosa, 1963; Schorscher et al., 1982; Dorr, 1969; Ladeira, 1991), showing the main gold mines and occurrences hosted by: (a) Archean banded-iron-formation: 1= Morro Velho, 2= Raposo, 3=Cuiabá; 4= São Bento; (b) mylonitic Archean volcano-sedimentary rocks: 5= Bela Fama, 6= Juca Vieira, 7= Paciência; (c) Early Proterozoic Witwatersrand-type conglomerates: 8= Cata Branca, 9= Serra do Gandarela; (d) Early Proterozoic graphitic phyllite: 10= Passagem de Mariana; and (e) Lake Superior-type iron-formation: 11= Congo Soco, 12= Maquiné, 13= Pitangui, 14= Cauê, 15= Conceição. Dashed line= staurolite in isograd (modified after Hoefs et al., 1982). .... 152**

**Figure 5.2. Simplified map of the Itabira District Map (modified after Dorr and Barbosa, 1963; Schorscher et al., 1982; Chemale and Quade, 1986). The iron mine open pits correspond to the northern and western sectors of the iron-formation unit which is complete outcrop. .... 153**

**Figure 5.3. Simplified geologic map of the Conceição mine (modified after Leao de Sá and Borges, 1991). .... 158**

Figure 5.4. Picture of the southern part of Conceição-iron-mine open pit, showing (a) the tectonic contact between the volcano-sedimentary sequence, iron-formation unit, indicated by thrust fault symbol, as in figure 3; (b) the intrusive rocks indicated by "i"; and (c) the location of the Conceição orebody, indicated by "CG". . . . .	159
Figure 5.5. Block diagram of the Conceição open pit based on mapping and drill log information of CVRD. . . . .	160
Figure 5.6 D1 asymmetric tight fold, showing the sense of shearing during D1 and the S1-mylonitic foliation. . . . .	163
Figure 5.7. Lower hemisphere, equal-area, stereographic projections of structural data from the Conceição mine. A. Poles to the S1 foliation (open circles); Le (star); measured in this work. B. Kamb contour of Poles to the S1 foliation (Souza Filho, 1989). C. Kamb contour of mineral lineation (Souza Filho et al., 1989). . . . .	164
Figure 5.8. Vertical section of the Conceição gold orebody (yellow to dark brown vein) folded by parasitic D2-fold. . . . .	168
Figure 5.9 Geological map of the level 901 of the Conceição orebody . . . . .	170
Figure 5.10. Detail of the Conceição auriferous vein, showing the dismembered yellow quartz vein with a border of goethitic and hematitic alteration. . . . .	172
Figure 5.11. Back-scattered electron image showing gold grains in open spaces parallel to S1-foliation in goethite-rich band. . . . .	173
Figure 5.12. Octahedral gold grains of the Conceição orebody. . . . .	175

## CONCLUSIONS AND RECOMMENDATIONS

Figure 1. Proposed evolutionary model for the Minas Supergroup (adapted from Teixeira and Figueiredo, 1991). Stage I= opening of the Minas basin (2.4-2.6 Ga, Babinski et al., 1993); Stage II A= basin closure following by folding, metamorphosim and thrusting of the Minas sequence (1.9- 2.2 Ga, Teixeira et al., 1991); B= detail of A, showing hydrothermal circulation during the basin closure. . . . .	189
--	-----

## **APPENDIX 1**

## LIST OF TABLES

### CHAPTER I

<b>Table 1.1. The stratigraphic column of the Early Proterozoic Minas Supergroup. ....</b>	<b>19</b>
<b>Table 1.2. Mineral abundances of jacutinga, itabirite and compact hematite body. ....</b>	<b>36</b>
<b>Table 1.3. Electron microprobe and scanning electronic microscopic (*) energy dispersive system analyses of gold grains of the Cauê orebodies. AN1 is an octahedral crystal; the other gold grains are stretched or bent. (Values en wt %). ....</b>	<b>48</b>
<b>Table 1.4. Electron microprobe analyses of Pd-Cu oxide shown in the Figure 12e (* average of two analyses in wt %). ....</b>	<b>52</b>
<b>Table 1.5. Electron microprobe analyses of palladium and palladseite shown in the Figure 12f (values in wt %; * average of two analyses). ....</b>	<b>53</b>
<b>Table 1.6. Major elements, and trace and precious metal contents of Cauê iron-formation specimens (1= hematite vein in jacutinga from Aba Norte; 2= jacutinga from Aba Norte; 3= hematite vein in jacutinga from Corpo X; 4= jacutinga close to hematite vein from Corpo X; 5= quartz vein in jacutinga from Corpo Y; 6= Jacutinga from Corpo Y; 7= jacutinga from Corpo Y; 8= jacutinga from Aba Leste; 9= jacutinga from Aba Leste; 10= itabirite; 11= compact hematite body; and 12= ferruginous quartzite). A= average of 133 samples of Lake Superior-type oxide facies iron-formation from 7 regions of Canada (Gross, 1988); and B= Average of REE elements of Lake Superior-type oxide facies iron-formation (Fryer, 1977). ....</b>	<b>54</b>
<b>Table 1.7: Gold grades of samples from the Cauê gold orebodies analyzed by fire-assay techniques. ....</b>	<b>56</b>

**CHAPTER II**

<b>Table 2.1: Wavelength-dispersive electron microprobe (EMP) analyses of palladian gold from polished sections of jacutinga, Corpo Y orebody. . . . .</b>	<b>83</b>
--	-----------

**CHAPTER III**

<b>Table 3.1: Wavelength-dispersive system analyses by electron-microprobe of palladium and palladseite, shown in Figures 2 and 3, from jacutinga of the Corpo Y orebody. Data reported by Davis et al. (1977) and an average of 4 analyses obtained by energy-dispersive system analyses (*, with 0.15% Mn) are given for comparison. . . . .</b>	<b>109</b>
--	------------

<b>Table 3.2: Wavelength-dispersive analyses by electron-microprobe of palladium-copper oxide from jacutinga of Corpo Y orebody. Arabic numbers correspond to the analyses plotted in Figures 4 (grain I), 5 (grain II) and 6 (grain III). . . . .</b>	<b>116</b>
--	------------

**CHAPTER IV**

<b>Table 4.1: Pb isotope results on minerals from the iron-formation and amphibolite of the Cauê mine. . . . .</b>	<b>139</b>
--	------------

**CHAPTER V**

<b>Table 5.1: The stratigraphic column of the Early Proterozoic Minas Supergroup. . . . .</b>	<b>156</b>
---	------------

<b>Table 5.2: Mineral abundances of jacutinga, itabirite and compact hematite body of the Conceição mine. . . . .</b>	<b>169</b>
---	------------

<b>Table 5.3: Electron microprobe energy dispersive system analyses of gold grains of the Conceição orebody. CO-3 is an octahedral crystal; the other gold grains are bent. (Values en wt %). . . . .</b>	<b>176</b>
---	------------

<b>Table 5.4: Major elements, and trace and precious metal contents of Conceição iron-formation specimens (41a= dismembered auriferous quartz vein with hematitic alteration border; 41c and 41g= jacutinga from the hanging wall of the auriferous quartz vein; 41d= jacutinga from the footwall of the auriferous quartz vein; FAU-06-07= itabirite). . . . .</b>	<b>178</b>
<b>Table 5.5: Tonnage, metal content and average gold grade of Conceição gold orebody from different levels mined between 1987 to 1990 (Andrade, 1991, pers. communication). . . . .</b>	<b>179</b>

## APPENDIX

<b>Table 1: Summary of important tectonothermal events in the São Francisco craton (After Teixeira and Figueiredo, 1991; Machado et al., 1992 and Babinski et al., 1993). . . . .</b>	<b>203</b>
<b>Table 2: Summary of the principal ore deposits of the São Francisco craton. . . . .</b>	<b>205</b>

## INTRODUCTION

Gold-bearing iron-formation are known throughout the world and form an important mineral exploration target. Some of the classic examples include the Homestake deposit in the United States (Lindgren, 1933; Rye and Rye, 1974; Sawkins and Rye, 1974), the Morro Velho Mine in Brazil (Orville, 1902; Lindgren, 1933; Gair, 1962 and Ladeira, 1985, 1991) Vulbachikwe in Zimbabwe (Fripp, 1976a,b; Saager et al., 1987; Oberthur et al, 1990), as well as deposits in Western Australia (Phillips et al., 1984; Groves et al., 1987), Canada (Fryer et al., 1979; Kerrich and Fryer, 1979; Macdonald, 1983; Padgham, 1984; Anglin and Franklin, 1985; Kerswill, 1986; Wyman et al., 1986; Lhotka and Nesbitt, 1989, Gibbins et al., 1991), India (Hamilton and Hodgson, 1986), and several mines in Brazil (Fleischer and Routhier, 1973; Abreu et al., 1988; Vial, 1988a e 1988b; Vieira, 1988; Vieira and Oliveira, 1988; Ladeira, 1991; Leao de Sa and Borges, 1991; Vieira, 1991).

Gold deposits in Lake Superior-type iron-formation are rare and have only been identified in the Itabira District of Brazil. In contrast, gold deposits in Algoma-

type iron-formations are common and extensively modelized. The various genetic models for Algoma-type gold deposits are presented here before introducing the content of this thesis.

There is little consensus on the genesis of the gold deposits hosted by Algoma-type iron-formation and three genetic models (syngenetic, epigenetic, and multistage or remobilization) have been proposed to explain the processes by which gold may have been concentrated in these rocks.

The syngenetic model involves deposition and/or early diagenetic formation of sulfide facies banded iron-formation and gold precipitation at the seawater-sediment interface in an oceanic basin in which oxide- and/or carbonate-facies banded iron-formation are the dominant precipitates. This implies a local sulfur source and/or suitable pH-Eh conditions which promote to the precipitation of Fe sulfides rather than Fe oxides (James, 1954).

Different fluid sources have been suggested for the syngenetic model. Fripp (1976a, 1976b), for example, proposed that seawater may convect through the oceanic crust and deposit gold from Au-rich brines. On the other hand, Kerrich and Fryer (1979) suggested that gold may be deposited from metamorphic H<sub>2</sub>O-CO<sub>2</sub>-rich fluids emanating from the crust onto the sea floor. These same fluids may have formed epigenetic deposits lower in the volcanic-sedimentary pile (Fig.1). In the case

of metamorphic fluid sources, some involvement of heated seawater is almost inevitable and Cl complexes would be responsible for metal transport. The criteria in favor of this model are according to Fripp (1976): (1) gold and sulfides are restricted to banded iron-formation (BIF) horizons which are laterally persistent; (2) absence of widespread wall rock alteration in the iron-formation; (3) geochemical characteristics of mineralized zones typical of volcanogenic-exhalative deposits (e.g. rare-earth element patterns); and (4) absence of sulfide and gold mineralization in the iron-rich host rock.

In recent years many researchers have postulated the epigenetic origins for gold deposits hosted by banded iron-formations (Fyon et al., 1983 ; Mason and MacConnell, 1983; Macdonald, 1983; Phillips et al., 1984; Wyman et al., 1986; Groves et al, 1987; Groves et al, 1988; Lhotka and Nesbitt, 1989; Vieira, 1991). Phillips et al. (1984) suggested that the stratabound deposits simply represent epigenetic mineralization derived from similar sources as vein-hosted gold but which was deposited in different host rocks.

The epigenetic model involves selective replacement of oxide and/or carbonate facies BIF by post-depositional sulfur-bearing fluids chemically similar to those responsible for the epigenetic volcanic- or sediment-hosted gold deposits

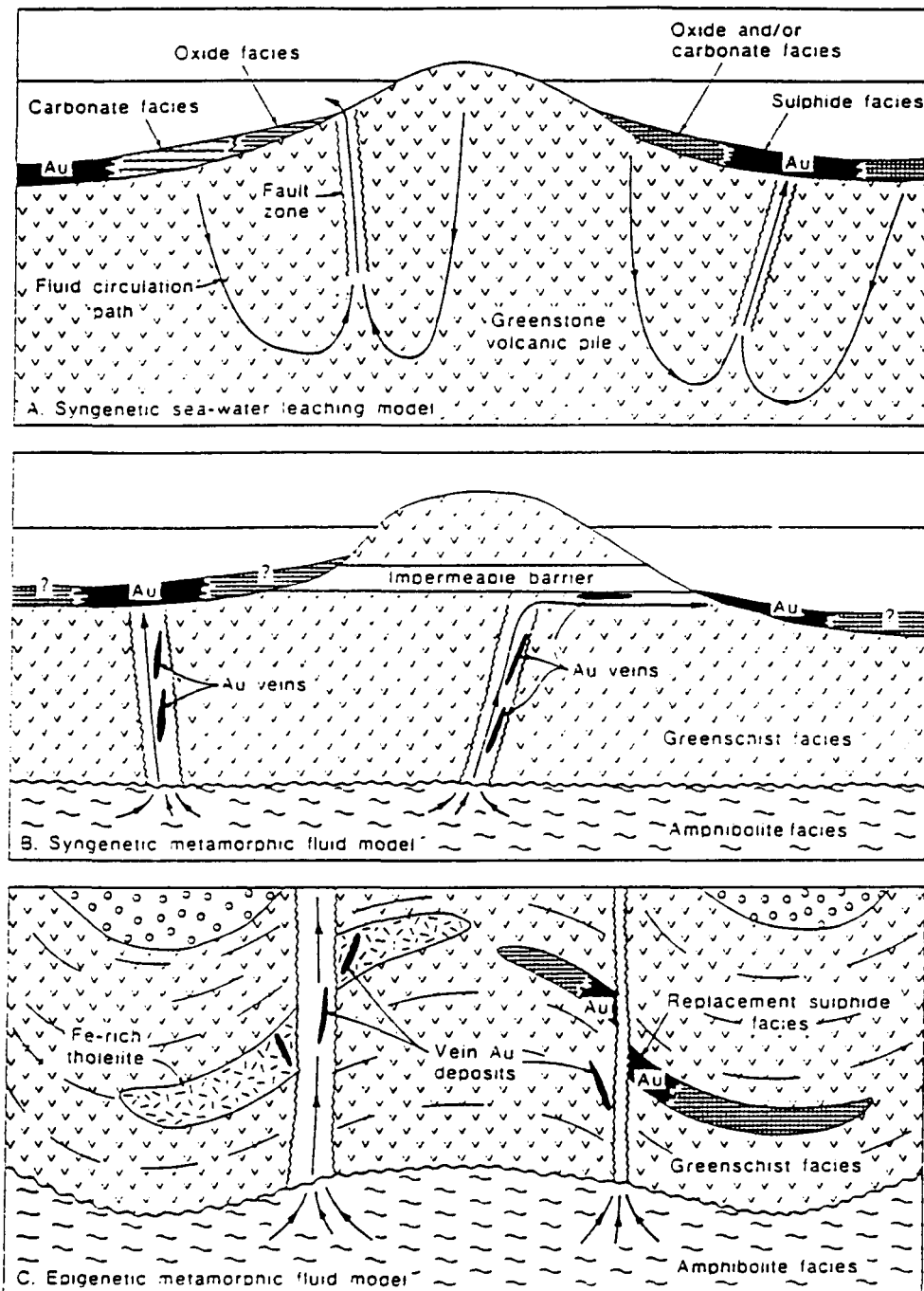


Figure 1. Alternative models for Archean iron-formation-hosted gold deposits:  
 A: Syngenetic seawater-leaching model adapted from Frip's (1976) model; B: Syngenetic metamorphic model (adapted from Kerrich and Fryer, 1979); and C: Epigenetic metamorphic fluid model (Phillips et al., 1984). After Groves et al., 1987.

elsewhere in volcanic-sedimentary sequences (Fig. 1). In this model, fluid transport is via fractures and faults in the banded iron-formation, and there is selective replacement of Fe-rich bands. Phillips et al. (1984), Groves et al. (1987) and Groves et al., (1988) listed the evidence that lend substantial support for the epigenetic model for BIF-hosted gold deposits in greenstone belts of the Yilgarn block, western Australia. The evidence is: (1) strong structural control of gold occurrences in places similar to that of volcanic-hosted deposits of certain epigenetic origin; (2) unequivocal evidence for widespread sulfidation and carbonate alteration of BIF in some deposits; (3) occurrences of anomalous Au, Sb and As contents; (4) gold to base metal ratios similar to those of volcanic-hosted gold ores and different of volcanogenic massive-sulfide or exhalative sediments; (5) indications from fluid inclusions that metamorphic fluids were involved in gold deposition; (6) lack of BIF-hosted gold deposits in terranes where sulfide-facies BIF is widespread (e.g. Norseman Wiluna Belt, Australia); (7) low background Au values in BIF, both regionally and along strike from mineralization; and (8) Pb-Pb model ages for Fe-sulfides are similar to volcanic-hosted gold deposits and younger than syngenetic base-metal deposits in the same terrane.

Both vein and stratabound gold deposits are present in many gold districts around the world, and hypotheses which involve both syngenetic and epigenetic process together have been proposed. The multistage model postulates that gold is a primary component of the iron formation and is remobilized and concentrated during

later events ( Rye and Rye, 1974; Sawkins and Rye, 1974; Fripp, 1976a; Saager et al., 1987; Oberthur et al, 1990; Ladeira, 1991).

Recently Oberthur et al. (1990) pointed out that the BIF-hosted gold occurrences from the greenstone terranes of the Zimbabwe and Kaapvaal cratons are not the product of a single universal metallogenic process, but may be explained by several different genetic processes, such as primary syn-sedimentary formation, diagenetic changes, metamorphic remobilization, and epigenetic hydrothermal emplacement.

Little is known about gold deposits in the Lake Superior-type iron-formation. The deposits in the Itabira Iron District of Brazil are the only known deposit hosted in a Lake Superior-type iron-formation in the world, and so they provide a unique opportunity to study the processes related to gold mineralization in this geological setting. In addition these deposits are PGE-bearing, and represent a new geological environment for PGE mineralization that has not yet been described in the scientific literature.

The purpose of this thesis is to explain the genesis of palladium-bearing gold ores in the iron-formation of the Cauê and Conceição mines based on: (1) mapping and structural analysis; (2) petrological and mineralogical studies; (3) whole rock

geochemistry; (4) mineral chemistry; and (5) geochronological data. The following is a brief outline of the thesis.

Chapter 1 contains the geological and structural framework of the Cauê iron mine in addition to the structural controls and geometry, hydrothermal alteration, ore mineralogy, and whole rock geochemistry of the palladium-bearing gold orebodies. This chapter also presents a deformation history of the palladium-bearing gold mineralization and a genetic model is proposed. This paper was accepted for publication in Economic Geology and the coauthors are M. Gauthier, M. Bardoux, E. Leao de Sá, J.T. Fonseca, and F. C. Santana.

In Chapters 2 and 3, textural details and analytical data for palladium gold (Chapter 2) and palladium minerals (Chapter 3) from jacutinga of the Cauê mine are reported and discussed in terms of their genesis. These papers were accepted to publication in Mineralogical Magazine. The coauthors of the second paper are M. Gauthier and M. Bardoux and of the third paper is M. Gauthier.

In Chapter 4, the results of lead isotope studies of the Cauê mine rocks are reported and discussed together with geological and structural data in order to determine the timing of gold-palladium deposition and to place the mineralizing event in a regional tectonic framework. This paper will be sent to the Journal of South American Earth Science.

In Chapter 5, the geological and structural framework of the Conceição mine is presented in addition to the structural control and geometry, hydrothermal alteration, ore mineralogy, and geochemical investigation of the palladium-bearing gold orebody. A comparison with the Cauê palladium-bearing gold orebodies is presented. This communication will be sent to "Revista Brasileira de Geociências".

In the Conclusion section, the contribution of this study to the understanding of the genesis of palladium-bearing gold deposits hosted by iron-formation and the resulting implications for the exploration of this type of palladium-bearing gold deposit are discussed. Future studies are suggested that may clarify specific problems and, therefore, better explain the occurrence of PGE and gold in the Lake Superior-type iron-formation.

Finally, in Appendix 1, the summary of the São Francisco craton tectonic evolution and its main ore deposits is presented. Its purpose is to provide the reader with a overall geological context of the study area.

## REFERENCES

- Abreu, A. S., Diniz, H. B., Prado, M.G.B. and Santos , S.P., 1988, Mina de ouro de Sao Bento, Santa Barbara, Minas Gerais. In Depósitos Minerais do Brasil, Departamento Nacional de Minas e Energia, Brasília, v. 3, p. 393-411.
- Anglin. S.D. and Franklin, J. M., 1985, Gold mineralization in the Beardmore-Geraldton area of the northwest Ontario: structural considerations and the role of iron formation. In Current research part A. Geological Survey of Canada, Paper 85-1A, p. 193-201.
- Fleischer, R. and Routhier, P., 1973, The "Consanguineous" Origin of Tourmaline-bearing Gold Deposit: Passagem de Mariana (Brazil): Economic Geology, v. 68, p. 11-22.
- Fripp, R. E. P., 1976a, Gold metallogeny in the Archaean of Rhodesia. In The Early History of the Earth. Edited by B.F. Windley. Wiley, London p. 455-466.
- Fripp, R. E. P., 1976b, Stratabound gold deposit in Archean banded iron-formation, Rhodesia: Economic Geology, v. 71, p. 58-75.
- Fryer, B. J., Kerrich, R., Hutchinson, R.W., Peirce, M.G. and Rogers, D.S, 1979, Archaean precious-metal hydrothermal systems, Dome Mine, Abitibi Greenstone Belt. I. Patterns of alteration and metal distribution: Canadian Journal of Earth Science, v. 16, p. 421-439.
- Fyon, J. A., Crocket, J.H. and Schwarcz, H.P., 1983, The Carshaw and Malga Iron Formation-hosted gold deposits of the Timmins Area: In geology of gold in Ontario. Edited by A.C. Colvine, Ontario Geological Survey, Miscellaneous Paper 110, p.98-110.
- Gair, J. E., 1962, Geology and ore deposits on the Nova Lima and Rio Acima Quadrangles, Minas Gerais, Brazil: United States Geological Survey Professional Paper, 342A, p.67.
- Gibbins, W. A., Padgham, W. A., Atkinson, S., Brophy, J. A., and Gault, D., 1991, The Central Iron Formation Zone, Slave Structural Province, Northwest Territories, Canada- A gold-rich Archean metallotect: Brazil Gold'91: An International Symposium on the geology of gold, Belo Horizonte, 1991, A. A. Balkema, Proceedings, p.159-165.
- Groves, D. I., Phillips, G. N., Falconer, L. J., Houstoun, S. M., Ho, S. E., Browning, P., Dahl, N., and McNaughton, N. J., 1987, Evidence for an epigenetic origin for

- BIF-hosted gold deposits in the greenstone belts of the Yilgarn Block, Western Australia: In Recent Advances in Understanding Precambrian Gold Deposits.** Edited by S.E. Ho and D.I. Groves. Geology Department and University Extension. University of Western Australia, Publication 11, p. 167-179.
- Groves, D. I., Ho, S. E., McNaughton, N. J., Mueller, A. G., Perring, C. S., Rock, N. M. S., 1988. Genetic models for Archaean lode-gold deposits in western Australia: In Recent Advances in Understanding Precambrian Gold Deposits.** Edited by S.E. Ho and D.I. Groves. The Geology Department & University Extension. University of Western Australia, Publication 12, p. 1-22.
- Hamilton, J. V. and Hodgson, C. J., 1986, Mineralization and structure of the Kolar gold field, India: Gold'86, an international symposium on the geology of gold deposits.** Edited by A.J. Macdonald. Toronto, Ontario, p. 270-283.
- James, H. L., 1954, Sedimentary facies of iron-formation: Economic Geology, v. 49, p. 235-293.**
- Kerrich, R., and Fryer, B. J., 1979, Archean precious-metal hydrothermal systems, Dome mine, Abitibi greenstone belt: II, REE and oxygen isotope relations: Canadian Journal of Earth Science, v. 16, p. 440-458.**
- Kerswill, J. A., 1986, Gold deposits hosted by iron formation in the Contwoyto Lake area, Northwest Territories: Gold'86 poster paper abstracts.** Edited by A.M. Chater. Geological Association of Canada, Mineral Deposits Division, p. 82-85.
- Ladeira, E., 1991, Genesis of gold in Quadrilátero Ferrífero: a remarkable case of permanency, recycling and inheritance- A tribute to Djalma Guimaraes, Pierre Routhier and Hans Ramberg: Brazil Gold'91: An International Symposium on the geology of gold, Belo Horizonte, 1991, A.A. Balkema, Proceedings, p. 11-30.**
- Ladeira, E., 1985, Metalogênese do ouro na Mina de Morro Velho e no Distrito de Nova Lima, Quadrilátero Ferrífero, Minas Gerais, Brasil: Contribuições à Geologia e à Petrografia, Sociedade Brasileira de Geologia, Núcleo Minas Gerais, p.95-151.**
- Leao de Sa, E. and Borges, N. R. A., 1991, Gold mineralization in Cauê and Conceição iron ore mines - Itabira- MG : Field and mine trip to Quadrilátero Ferrífero, Minas Gerais, Brazil, Field guide book of Brazil Gold'91: An International Symposium on the geology of gold. Belo Horizonte, p. 74-85.**
- Lhotka, P. G., and Nesbitt, B. E., 1989, Geology of unmineralized and gold-bearing iron formation, Contwoyto Lake- Point Lake region, Northwest, Canada: Canadian Journal of Earth Science, v. 26, p. 46-64.**

- Lindgren, W., 1933, Mineral Deposits. McGraw-Hill Book Company, Inc., New York, 4th ed., 930p.
- Macdonald, A. J., 1983, The iron formation-gold association: evidence from the Geraldton Area: In geology of Gold in Ontario, edited by A.C. Colvine, Ontario Geological Survey, Miscellaneous Paper 110, p.75-83.
- Mason, J. K. and McConnell, C. D., 1983, Gold Mineralization in the Beardmore-Geraldton Area: In Geology of Gold in Ontario. Edited by A.C. Colvine, Ontario Geological Survey, Miscellaneous Paper 110, p. 84-97.
- Oberthur, T. S., R. and Tomschi, H.-P., 1990, Geological, mineralogical and geochemical aspects of Archean banded iron-formation-hosted gold deposits: some examples from Southern Africa: Mineralium Deposita, v. 25, p. S125-S135.
- Orville, A. D., 1902, Notes on Brazilian Gold Ores: Translation of American Institute of Mining and Engineering, v. 33, p. 282-287.
- Padgham, W. A., 1984, Gold deposits of N.W.T.; classes, styles, genesis, exploration methods and success probabilities: Contributions to the Geology of the Northwest Territories, v. 1, p. 121-129.
- Phillips, G. N., Groves, D. I., Martyn, J. E., 1984, An epigenetic origin for Archean banded iron formation hosted gold deposits: Economic Geology, v. 79, p. 162-171.
- Rye, D. M. and Rye, R. O, 1974, Homestake gold mine, South Dakota: I Stable isotope studied: Economic Geology, v. 69, p. 293-317.
- Saager, R. O., Oberthur, T. S., and Tomschi, H. P., 1987, Geochemistry and mineralogy of banded iron-formation-hosted gold mineralization in the Gwanda Greenstone Belt, Zimbabwe: Economic Geology, v. 82, p. 2017-2032.
- Sawkins, F. J. and Rye, D. M., 1974, Relationship of Homestake type gold deposits to iron-rich Precambrian sedimentary rock: Institute of Mining and Metallurgy, Transactions, Section B, v. 84, p. B37-B38.
- Vial, D. S., 1988a, Mina de ouro da Passagem , Mariana, Minas Gerais. Principais Depósitos Minerais do Brasil, Departamento Nacional de Produção Mineral, Brasília, v.3, p. 421-430.
- Vial, D. S., 1988b, Mina de Ouro de Cuiabá, Quadrilátero Ferrífero, Minas Gerais: Principais Depósitos Minerais do Brasil, Departamento Nacional de Produção Mineral, Brasilia, p.413-419.

Vieira, F. W. R., 1991, Textures and processes of hydrothermal alteration and mineralization in the Nova Lima Group, Minas Gerais, Brazil: Brazil Gold'91: An International Symposium on the geology of gold, Belo Horizonte, 1991, A.A.Balkema, Proceedings, p.319-325.

Vieira, F. W. R., 1988, Processos epigenéticos de formação dos depósitos auríferos e zonas de alteração hidrotermal do Grupo Nova Lima, Quadrilátero Ferrífero, Minas Gerais: Congresso Brasileiro de Geologia, 35<sup>th</sup>, Sociedade Brasileira de Geologia, Belem, 1: 76-87.

Vieira, F. W. R., and Oliveira, G. A. I., 1988, Geologia do Distrito Aurífero de Nova Lima, Minas Gerais: Principais Depósitos Minerais do Brasil, Departamento Nacional de Produção Mineral, Brasília, p. 377-391.

Wyman, D. A., Kerrich, R. and Fryer, B.J, 1986, Gold Mineralization overprinting iron formation at the Agnico- Eagle Deposit, Quebec, Canada: mineralogical, microstructural and geochemical evidence. Gold'86, An International Symposium on the geology of gold deposits, Toronto, Proceedings, p. 108-123.

## **CHAPTER I**

**PALLADIUM-BEARING GOLD DEPOSIT HOSTED BY PROTEROZOIC LAKE  
SUPERIOR-TYPE IRON-FORMATION AT CAUE IRON MINE, ITABIRA  
DISTRICT, SOUTHERN SAO FRANCISCO CRATON, BRAZIL:  
GEOLOGIC AND STRUCTURAL CONTROLS**

## 1.1 INTRODUCTION

The southern part of the São Francisco Craton (Fig. 1.1, including the Quadrilátero Ferrífero and the Itabira District) is known as a major producer of iron ore (Dorr, 1965; Dorr, 1973; Melo et al., 1986; Walde, 1986; Hoppe et al., 1987), but it is also an important gold province (Fleischer and Routhier, 1973; Abreu et al., 1988; Ladeira, 1988; Vial, 1988; Vieira and Oliveira, 1988; Fleischer and Vial, 1991; Ladeira, 1991; Leao de Sá and Borges, 1991). The Morro Velho mine alone has produced about 500 t Au (Ladeira, 1991). The gold deposits in southern São Francisco craton (Fig. 1.1) are hosted by Archean banded-iron-formation (e.g., Morro Velho, Raposos, Cuiabá, and São Bento mines) and mylonitized volcano-sedimentary rocks (e.g., Bela Fama, Juca Vieira, and Paciência occurrences) as well as Early Proterozoic Witwatersrand-type conglomerates (e.g., Cata Branca showing and Serra do Gandarela prospect), graphitic phyllites (Passagem de Mariana mine), and Lake Superior-type iron-formations (e.g., Congo Soco, Maquiné, Pitangui, Cauê and Conceicao mines) (Ladeira, 1991; Leao de Sá and Borges, 1991).

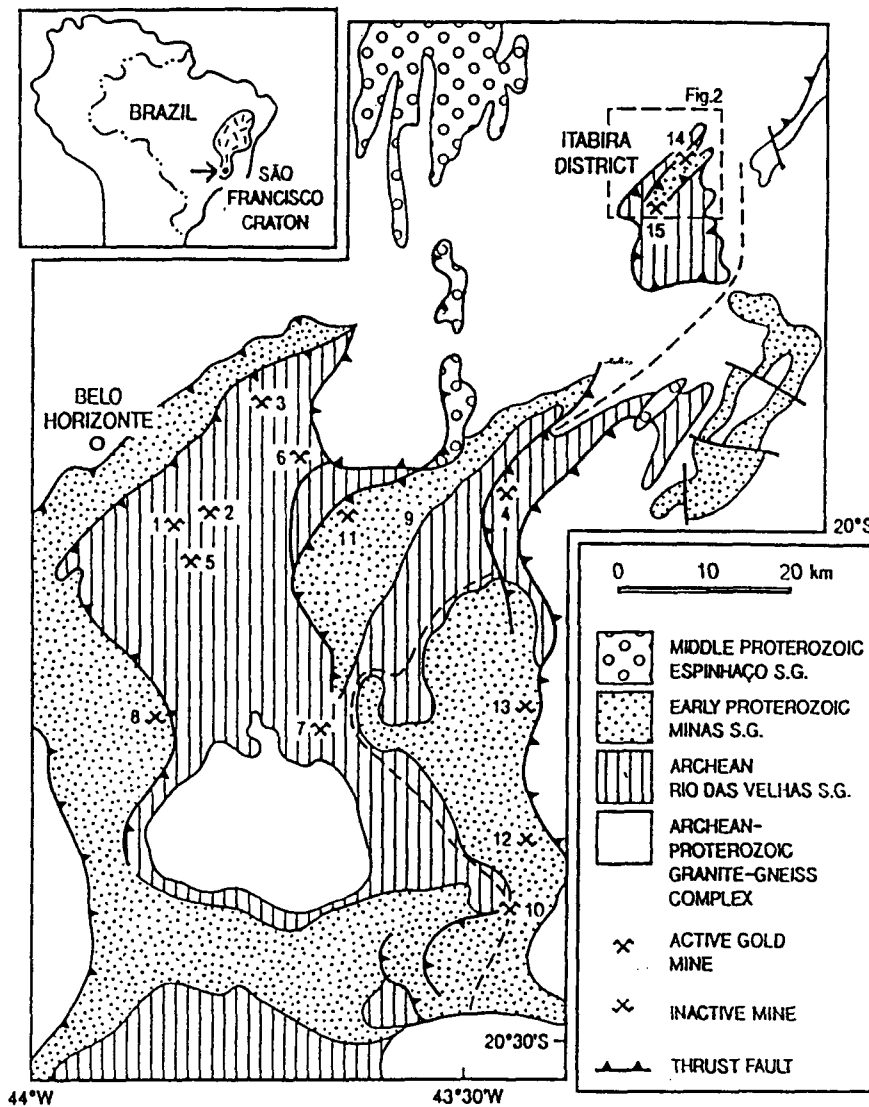


Figure 1.1.. Schematic geologic map of the southern part of the São Francisco Craton (modified after Dorr and Barbosa, 1963; Schorscher et al., 1982; Dorr, 1969; Ladeira, 1991), showing the main gold mines and occurrences hosted by: (a) Archean banded-iron-formation: 1= Morro Velho, 2= Raposos, 3=Cuiabá; (b) mylonitic Archean volcano-sedimentary rocks: 5= Bela Fama, 6= Juca Vieira, 7= Paciência; (c) Early Proterozoic Witwatersrand-type conglomerates: 8= Cata Branca, 9= Serra do Gandarela; (d) Early Proterozoic graphitic phyllite: 10= Passagem de Mariana; and (e) Lake Superior-type iron-formation: 11= Congo Soco, 12= Maquiné, 13= Pitangui, 14= Cauê, 15= Conceição. Dashed line= staurolite in isograd (modified after Hoefs et al., 1982).

The Congo Soco, Maquiné, Pitangui, Cauê, and Conceição deposits appear to be the only deposits in the world in which gold and palladium occur together in a Proterozoic Lake Superior-type oxide-facies iron-formation (Olivo et al., 1993). Congo Soco, Maquiné and Pitangui are inactive gold mines. Bensusan (1929) reported that 12 tons of gold were extracted from 1826 to 1839 from the Congo Soco mine and 5 tons from 1865 to 1896 from the Maquiné mine. In the Cauê (earlier called "Santa Barbara") and Conceição mines, gold ore was mined during the 18<sup>th</sup>-19<sup>th</sup> centuries by Portuguese and English companies (Bensusan, 1929; Dorr and Barbosa, 1963). Mining stopped when the water table level was reached. Since 1986, the Companhia Vale do Rio Doce (CVRD) has selectively extracted palladium-bearing gold ore as a by-product from the Cauê and Conceição iron mines. Gold ore reserves are estimated at 100,000 t grading 30 g/t Au (Leao de Sá and Andrade, 1990), and the annual production is approximately 500 kilograms of palladium-bearing gold bullion ( L.P. Andrade, oral communication, 1993).

Despite the originality of these deposits, little is known about their genesis. Bensusan (1929) reported that the auriferous shoots in the Maquiné mine were structurally controlled ("dipping 18° E"). For the Cauê and Conceição mines, Polônia and Souza (1988) suggested, based on petrographic studies, that gold mineralization was associated with a shear zone. Leao de Sa and Borges (1991) mapped the Corpo Y orebody and showed that zones of the highest grades are aligned parallel to a pervasive stretching lineation trending N80E/22°. Subsequent to the publication of

these papers, four new orebodies have been exposed in the Cauê mine, providing complementary information to further understand the genesis of the Cauê palladium-gold ores.

The purpose of this paper is to present the geological and structural framework of the Cauê mine where palladium-gold ores and their hosting lithologies are best exposed. Macroscopic and microscopic fabrics and hydrothermal alteration affecting the palladium-gold mineralization and ore mineralogy are described in order to propose a genetic model.

## 1.2 REGIONAL GEOLOGIC SETTING

The southern part of the São Francisco Craton comprises four major lithostratigraphic units (Fig. 1.1, Dorr and Barbosa, 1963; Dorr, 1969; Schorscher et al., 1982): (1) the Archean to Proterozoic Granite-Gneiss Complex; (2) the Archean volcano-sedimentary Rio das Velhas Supergroup dated between 2772 to 2776 Ma (Machado et al., 1992); (3) the Early Proterozoic Minas Supergroup, an overlying metasedimentary sequence that hosts the gold deposits discussed in this paper; and (4) the Middle Proterozoic Espinhaço Supergroup, a metasedimentary sequence with minor metavolcanic rocks dated at 1700 Ma (Dossin et al., 1993). All these units are cut by several types and generations of intrusive rocks.

The Minas Supergroup, which host the Cauê deposits, comprises conglomerates, phyllites, Lake Superior-type iron-formations, carbonates, quartzites, and graywackes (Table 1.1, Dorr, 1969; Ladeira, 1991). Pb/Pb isochron ages for carbonates from the Gandarela Formation and the Piracicaba Group (Table 1.1, Babinski et al., 1991) and U/Pb ages (Machado et al., 1992) from the Quadrilátero Ferrífero suggest that deposition of the Minas Supergroup took place between 2.6 and 2.4 Ga (Babinski et al., 1993). The data also suggest that these rocks were metamorphosed at approximately 2.0 Ga (Babinski et al., 1991).

Metamorphic temperatures in the Minas Supergroup in the southern São Francisco Craton increase from west to east from 390° C to 710° C (Schorscher, 1975; Hoefs et al., 1982; Muller et al., 1982). A staurolite in/chloritoid out isograd has been mapped along a NNE-SSW direction in the eastern part of this region (Fig. 1.1, Hoefs et al., 1982). Mineral reactions and oxygen isotope temperatures indicate amphibolite facies (> 600° C) transitional to granulite facies further east of the isograd (Hoefs et al., 1982).

The Transamazonic orogeny (c.a. 2 Ga) produced isoclinal recumbent folds together with thrust faults causing imbrications in the Minas sequence located in the western part of the São Francisco Craton (Fig. 1.1, Rosière, 1981; Hoppe et al., 1987). In the eastern part, parautochthonous and allochthonous nappes, comprising the Itabira District discussed herein, are thrusted westward and northwestward (Hoefs

SUPERGROUP	GROUP	FORMATION	LITHOLOGIES	ENVIRON- MENT	APPARENT THICKNESS (m)	COMMENTS
		SABARA	Chorite schist and phyllite, metatuff, graywacke, tilloid, conglomerate, quartzite, minor iron-formation	Molasse (?)	3,000	detrital zircon U/Pb age 2,125 +/- 4 Ma (Machado et al., 1992)
LOCAL EROSIONAL UNCONFORMITY						
MINAS	PIRACICABA	BARREIRO	Phyllite and graphitic phyllite	Stable shelf	150	Pb/Pb isochron age 2,050 (+/- 230) Ma (Babinski et al., 1991)
		FECHO DO TABOES	Orthoquartzite	Stable shelf	125	
		FUNIL	Quartzose phyllite, dolomitic phyllite, siliceous dolomite	Stable shelf	410	
		CERCADINHO	Quartzite and phyllite, minor conglomerate and dolomite	Stable shelf	600	
LOCAL EROSIONAL UNCONFORMITY						
ITABIRIA	GANDARELA		Dolomite and minor limestone, dolomitic itabirite, itabirite, dolomitic phyllite	Stable shelf	600	Pb/Pb isochron age 2,420 +/- 25 Ma (Babinski et al., 1991)
	CAUÉ		Itabirite (oxide-facies iron-formation), dolomitic itabirite, minor phyllite and dolomite	Stable shelf	350	Host unit of palladium-bearing gold deposits
	BATATAL		Phyllite, slightly graphitic phyllite, minor metachert and iron-formation	Stable shelf	250	Host unit of the Passagem de Mariana Gold Deposit
CARACÁ	MOEDA		Paralic facies: orthoquartzite, conglomerate, phyllite; Blanket facies: sericitic quartzite, quartzose phyllite, quartzite	Stable shelf	1000 150	Witwatersrand-type gold deposits

Table 1.1. The stratigraphic column of the Early Proterozoic Minas Supergroup

et al., 1982; Muller et al., 1982, Schorscher et al., 1982; Belo de Oliveira, 1986; Belo de Oliveira and Teixeira, 1990). Although the relative age of these structures is not yet established, they are considered to be Early Proterozoic by Schorscher et al. (1982) or Late Proterozoic by Belo de Oliveira and Teixeira (1990).

### 1.3 CAUÊ MINE GEOLOGY

#### 1.3.1 Geologic Units

The Cauê mine located in the northeastern part of the Itabira Iron District (Fig. 1.2, Dorr and Barbosa, 1963; Schorscher et al., 1982; Chemale and Quade, 1986) comprises three metamorphosed lithostratigraphic units (Fig. 1.3): (1) a volcano-sedimentary sequence, correlated with the Rio das Velhas Supergroup in the Quadrilátero Ferrífero; (2) an iron-formation unit, referred to as Cauê Formation of the Itabira Group, which is part of the Early Proterozoic Minas Supergroup; and (3) a quartzite unit, correlated with the Piracicaba Group of the Minas Supergroup. Dykes of intrusive rocks occur in the iron-formation and in the quartzite units and slices of amphibolite and talc schist are tectonically imbricated with the iron-formation unit. With the exception of intrusive contacts, all contacts between the various units are structural and interpreted as thrust faults. These contact zones have been highly altered by hydrothermal fluids and weathering characterized by assemblages of kaolinite, limonite and dismembered quartz veins. Locally, these assemblages define

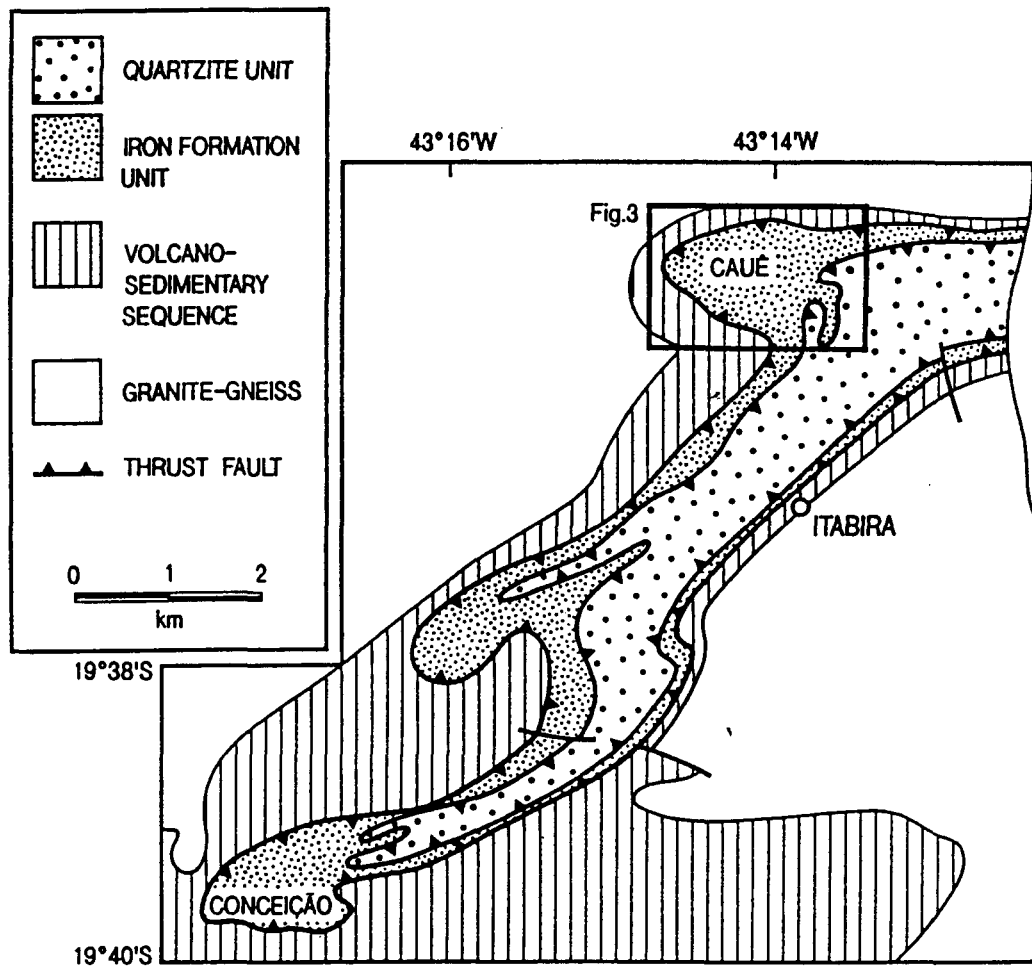
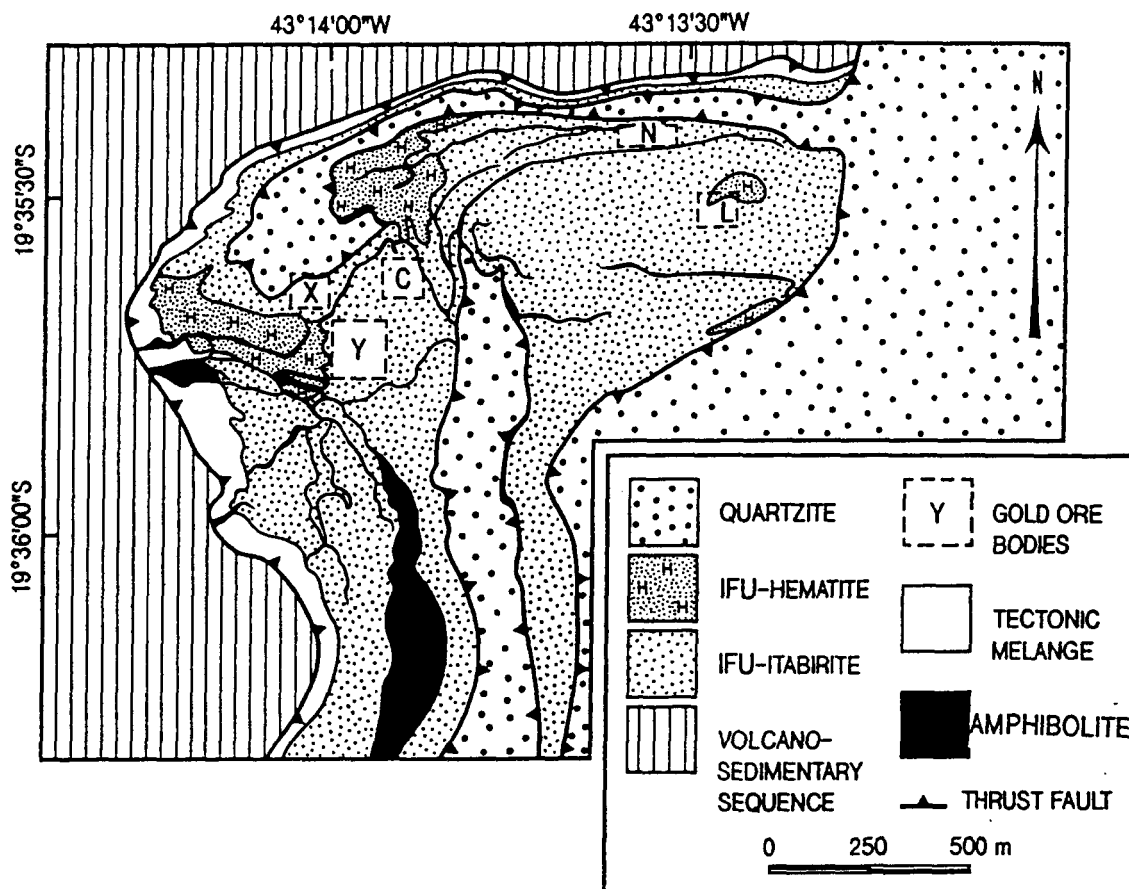


Figure 1.2. Simplified map of the Itabira District Map (modified after Dorr and Barbosa, 1963; Schorscher et al., 1982; Chemale and Quade, 1986). The iron mine open pits correspond to the northern and western sectors of the iron-formation unit which is complete outcrop.



**Figure 1.3.** Simplified geologic map of the Cauê mine (modified after Leao de Sá and Borges, 1991). The open pit of the Cauê iron mine corresponds to itabirite and hematite (iron-formation unit; IFU) outcrop. (N=Aba Norte; L=Aba Leste; C= Central; X=Corpo X; Y=Corpo Y gold orebodies).

thick zones interpreted as tectonic mélange; elsewhere, they define discrete fault planes.

(1) Volcano-Sedimentary Sequence: With an apparent thickness of two hundred meters, this sequence structurally underlies the iron-formation unit. It is composed of talc schist, mica-carbonate schist, and actinolite-biotite-quartz schist with subordinate proportions of quartzite, iron-formation, and amphibolite. Garnet-chlorite schist occurs mainly near the tectonic contacts with the overlying iron-formation unit. Chalcopyrite, pyrite and ilmenite are common accessory minerals in all rock types.

(2) Iron-Formation Unit: With an apparent thickness estimated at 200-250 m, this unit comprises itabirite, several compact hematite bodies, and jacutinga. Itabirite is composed of alternating centimeter- to millimeter-wide bands of hematite +/- magnetite (partly replaced by hematite), and quartz (+/- subordinate feldspar and kaolin). The compact hematite bodies are composed of 95% hematite and contain isolated magnetite porphyroblasts. Jacutinga, which host s the palladium-gold ore is a hydrothermally altered ironstone consisting of interlayered quartz, hematite, magnetite (+/- goethite) and white phyllosilicate (talc, phlogopite and kaolin) bands, with minor amounts of tourmaline, apatite, and monazite. Fe-Mg-Ca carbonate grains are common as inclusions in quartz grains. This unit forms part of a Lake Superior-type iron-formation (Hoppe et al., 1987).

(3) Quartzite Unit: With an apparent thickness estimated at 200 m, this unit consists of white massive quartzite, composed of fine- to medium-grained quartz and variable amounts of muscovite (+/- kyanite) and hematite. Where in contact with the iron-formation unit, the quartzite is more ferruginous.

Intrusive Rocks: Throughout the Cauê mine, intrusive rocks form lenticular bodies that are either concordant or discordant with the iron-formation and the quartzite units and are discontinuous throughout the volcano-sedimentary sequence (Fig. 1.3). The silicates in these intrusive rocks are generally replaced by kaolinite but relict grains of ilmenite intergrown with hematite are observed. The freshest rocks contain hornblende, ilmenite intergrown with hematite, plagioclase, and quartz with secondary biotite, epidote, chlorite and carbonate. Trace amounts of chalcopyrite and pyrrhotite have been observed.

Tectonically imbricated slices of talc schist and amphibolite have been observed locally in the iron-formation unit. The talc schist slices are not more than ten meters wide and occur near the contact between iron-formation and the underlying volcano-sedimentary sequence in the central part of the Cauê mine. They contain trace amounts of hematite. The amphibolite slices may reach 70 meters in thickness and occur in the central-southern sector near the contact with the quartzite unit. Except for the presence of late kinematic muscovite, these slices have modal compositions very similar to those of the intrusive rocks.

### 1.3.2 Structure and Metamorphism

Three episodes of mesoscopic and macroscopic folding are recognized in the five structural domains (central, east, north, south and west; Fig. 1.4) of the Cauê mine. Thrust faults and boudins are observed in association with D1 and D2 folding events.

**D1 folds and fabrics:** D1 folds are tight to isoclinal in the north and west domains and develop progressively into sheath folds in the central and east domains. Where the ENE elongation lineation (Le) and S1 foliation are well developed, there are commonly veins of hematite and quartz.

In the iron-formation unit, compact hematite bodies occur commonly in the cores of the sheath folds at map (Fig. 1.5) and outcrop scales (Fig. 1.6a). Sheath folds fold lithological layering. The long axes of sheath folds range up to 1 meter in length and are parallel to the mineral elongation lineation, Le, and stretched quartz veins (Fig. 1.6b). Cross sections normal to D1 sheath-fold long axes exhibit flattened elliptical to circular shapes with orthogonal dimensions of 3-6 cm and 15-30 cm and shape ratios (B/C) ranging from 4 to 13. The plane of sheath flattening is parallel to S1. Mafic intrusive rocks are locally concordant to, and outline, the sheath folds (Fig. 1.3); however, some are discordant to these structures (Fig. 1.3 and 1.5), suggesting a pre- to syn-D1 emplacement for the intrusive bodies. In the volcano-sedimentary

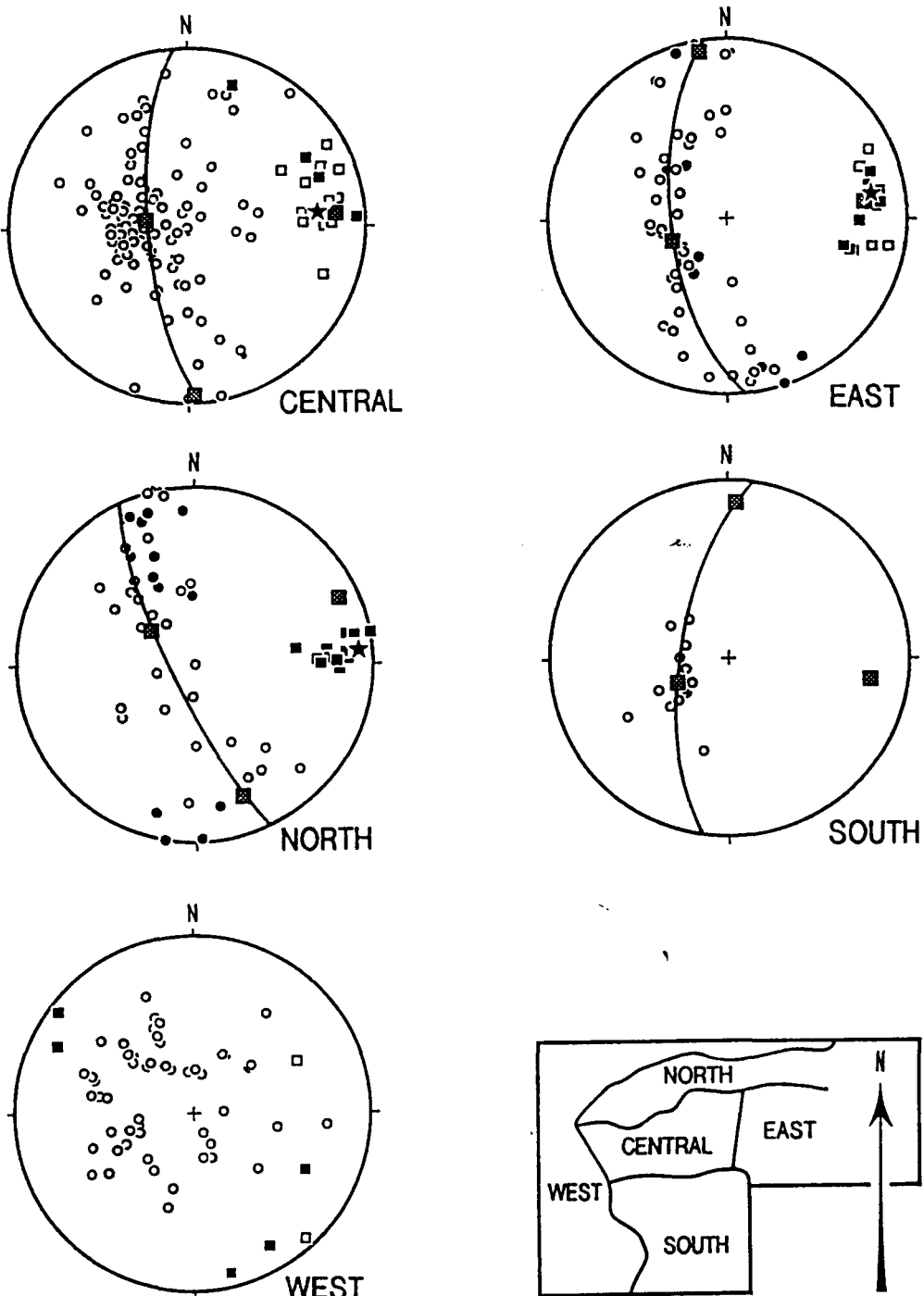


**Figure 1.4.** Lower hemisphere, equal-area, stereographic projections of structural data from the Cauê mine structural domains outlined in the inset. Open circles: poles to the S1 foliation; filled circles: poles to the S2 foliation; open boxes: fold axis of D1-folds; filled boxes: fold axis of D2-folds; great circle girdle: best-fit plane to S1 foliation poles with eigenvectors (stippled box); stars: mean elongation lineation.

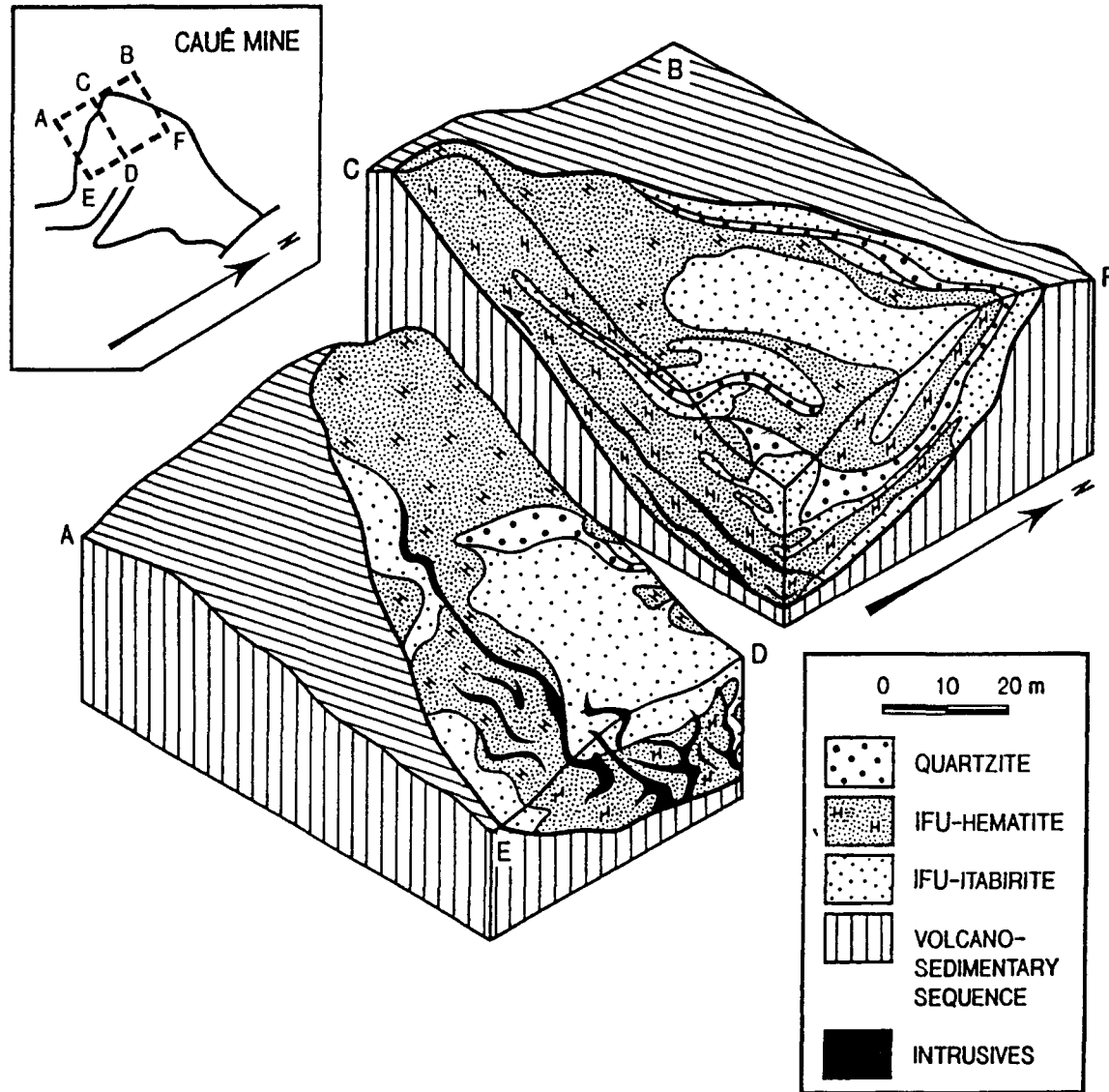
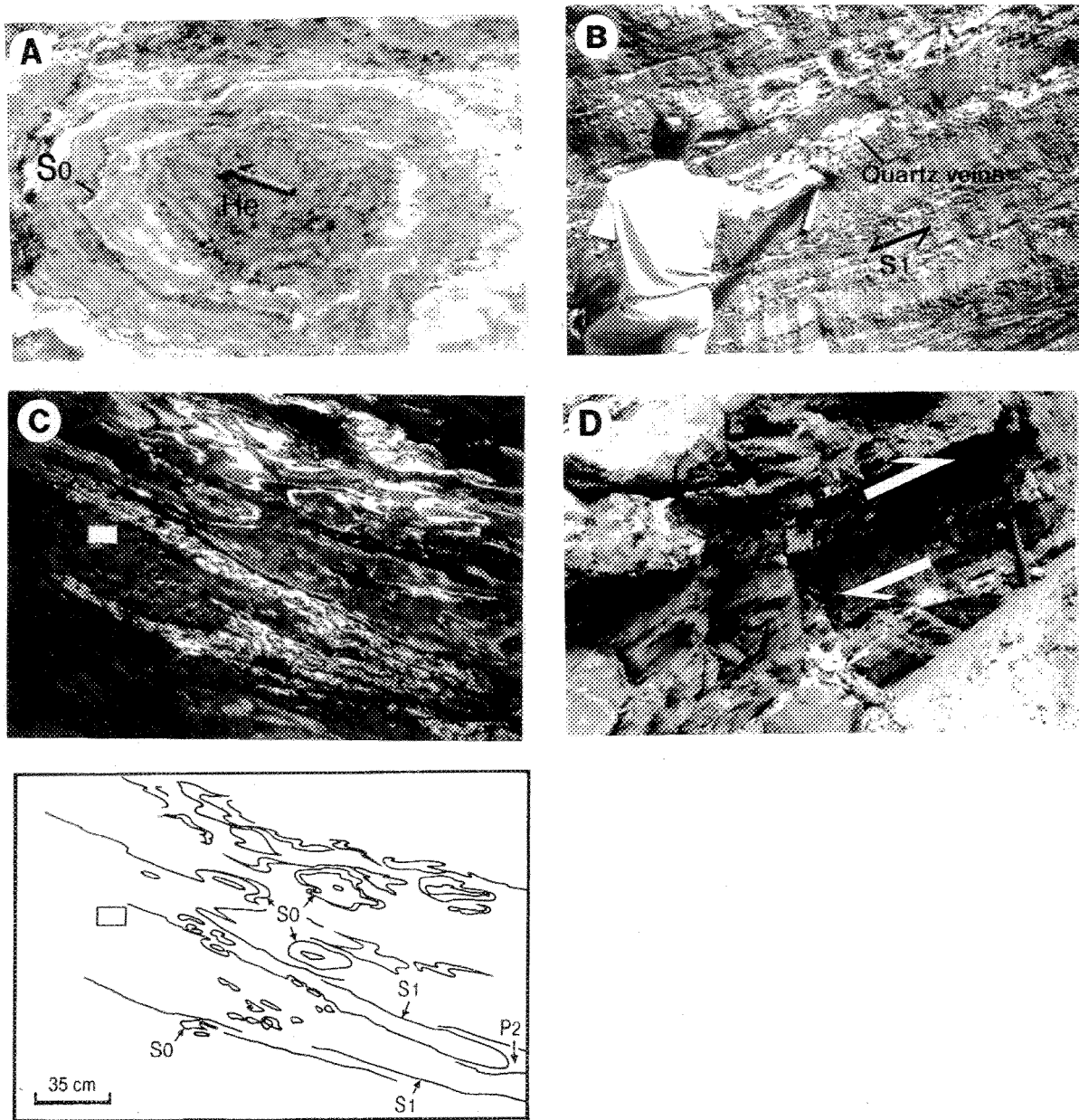


Figure 1.5. Block diagram of the core of the macroscopic sheath fold in the central-west area of the Cauê mine based on open pit mapping and drill log information of CVRD.



**Figure 1.6** A. Sheath fold with a compact hematite core (He); from the east structural domain. B. Stretched quartz bands parallel to the long axes of sheath folds, observed in the XZ plane of a finite strain ellipsoid (from Corpo Y gold orebody, central structural domain). C. A complex F1-F2 fold pattern from Corpo Y gold orebody, central structural domain. D. Mesoscopic duplex structures in the iron-formation unit showing the shear sense (arrows= shear sense).

sequence (west domain), D1 isoclinal folds reach amplitudes of 5 m, but sheath folds are absent.

The S1 foliation is defined by the preferred shape orientation of specular hematite and white phyllosilicate and by planar to lenticular ribbons of fine-grained quartz aggregates. In the south domain, where iron-formation is least deformed, C/S fabrics are preserved and they become coplanar in the central, east, and north domains, where rocks are most strained. In these domains, S1 is parallel to millimeter-to-centimeter-scale compositional layering (Fig. 1.6b).

The Le fabric is most conspicuous in the iron-formation unit. It is defined by elongate hematite grains in the plane of S1-foliation, which is broadly parallel to the D-1 fold axes. In mafic intrusive rocks, the Le is defined by elongate hornblende and ilmenite grains. Despite two subsequent phases of deformation, the Le orientation is nearly constant throughout the iron-formation and plunges 10-25° in a N80-85E direction (Fig. 1.4).

Quartz and hematite veins occur parallel to the S1-foliation. They are mainly recognized in D1 hinge zones where they are discordant to S0. As a result of intense transposition, the veins are parallel to S0 in the flanks of D1-structures. They were folded during D2 deformation.

**D2 Folds and fabrics:** D2 folds are asymmetrical tight folds. In this folding phase developed: (1) the L2 lineation, characterized by millimeter-scale parasitic ENE fold axes (FA2); and (2) the S2 foliation, which transposed S1 foliation and developed essentially in the north domain. S2 also overprints S1 in D2 fold hinges.

In the eastern and central sectors of the Cauê mine, D1-sheath folds and the S1-foliation are highly contorted and disrupted due to progressive deformation. Some D1-structures were refolded through greater than 180° and have formed "rolling" structures and isolated ball-shaped structures during progressive D1-D2 deformation (Fig. 1.6c).

**D3 folds and fabrics:** D3 structures are open folds (F3) with an associated N-S cleavage crenulation (S3), commonly spaced 2-5 millimeters. The L3 crenulation lineation formed during this fold phase and trends broadly N-S with a moderate to horizontal dip. Meter- to centimeter-scale talc-hematite-quartz veins were also generated during D3 folding and are commonly parallel to S3.

**Boudinage:** Boudins occur at all scales (millimeters to tens of meters). They occur within either (1): S1 planes parallel to the Le, indicating that Le is the axis of maximum elongation or (2) in the S2 foliation planes (e.g. hematite-rich boudins of the Aba Norte gold orebody).

**Thrust Faults:** These faults repeat and truncate geologic units forming several imbricated sheets (Fig. 1.3). Duplex structures formed by imbricated thrust faults are observed mesoscopically (Fig. 1.6d). Because these faults are parallel to C-S planes (Leao de Sá and Borges, 1991) and are reactivated and folded by D2 event, they are interpreted as syn-D1 features. These structures were also reactivated during D3 as indicated by late N-S lineations on fault surfaces.

**Interference Patterns:** Refolding of macroscopic D1 folds by D2 folds generated complex fold interference patterns (Figs. 1.3 and 1.6c) analogous to a dome and basin pattern that has been flattened in the S1 plane and stretched parallel to Le so that all limbs and hinges of D1 and D2 structures are broadly parallel. This pattern cannot be generated by refolding any number of coaxial fold generations and are not similar to the classical interference patterns described by Ramsay (1967) and Thiessen (1986). Instead, the D1-D2 interference patterns are more analogous to those observed in ductile shear zones that have undergone progressive non-coaxial shear (Berthé and Brun, 1980; Cobbold and Quinquis, 1980; Goscombe, 1991).

**Metamorphism:** Oxygen isotope data on quartz and hematite parallel to S1 foliation from itabirite in the Cauê mine indicate an average metamorphic temperature of 610° C (Hoefs et al., 1982 and Muller et al, 1982). This temperature is consistent with data obtained from similar rocks of the Conceição and the Dois Córregos mines and with the metamorphic assemblage described from the country rocks (Hoefs et al.,

1982 and Muller et al., 1982). The metamorphic assemblages in mafic intrusive rocks and in rocks of the volcano-sedimentary sequence described in this paper indicate retrograde metamorphism from amphibolite to greenschist facies.

## 1.4 NATURE OF D1-D2 DEFORMATION IN THE CAUÊ MINE

### 1.4.1 Progressive Simple Shear Regime:

The D1 and D2 structures in the Cauê mine are interpreted to have been generated in a progressive simple shear regime. This interpretation is supported by several field observations. First, C/S fabrics are preserved in the least deformed domains and are indicative of non-coaxial shear (Berthé et al., 1979). Secondly, the symmetrical scatter of both D1 and D2 fold axes around the ENE directions in S1/S2 planes is consistent with extreme rotation of fold axes towards the transport directions with progressive non-coaxial shear (Fig. 1.4, Bell, 1978; Berthé and Brun 1980; Cobbold and Quinquis, 1980, Skjernaa, 1980, Goscombe, 1991). Finally, some D1 features were refolded through greater than 180° and have formed "rolling" structures and isolated ball-shaped structures during the progressive D1-D2 deformation (Fig. 1. 6c). In addition, sheath folds occur at various scales, and are commonly described in shear zones that have experienced non-coaxial shear (Quinquis et al, 1978; Minnigh, 1979; Berthé and Brun, 1980; Cobbold and Quinquis, 1980; Lacassin and Mattauer, 1985; Skjernaa, 1989; Goscombe, 1991). The simplest kind of progressive

deformation that is both continuously non-coaxial and rotational is a progressive simple shear (Quinquis et al., 1978).

#### **1.4.2 Shear Sense**

Shear sense during the development of S1-Le fabrics has been determined in the field from mesoscopic-scale duplex structures (Fig. 1.6d), asymmetrical folds, and C/S fabrics by using a method discussed in Boyer and Elliott (1982), Bell and Hammond (1984), McClay and Insley (1986), and Hanmer and Passchier (1991). The sense of progressive shear is consistently east-over-west throughout the iron-formation unit in the Cauê mine. It is concordant with the sense of shear determined in the iron-formation unit in other sectors of the Itabira District (Souza Filho et al, 1989).

#### **1.4.3 Bulk Shear Strain**

In the iron-formation unit at the Cauê mine, high bulk shear strains during D1 are supported by: (1) the very elongate nature and flattened ellipsoidal cross section (high B/C ratios) of D1 sheath folds (Lacassin and Mattauer, 1985; Skjernaa, 1989); (2) the co-planar C/S foliation (S1 mylonitic foliation); and (3) the tightly constrained distribution of D1 fold axes around the ENE direction (Fig. 1.4; Skjernaa, 1980). In addition, macroscopic- or mesoscopic-scale sheath folds are associated with bulk

strains greater than 10 (Bell, 1978; Lister and Price, 1978; Cobbold and Quinquis, 1980; Skjernaa, 1989). Bulk shear strain during D2 in the central, north, and east structural domains is interpreted to be moderate to high ( $\sigma > 4$ - higher in the north domain), based on the tightly constrained distribution of D2 fold axes around the L<sub>e</sub> orientation (Fig. 1.4, Skjernaa, 1980).

In the volcano-sedimentary sequence (west structural domain), the absence of sheath folds and the weak rotation of D1 and D2 structural elements (Fig. 1.4) suggest a weaker shear strain during D1 and D2.

#### 1.4.4 Décollement Surfaces

Four observations suggest that the iron-formation unit was detached from the underlying sequence along décollement surfaces during D1 and probably D2 events (Fig. 1.3): (1) the laterally extensive nature of the iron-formation unit; (2) the higher bulk shear strain relative to the surrounding units; (3) the consistent east-over-west sense of shear throughout the iron-formation unit; and (4) the thrust-faulted contacts with the adjacent volcano-sedimentary sequence. The fundamental evidence for a major décollement is based on the truncation of mafic intrusive bodies by the contact of the iron-formation unit and the volcano-sedimentary sequence (Figs. 1.3 and 1.5).

## 1.5 PALLADIUM-BEARING GOLD OREBODIES OF THE CAUÊ MINE

Five gold orebodies have been mined at the Cauê mine. They are referred to as: Corpo Y, Corpo X, Central, Aba Leste and Aba Norte (Fig. 1.3). The Corpo Y, Corpo X, and Central have been intermittently mined respectively since 1986, 1991, 1993, and Aba Leste and Aba Norte were mined in 1991 and are now inactive. These orebodies are hosted by jacutinga in the iron-formation unit. Because the compositional bands in jacutinga may range from several millimeters to tens centimeters in thickness, the mineral abundances vary from one sample to another, as shown in Table 1.2. This rock represents possibly an altered carbonate-bearing oxide-facies iron-formation (referred to as dolomitic itabirite) as proposed by Dorr and Barbosa (1963) and Olivo et al., (1994).

### 1.5.1 Structural Controls and Geometry

The Corpo Y, Corpo X, Central and Aba Leste orebodies are stratabound and are encountered in the domains of high bulk shear strain (Central, East and North, Figs. 1.3 and 1.4). They are parallel to the S1-mylonitic foliation which is commonly parallel to the composition layering (S0) in the limbs of D1-D2 structures.

Although gold grains from Corpo Y occur in hematite as well as white phyllosilicate bands of jacutinga parallel to the S1-mylonitic foliation, the highest gold

	JACUTINGA					ITABIRITE	COMPACT HEMATITE
	CORPO Y	CORPO X	CENTRAL	ABA LESTE	ABA NORTE		
Hematite	35-65%	50-90%	55-90%	55-80%	54-50%	55-70%	99-100%
Quartz	5-15%	10-35%	5-30%	0-5%	40-45%	30-45%	
Magnetite	tr.	tr.		tr.		tr.	tr.
Kaolin	5-30%	0-5%	0-10%	10-30%	0-5%	tr.	
Goethite	15-30%	0-5%	0-5%	10-30%	0-5%	tr.	tr.
Talc	tr.	tr.	5-20%	tr.	tr.		
Phlogopite	tr.	tr.		tr.	0-5%		
Feldspar	tr.	tr.		tr.	tr.	tr.	
Tourmaline	tr.	tr.	tr.	tr.	tr.		
Carbonate	tr.	tr.	tr.		tr.		
Monazite	tr.						
Apatite	tr.						

Table 1.2. Mineral abundances of jacutinga, itabirite and compact hematite body.

concentrations occur in quartz veins (Leao de Sá and Borges, 1991) stretched parallel to the elongation lineation in the plane of S1 mylonitic foliation (Fig. 1.7). The Le in this domain plunges 22° at N82E. These gold rich bands and veins were dismembered by the progressive high bulk shear deformation and repeated by tight folds generated during the D2 progressive deformation, exhibiting a repeated and segmented pipe-like geometry. The main ore shoot is on average 0.2 meters thick and 70 meters long and extends for at least 250 meters down dip in the direction of Le ( Fig. 1.7b, Leao de Sá and Borges, 1991).

The geometry of the other orebodies in three dimensions is poorly understood because the open-pit extraction of palladium-gold ore is intermittent, as a result of iron mining operations. Also, drill cores, galleries and shafts are not available in these palladium-gold ore sites. In the Corpo X and Central orebodies, the highest palladium-gold concentrations occur in hematite-rich veins parallel to S1-mylonitic foliation, containing local centimeter-size quartz-talc concentrations outlined by goethite. In the Corpo X orebody (Fig. 1.8), the mineralized hematite extend for 28 meters, varying from 1 to 5 meters in thickness. In the Central orebody (Fig. 1.9), there are two rich hematite veins with local coarse quartz-talc concentrations, extending up to 20 m in length and varying from 20 cm to 7 m in thickness. Having a ribbon-like geometry concordant to S1-planes, these hematite veins were segmented

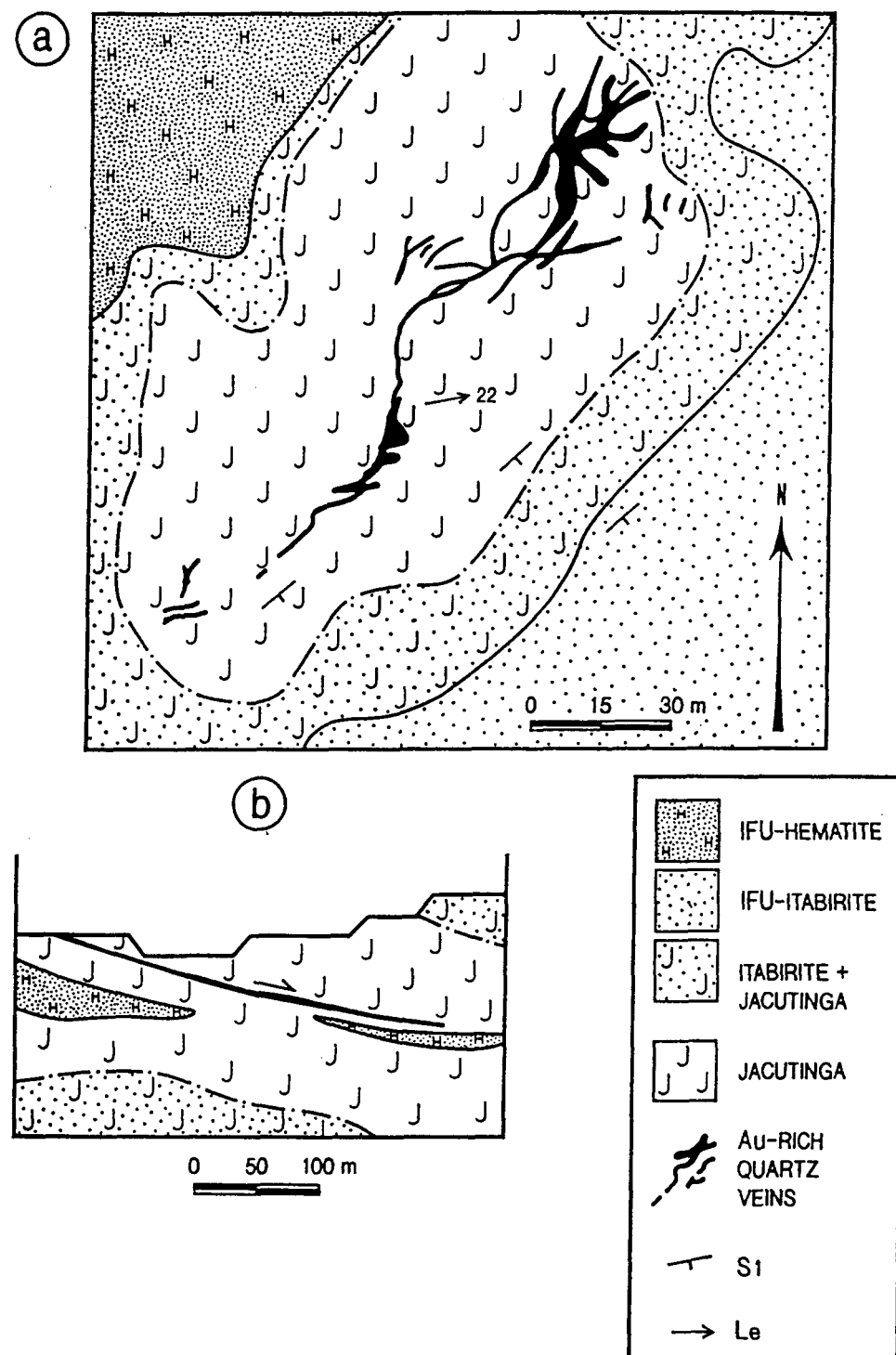


Figure 1.7. A. Map of level 868 of the Corpo Y gold orebody (modified after Leao de Sá and Borges, 1991). B. Schematic geological section of the Corpo Y gold orebody based on drill core data (modified after Leao de Sá and Borges, 1991).

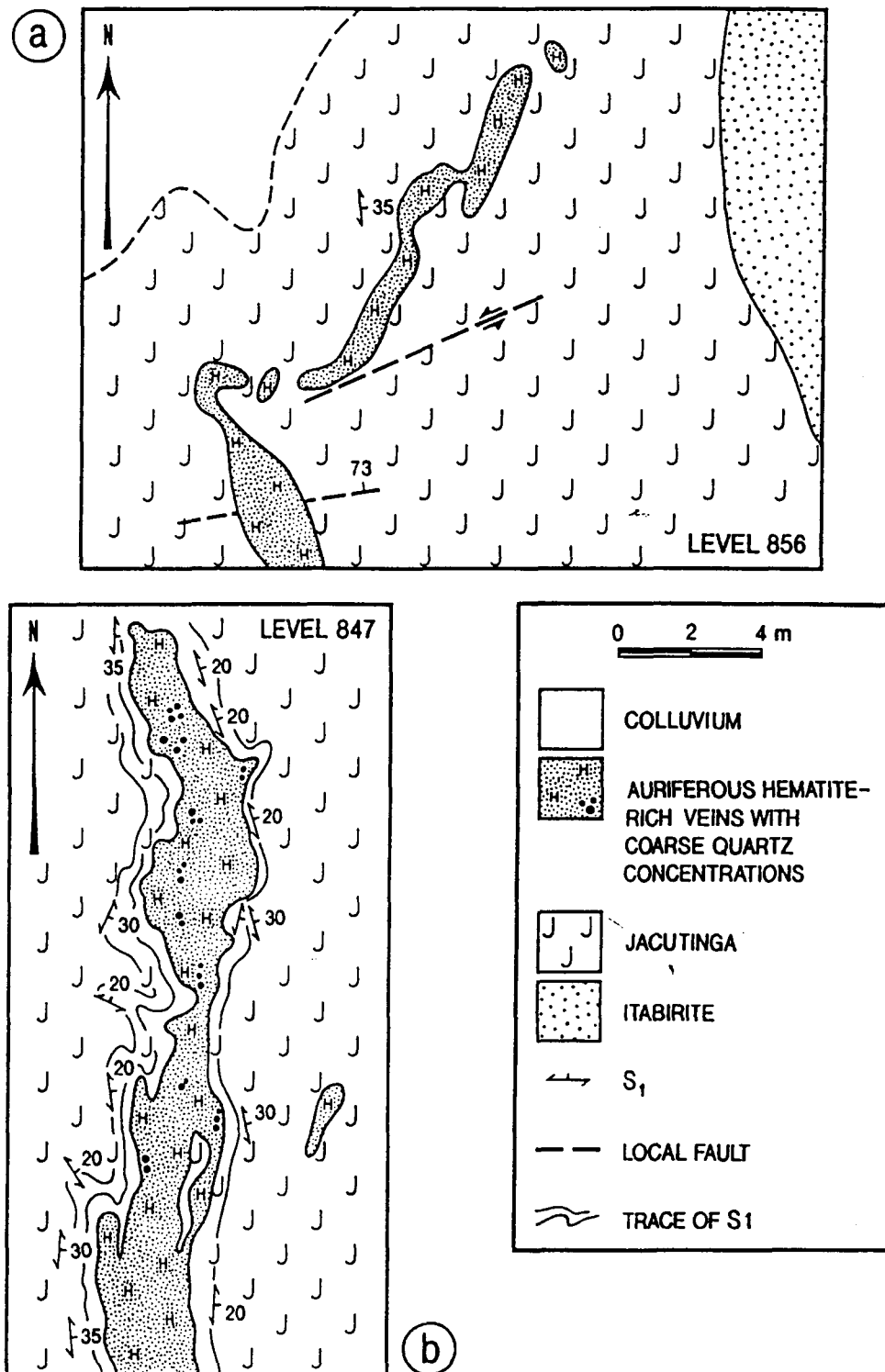


Figure 1.8. A. Map of level 856 of the Corpo X palladium-bearing gold orebody located in Figure 1.3. B. Map of level 847 of the Corpo X palladium-bearing gold orebody located in Figure 1.3.

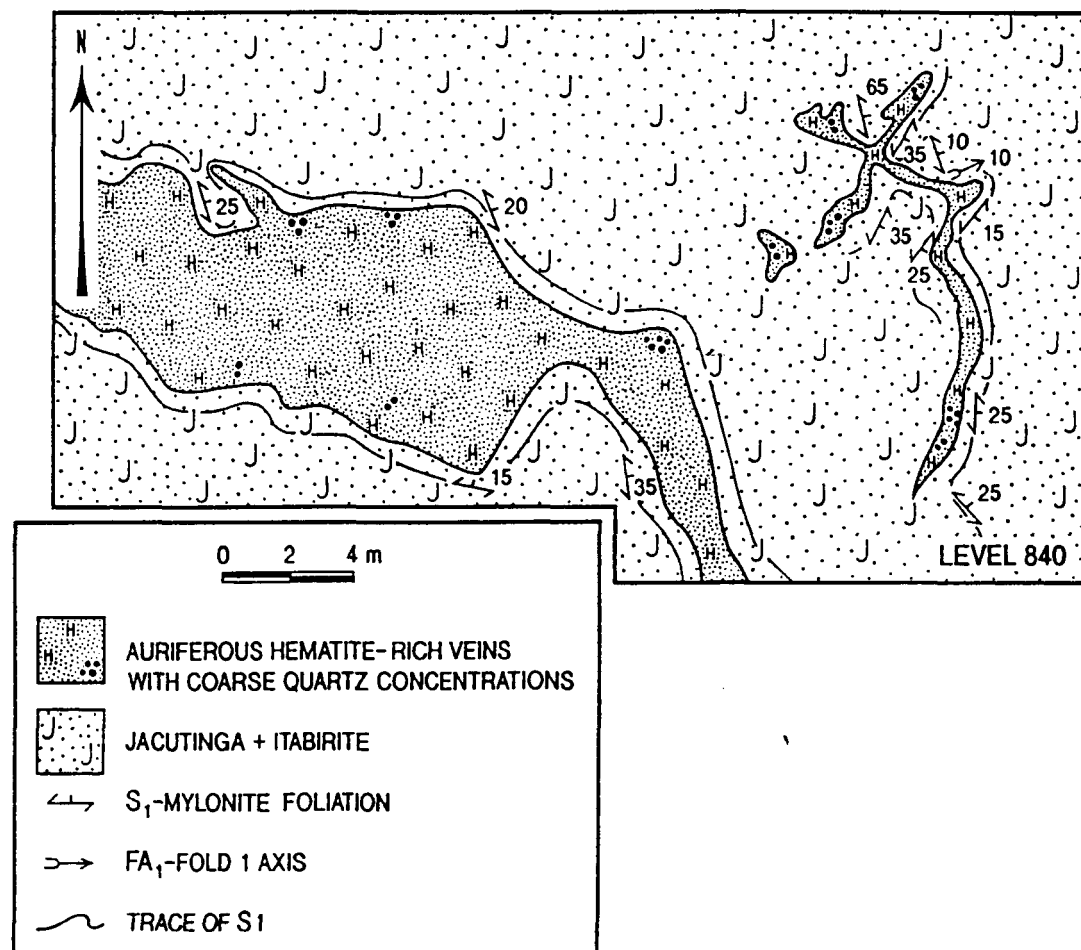


Figure 1.9. Map of level 840 of the Central palladium-bearing gold orebody located in Figure 1.3.

and folded by progressive deformation. Remobilization of hematite occurred in the hinges of D2-folds (Fig. 1.9). In the Aba Leste orebody, gold-palladium ore is disseminated in the jacutinga layer and in dismembered hematite-rich veins occurring in this layer. Both the jacutinga layer and hematite-rich veins are parallel to S1 foliation (Fig. 1.10).

In contrast to the other orebodies, the Aba Norte orebody is not parallel to the S1 mylonitic foliation; instead, it cuts S1 and S0, and is parallel to S2 foliation (Fig. 1.11). This orebody consists of a boudinaged hematite-rich vein with local concentrations of quartz-kaolin outlined by goethite. The hematite vein is 140 meters long and varies from a few centimeters to five meters in thickness.

### **1.5.2 Hydrothermal Alteration and Effects of Weathering in Jacutinga**

The main hydrothermal-metamorphic minerals, i.e. talc, phlogopite, quartz, hematite, and tourmaline, are all aligned parallel to the S1 foliation, as observed in some relatively unweathered samples of jacutinga. Although the formation of talc and phlogopite indicate pervasive alteration in ore-bearing layers, these minerals are restricted to the jacutinga layers. These minerals were also described in other gold deposits hosted by jacutinga in the Quadrilátero Ferrífero (Bensusan, 1929; Dorr and Barbosa, 1963).

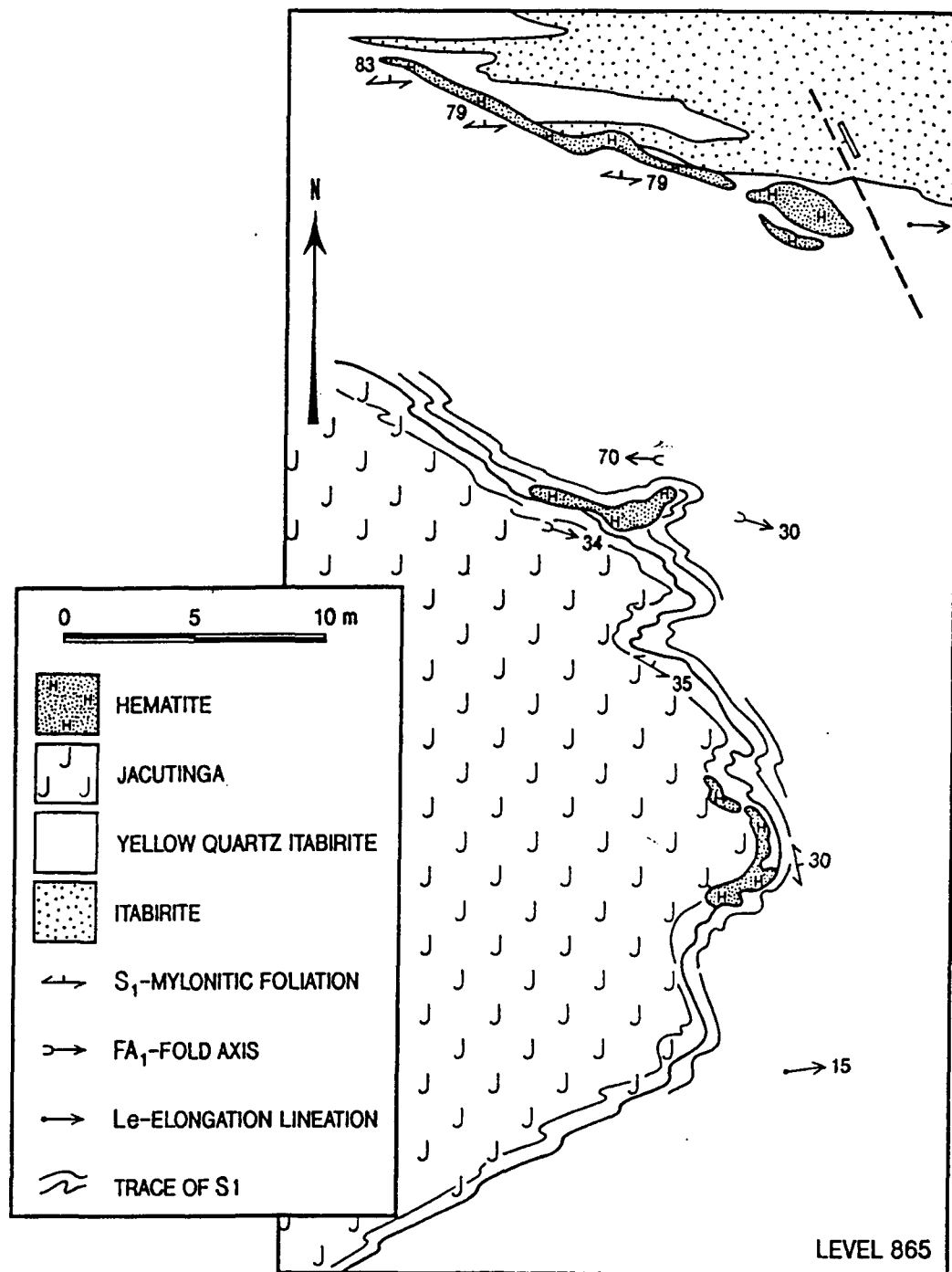


Figure 1.10. Map of level 865 of the Aba Leste palladium-bearing gold orebody located in Figure 1.3.

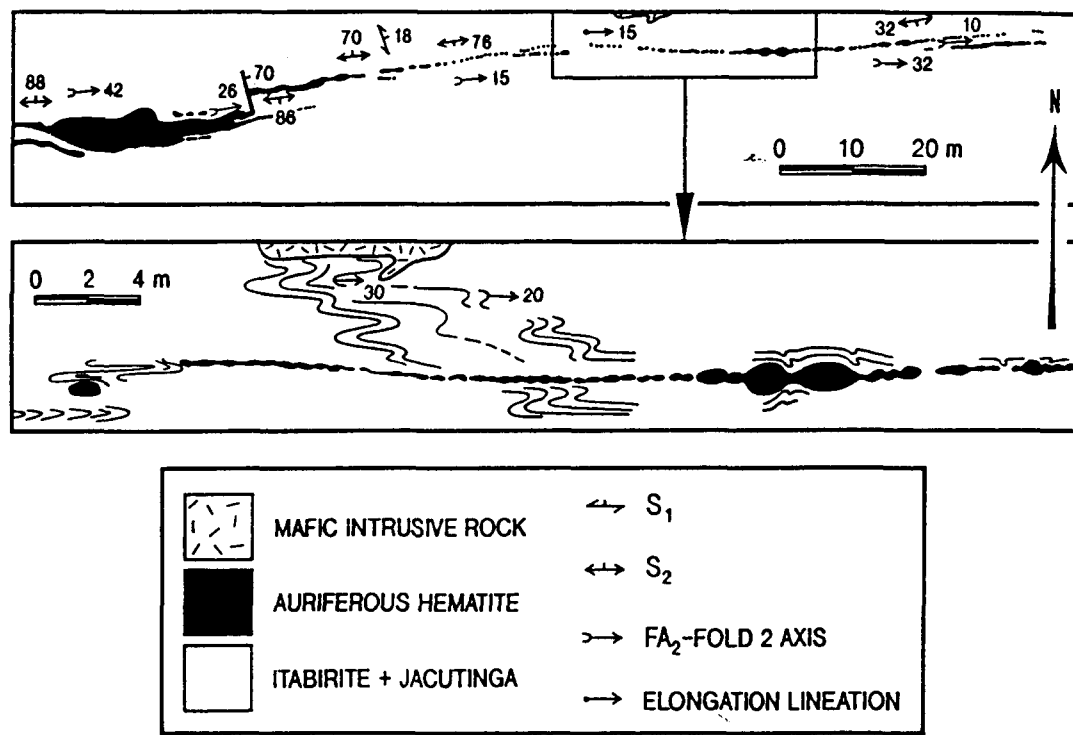
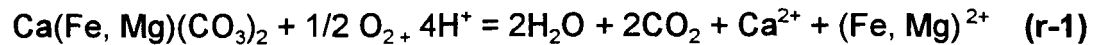
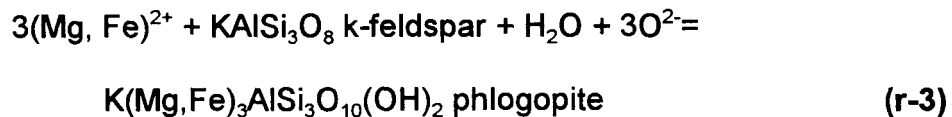
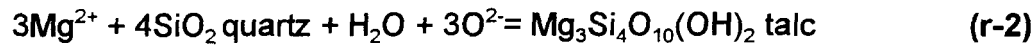


Figure 1.11. Map of level 880 of the Aba Norte gold orebody located in Figure 1.3.

The hydrothermal fluids may have reacted with the dolomitic itabirite causing the dissolution of Fe-bearing dolomite according to following reaction:



The products of carbonate dissociation may have reacted with quartz and k-feldspar to form talc and phlogopite, according to the following reactions:



In the Corpo X, Central, and Aba Leste orebodies, hematite-rich veins parallel to S1 are evidence of enrichment in hematite during D1-deformation. Hematite may have formed by reaction of Fe-calcite in dolomitic itabirite with oxygen derived from the hydrothermal fluids (r-4).



Emplacement of quartz veins is more conspicuous in the Corpo Y orebody, where high gold grades are hosted by quartz veins. In the other orebodies quartz

occurs as local concentrations (1-3 cm) in the hematite veins. Tourmalinization is not widespread, rather it is restricted to palladium-gold rich ore. Tourmaline grains occur in white phyllosilicate and hematite bands parallel to S1 foliation. Whereas some tourmaline grains contain gold inclusions, other tourmaline grains occur as inclusions in gold grains, suggesting synchronous gold and tourmaline deposition or recrystallization during metamorphism. Monazite was also observed in one sample of jacutinga from the Corpo Y orebody and apatite occurs as micrometric grains commonly associated with the goethitic-kaolinitic matrix of the jacutinga.

Weathering alteration in the Cauê mine extends to a depth of more than 200 meters. Weathering is strongest in the jacutinga due to the compositional heterogeneity of the host rock, in comparison with the non-auriferous iron-formation (itabirite and hematite bodies, Table 1.2). The main weathering minerals are kaolinite and goethite. The kaolinite is pseudomorphous after talc and phlogopite. Kaolinite also replaced k-feldspar grains which occur in boudins or in quartz bands. Some quartz grains are dissolved along their contact boundaries and the open spaces are filled with kaolinite. Hematite rims are altered to goethite.

The most weathered samples show a texture resembling the plumage colors of *Pipile jacutinga*, a Brazilian bird, which is black with white spots. This characteristic texture of weathered jacutinga has been used as a guide for gold prospecting in this region since the 18<sup>th</sup> century.

### 1.5.3 Ore Mineralogy

In the Corpo Y, Corpo X, Central and Aba Leste orebodies, gold grains are palladium-bearing. In Corpo Y gold occurs as: (1) free grains and inclusions in rotated tourmaline hosted by hematite bands located in the core of dismembered sheath folds (Fig. 1.12a); (2) elongated grains parallel to S1-mylonitic foliation planes of hematite bands (Fig. 1.12b); (3) free grains or inclusions in boudinaged quartz bands or veins (Fig. 1.12c); and (4) free grains parallel to the S2 foliation planes (Fig. 1.12d). Electron-microprobe (EMP) analyses of gold grains from polished sections of jacutinga reveal that palladium contents in these grains range from 1 to 5 percent and that the highest Pd concentrations are associated with small (commonly smaller than 10 microns) inclusions of Pd-Cu oxides, showing island-mainland and replacement (relict) textures (Olivo et al., 1994). Some disaggregated, elongated, flattened and bent grains were analyzed using SEM and EMP energy-dispersive spectrometry (EDS) revealing palladium contents of up to 20 percent (Table 1.3). Although copper is predominantly concentrated in palladium inclusions, it also occurs directly in gold and may reach total contents of 8 percent (Olivo et al., 1994). Gold grains also contain trace amounts of Ag (commonly less than 1%, Table 1.3 - and Olivo et al., 1994). From Corpo X, gold-bearing polished sections were not available for textural studies. Some gold grains, obtained by gravimetric concentration of disaggregated jacutinga, are flattened or bent and also contain Pd-Cu-oxide inclusions (Olivo et al.,

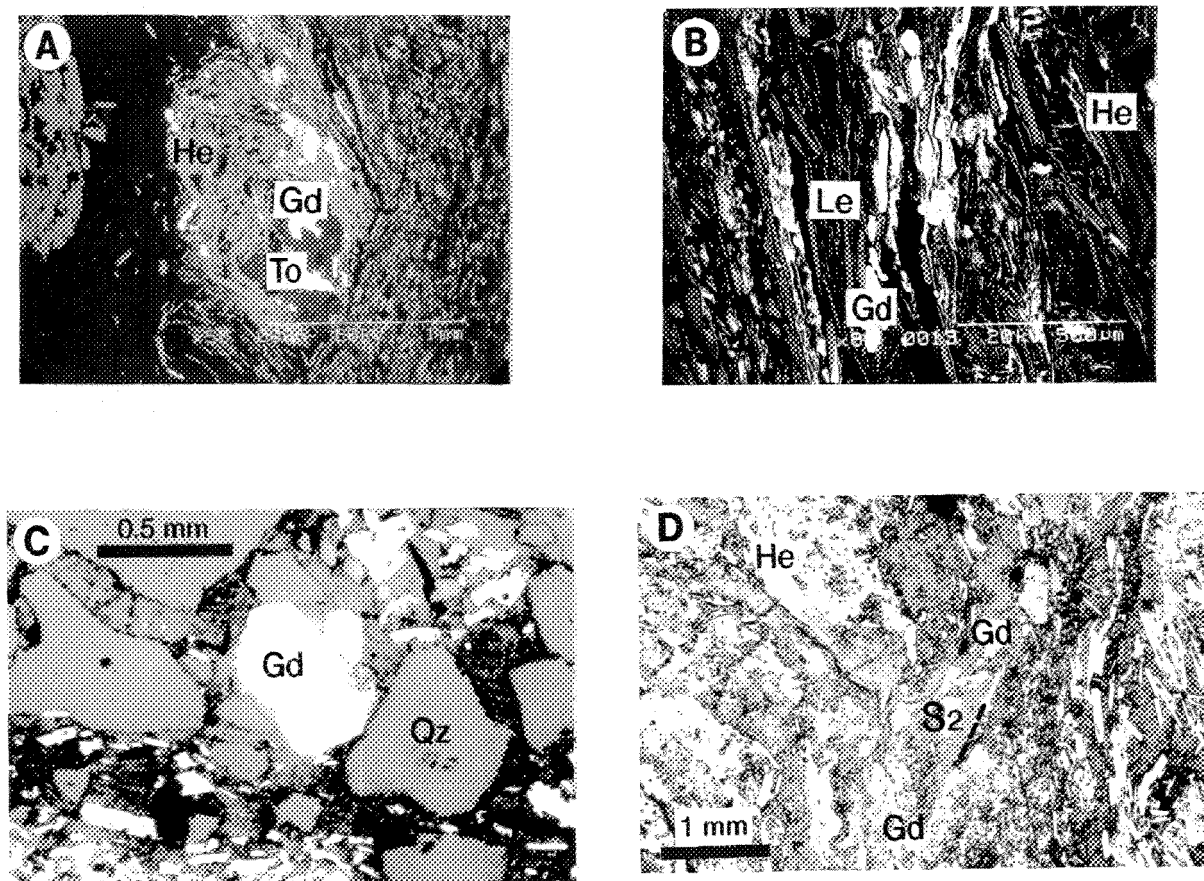


Figure 1.12 A. Back-scattered electron image showing gold (Gd) as free grains or as inclusions in tourmaline (To) in the core of a dismembered D1-sheath fold of the Corpo Y orebody. He=hematite. B. Back-scattered electron image showing stretched gold grains (Gd) parallel to the elongation lineation (Le) in the Corpo Y orebody. He=hematite. C. Photomicrograph of gold (Gd) grain in boudinaged quartz (Qz) veins parallel to S1 in the Corpo Y orebody. He=hematite. D. Photomicrograph of gold (Gd) grains in the S2 transposition foliation plane from the Corpo Y orebody. He=hematite.

	Au (%)	Pd (%)	Rh (%)	Cu (%)	Ag (%)	Fe (%)	Zn (%)	Te (%)
<b>Corpo Y</b>								
Y1a	90.70	7.57	n.d.	1.27	n.d.	0.49	n.d.	n.d.
Y1b	88.37	8.05	n.d.	1.73	n.d.	1.50	0.36	n.d.
Y1c	90.50	8.09	n.d.	1.13	n.d.	0.19	n.d.	n.d.
Y2a	87.76	10.40	n.d.	1.36	n.d.	0.48	n.d.	n.d.
Y2b	88.96	8.20	n.d.	1.48	n.d.	0.58	n.d.	n.d.
Y2c	89.78	8.65	n.d.	1.04	n.d.	n.d.	n.d.	n.d.
Y3	88.11	8.72	n.d.	1.92	n.d.	0.32	0.88	n.d.
Y4a	91.44	7.91	n.d.	0.64	n.d.	n.d.	n.d.	n.d.
Y3b	90.53	8.01	n.d.	0.96	n.d.	n.d.	n.d.	n.d.
Y4c	94.83	4.10	n.d.	n.d.	n.d.	n.d.	n.d.	n.d.
Y4d	95.09	3.80	n.d.	n.d.	n.d.	n.d.	n.d.	n.d.
Y5a	80.81	19.19	n.d.	n.d.	n.d.	n.d.	n.d.	n.d.
Y5b	78.47	19.22	n.d.	n.d.	n.d.	n.d.	n.d.	n.d.
Y6a	97.17	2.82	n.d.	n.d.	n.d.	n.d.	n.d.	n.d.
Y6b	99.07	0.93	n.d.	n.d.	n.d.	n.d.	n.d.	n.d.
Y7a	98.09	1.91	n.d.	n.d.	n.d.	n.d.	n.d.	n.d.
Y7b	98.20	1.80	n.d.	n.d.	n.d.	n.d.	n.d.	n.d.
Y8a	98.63	1.37	n.d.	n.d.	n.d.	n.d.	n.d.	n.d.
Y8b	98.25	1.75	n.d.	n.d.	n.d.	n.d.	n.d.	n.d.
<b>Corpo X</b>								
X1a	81.44	10.14	n.d.	3.51	0.59	3.23	1.09	n.d.
X1b	90.30	1.17	n.d.	4.62	n.d.	0.85	3.06	n.d.
X1c*	95.03	2.24	n.d.	n.d.	n.d.	2.73	n.d.	n.d.
X1d*	95.92	2.25	n.d.	n.d.	n.d.	1.84	n.d.	n.d.
X2a	97.60	1.52	n.d.	0.59	n.d.	0.28	n.d.	n.d.
X2b*	95.67	3.94	n.d.	n.d.	n.d.	0.39	n.d.	n.d.
X2c*	94.67	2.18	n.d.	n.d.	n.d.	3.15	n.d.	n.d.
X2d*	97.51	1.06	n.d.	0.71	n.d.	0.73	n.d.	n.d.
<b>Aba Leste</b>								
AL1a	93.70	6.30	n.d.	n.d.	n.d.	n.d.	n.d.	n.d.
AL1b	91.62	7.84	n.d.	0.29	n.d.	n.d.	n.d.	n.d.
AL2a	99.34	n.d.	n.d.	0.17	n.d.	0.11	n.d.	0.38
AL2b	98.09	n.d.	n.d.	1.91	n.d.	n.d.	n.d.	n.d.
AL3a	98.63	n.d.	n.d.	0.41	n.d.	0.50	n.d.	0.46
AL3b	100.00	n.d.						
AL3c	97.67	n.d.	n.d.	2.17	n.d.	0.15	n.d.	n.d.
AL4	98.26	0.97	n.d.	0.77	n.d.	n.d.	n.d.	n.d.
<b>Aba Norte</b>								
AN1a	97.52	n.d.	1.09	n.d.	1.39	n.d.	n.d.	n.d.
AN1b	97.29	n.d.	1.08	0.24	1.39	n.d.	n.d.	n.d.
AN1c	100.00	n.d.						
AN1d	96.95	n.d.	1.50	0.75	0.79	n.d.	n.d.	n.d.
AN2a	96.01	n.d.	n.d.	0.66	n.d.	1.74	n.d.	1.58
AN2b	98.46	n.d.	n.d.	0.66	n.d.	0.88	n.d.	n.d.
AN2c	99.86	n.d.	n.d.	n.d.	n.d.	0.14	n.d.	n.d.
AN3a	96.71	n.d.	0.54	0.68	0.96	0.32	n.d.	0.80
AN3b	96.81	n.d.	0.76	0.79	0.38	1.27	n.d.	n.d.

Table 1.3. Electron microprobe and scanning electronic microscopic (\*) energy dispersive system analyses of gold grains of the Cauê orebodies. AN1 is an octahedral crystal; the other gold grains are stretched or bent. (Values in wt %).

1994). EDS analyses of these gold grains gave Pd contents of up to 10 percent (Table 1.3).

In the Aba Leste, palladian gold grains occur as inclusions in S1-parallel hematite and as free grains on S1 surfaces (Olivo et al., 1994). The quality of polishing of the sections was inadequate for quantitative analysis of these grains. Palladian gold grains, obtained by gravimetric concentration of disaggregated rich primary ore, are flat and contain up to 7 percent Pd (Table 1.3). Palladium in these grains is not related to local concentrations of small inclusions; rather, it is homogeneously distributed throughout the gold grains (Olivo et al., 1994).

In the Aba Norte orebody, gold-bearing polished sections were not available for textural studies. Some gold grains, recovered from jacutinga and hematite veins, are either well-formed octahedral crystals or bent grains. In contrast with gold from other orebodies, these gold grains are not palladium-bearing; rather, they have rhodium contents of up to 1.5 percent estimated by EMP-EDS analyses (Table 1.3).

Although palladium occurs commonly associated with gold grains, some free palladium minerals are observed in gold-rich bands of jacutinga from Corpo Y. They are: palladium-copper oxide, palladium, and palladseite (Olivo et al., 1995). Palladium-copper oxide occurs as free, zoned grains in hematite bands, elongated parallel to the elongation lineation (Fig. 1.13a), and in white phyllosilicate bands and

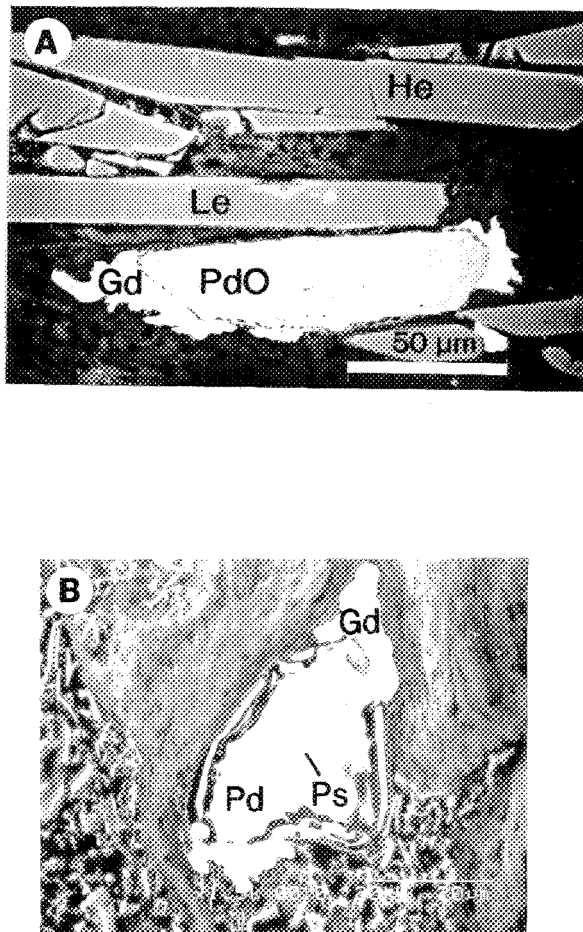


Figure 1.13 A. Secondary electron image of gold (Gd) coating around a zoned palladium-copper-oxide grain (PdO) from hematite-rich band parallel to elongation lineation (Le). From the Corpo Y orebody. Zoning is characterized by dark coloured zones with the highest Pd/Cu ratios alternating with light zones. He=hematite.  
B. Back-scattered electron image of gold (Gd) coating around palladium (Pd) with a core of palladseite (Ps) from a phyllosilicate-rich boudin parallel to the elongation lineation (Le). From the Corpo Y orebody.

quartz veins. The Pd, Cu and Hg contents are variable, as revealed by EMP analyses (Table 1.4); darker zones have higher Pd/Cu ratios than the lighter zones. Palladium grains occur in quartz veins and in boudinaged white phyllosilicate-rich bands parallel to the S1 mylonitic foliation. Palladium is alloyed with trace amounts of Au, Cu and Fe (Table 1.5). One grain of palladium in the kaolin boudin has a core of palladseite,  $(\text{Pd}, \text{Cu}, \text{Hg})_{17} \text{Se}_{15}$  (Fig. 1.13b, Table 1.5). Palladium-oxide and palladium grains are coated with films of gold and commonly do not exceed 100 microns. Although palladium arsenide-antimonides were also reported from gold washing concentrates at Itabira by Clark et al. (1974), Cabri et al. (1977) and Davis et al. (1977), no genetic link with iron-formation was mentioned.

#### 1.5.4 Whole Rock Geochemical Investigations

Some hand samples of jacutinga and quartz and hematite veins were selected for whole rock analysis. In addition, one sample of itabirite, massive hematite and ferruginous quartzite were also analyzed for comparison. Rare earth elements, platinum group elements, Au, Sc, Th, U, Cs, Hf, Ta, and Y were determined by instrumental neutron activation analysis (INAA). Major elements, Ag, Li, Sc, V, Cr, Co, Ni, Cu, Zn, Ga, Sr, Zr, Nb, Mo, Cd, Sn, Sb, Te, Ba, W, Pb, Bi and As were analyzed by Inducted coupled plasma (ICP). The results listed in Table 1.6 are only for those elements with concentration greater than the detection limits.

	<b>Dark bands*</b>	<b>Light bands*</b>
PdO (%)	93,06	89,13
CuO (%)	4,99	6,90
HgO (%)	0,26	1,13
AuO (%)	0,44	0,31
Fe <sub>2</sub> O <sub>3</sub> (%)	1,19	0,82
SeO <sub>2</sub> (%)	0,08	0,03
Sb <sub>2</sub> O <sub>5</sub> (%)	0,04	0,04
<b>TOTAL</b>	<b>100,06</b>	<b>98,36</b>
Pd (%)	77,04	74,31
Cu (%)	3,77	5,21
Hg (%)	0,23	1,00
Au (%)	0,40	0,36
Fe (%)	0,79	0,46
Se (%)	0,06	0,02
Sb (%)	0,02	0,03
Pd/Cu	20,44	14,26

**Table 1.4.** Electron microprobe analyses of Pd-Cu oxide shown in the Figure 1.13a  
(\* average of two analyses in wt %).

	PALLADIUM	PALLADSEITE*
Pd (%)	91,99	55,10
Cu (%)	1,31	3,02
Hg (%)	n.d.	3,05
Se (%)	n.d.	35,57
Au (%)	1,98	0,70
Fe (%)	1,31	0,57
TOTAL	96,65	97,38

Table 1.5. Electron microprobe analyses of palladium and palladseite shown in the Figure 1.13b (values in wt %; \* average of two analyses).

	1	2	3	4	5	6	7	8	9	10	11	12	A	B
SiO <sub>2</sub> (%)	18,71		2,61		90,16		42,72		4,61	45,51		89,49	49,4	
Fe <sub>2</sub> O <sub>3</sub> (%)	79,31		94,19		8,17		53		93,98	52,82		17,93	41,62	
Al <sub>2</sub> O <sub>3</sub> (%)	1,63		1,23		0,3		2,15		1,78	0,36		1,29	1,24	
MnO (%)	n.d.		0,51		0,02		1,46		n.d.	0,01		0,19		
TiO <sub>2</sub> (%)	0,07		0,06		n.d.		0,06		0,04	0,01		0,09		
Na <sub>2</sub> O (%)	0,02		0,02		0,02		0,02		0,02	0,02		0,03	0,1	
K <sub>2</sub> O (%)	0,24		0,21		0,1		0,19		0,11	0,19		0,25	0,17	
LOI (%)	0,85		1,3		0,25		2,55		0,95	0,15		0,6	4,18	
Au (ppb)	140	4700	40	50	500		12	95	15	n.d.	2	n.d.	11	
Pd (ppb)	37	n.d.	n.d.	180	n.d.		66	n.d.	25	n.d.	n.d.	n.d.		
Pt (ppb)	86	n.d.	n.d.	n.d.	n.d.		29	22	21	n.d.	60	n.d.		
Ag (ppm)	1,4	1,4	1,5	1	0,3	2,1	0,6	1,2	1,9	1,6	2,2	1,2		
Cu (ppm)	n.d.	13	1	4	3	2	5	2	3	2	2	4	tr.	
Ni (ppm)	14	25	2	17	6	19	25	44	20	14	24	26	10	
Cr (ppm)	288	422	354	218	433	394	231	269	229	364	196	584	60	
V (ppm)	17	18	87	26	4	13	27	15	18	12	20	35	10	
As (ppm)	24	19	26	n.d.	n.d.	13	22	n.d.	n.d.	n.d.	19	n.d.		
Sb (ppm)	6	n.d.	5	7	7	n.d.	9	6	12	n.d.	n.d.	9		
Zn (ppm)	n.d.	12	33	31	7	4	42	23	2	n.d.	3	6	700	
Pb (ppm)	6	17	2	5	6	n.d.	10	17	19	3	n.d.	9		
Cd (ppm)	5,2	2	2,6	3,9	n.d.	3,9	1,9	1,7	3,4	2,7	5,2	1,2		
Sn (ppm)	58	51	25	20	n.d.	35	n.d.	28	n.d.	35	n.d.	n.d.		
Ba (ppm)	50	84	61	50	11	19	83	61	13	10	32	136	70	
La (ppm)	26	75	9	5	n.d.	1	8	8	5	1	3	5		2,7-1,6
Ce (ppm)	62	180	10	9	n.d.	4	11	18	11	2	6	9		4,5-3,1
Nd (ppm)	18	95	n.d.	n.d.	n.d.	n.d.	n.d.	n.d.	n.d.	n.d.	n.d.	n.d.		2,4-1,4
Sm (ppm)	3,4	15,1	1,7	n.d.	n.d.	0,3	1,3	1,6	1,7	0,5	0,9	1		0,4-0,2
Eu (ppm)	5	0,6	0,7	n.d.	n.d.	n.d.	n.d.	0,6	n.d.	n.d.	n.d.	n.d.		0,2-0,1

Table 1.6. Major elements, and trace and precious metal contents of Cauê iron-formation specimens (1= hematite vein in jacutinga from Aba Norte; 2= jacutinga from Aba Norte; 3= hematite vein in jacutinga from Corpo X; 4= jacutinga close to hematite vein from Corpo X; 5= quartz vein in jacutinga from Corpo Y; 6= Jacutinga from Corpo Y; 7= jacutinga from Corpo Y; 8= jacutinga from Aba Leste; 9= jacutinga from Aba Leste; 10= itabirite; 11= compact hematite body; and 12= ferruginous quartzite). A= average of 133 samples of Lake Superior-type oxide facies iron-formation from 7 regions of Canada (Gross, 1988); and B= Average of REE elements of Lake Superior-type oxide facies iron-formation (Fryer, 1977).

Because of the weathering of the iron-formation, results reported here are only qualitative, particularly for the most mobile elements, and represent enrichments and depletions due to both hydrothermal alteration and weathering. In Table 1.6 the average for geochemical data of Lake Superior-type oxide-facies iron-formation published in Fryer (1977) and Gross (1988) are also given for comparison. Iron-formation samples from the Cauê mine yield higher  $\text{Fe}_2\text{O}_3$  total, Ni, Cr, V, As contents than the average values reported by Gross (1988). In addition, La and Ce contents are higher in jacutinga than in itabirite, hematite bodies of the Cauê mine, and the averages reported by Fryer (1977). This LREE enrichment could be explained by the occurrence of monazite in jacutinga.

Although the samples were analyzed for all the platinum-group elements, only Pd and Pt were detected, yielding values up to 180 ppb and 86 ppb, respectively. Gold contents in these samples are lower than the average grade of gold ore in jacutinga, indicating heterogeneous gold distributions. Gold was also analyzed by CVRD, using fire assay techniques, in 982 samples of jacutinga and D1 veins from Corpo Y (level 868), Corpo X (level 856), Aba Leste (level 865) and Aba Norte (level 880) by CVRD (Table 1.7). Corpo Y yields the highest gold grades (up to 7500 ppm) with an average grade of 155 ppm.

	CORPO Y (level 868)	CORPO X (level 856)	ABA LESTE (level 865)	ABA NORTE (level 880)
Range (ppm)	<0.1 - 7488.7	<0.1 - 148.0	<0.1 - 12.9	<0.1 - 135.3
Average (ppm)	155,5	10,6	0,8	1,8
Number of samples	304	54	94	530

Table 1.7: Gold grades of samples from the Cauê gold orebodies analyzed by fire-assay techniques.

## 1.6 DEFORMATION HISTORY OF PALLADIUM-BEARING GOLD MINERALIZATION

Detailed mapping and petrographic studies of the Cauê palladium-bearing gold orebodies suggest that the deposition of gold and palladium was contemporaneous with D1 deformation in the Corpo Y, Corpo X, Central and Aba Leste orebodies; whereas in Aba Norte, the richest gold orebody is contemporaneous with progressive D2-deformation. Palladian gold mineralization is located in high bulk shear strain sites (central, east and north domains) dismembered by east-over-west thrust faults.

Evidence of economic palladium and gold concentration synchronous with D1-deformation (Olivo et al., 1994) includes the occurrence of palladium gold as: (1) free grains or inclusions in syn-D1 tourmaline in the core of dismembered sheath folds (Fig. 1.12a); (2) slightly to strongly stretched grains parallel to the Le (Fig. 1.12b); and (3) free grains or inclusions in quartz-rich (Fig. 1.12c) and hematite-rich veins contemporaneous with D1, and deformed by D2 and D3. In addition, stretched palladium-copper oxide and palladium grains occur in hematite and white phyllosilicate bands and quartz veins parallel to S1 foliation (Fig. 1.13).

D1 deformation was ductile, non-coaxial, and progressive with high bulk shear strain. In this type of shear zone, the geometry of palladium-bearing gold orebodies and iron-formation is tentatively correlated with the third model of passive fold

development proposed by Cobbold and Quinquis (1980). According to this model, non-cylindrical passive folds develop mostly in regions between boudins. As segmentation of boudins progresses, the folds remain between the boudins (Fig. 1.14). The non-cylindricity of passive folds increases with progressive deformation, and at high shear strain ( $\sigma > 10$ ) "most deflections of realistic geological proportions become sheathlike" (Fig. 1.14; Cobbold and Quinquis, 1980). With progressive D1-deformation, sheath folds at the Cauê mine may have been transposed as rootless folds whose axes were progressively rotated parallel to the shear direction where deformation was more intense. Boudinaged auriferous quartz and hematite veins generated in this episode were also rotated parallel to the shear direction.

The continuous formation and deformation of quartz and hematite boudins as well as the irregular surface formed by D1 folds may have created the instability necessary to generate D2 folds in a regime of progressive simple shear. Tight D2 folds formed despite sheath fold formation because the bulk shear strain during D2 deformation was probably less intense than during D1 ( $\sigma < 10$ ). In this event, the Aba Norte hematite vein was formed and boudinaged parallel to S2-foliation. The third deformation event (D3) occurred at a higher crustal level and did not remobilize gold and palladium.

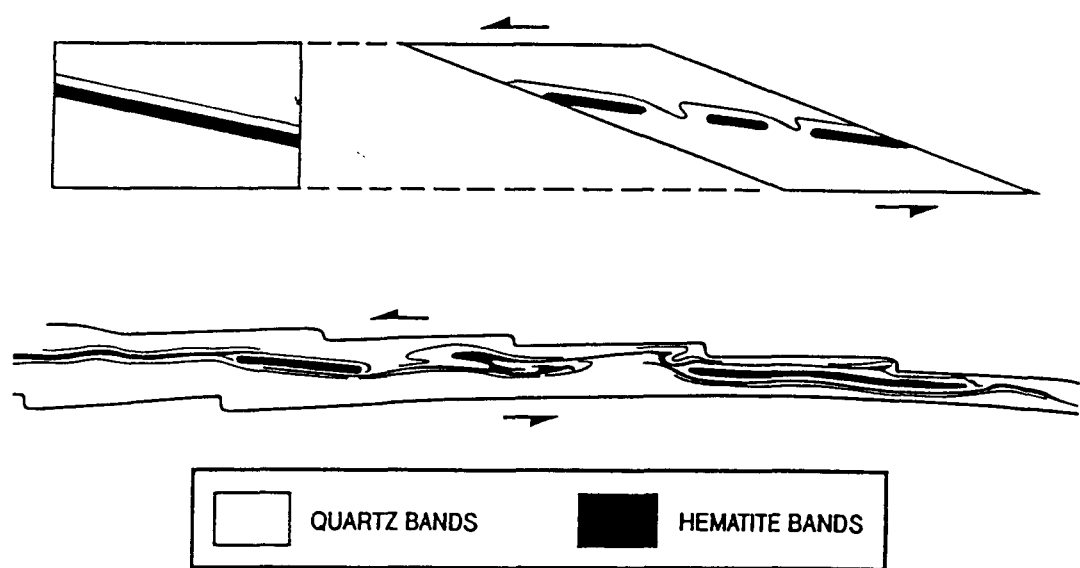


Figure 1.14. Passive model for development of sheath folds in a ductile, non-coaxial, and progressive tectonic regime with high bulk shear strain :  $\sigma$  greater than 10 (adapted from Cobbold and Quinquis, 1980). See text for explanation.

The purely ductile deformation process associated with the décollement of the iron-formation unit could enhance the rock permeability and provide the driving force for mineralizing fluid flow through chemically reactive host rocks (Boulter et al., 1987). In the Cauê mine, the chemically reactive host rocks were the jacutinga layers, and are discussed in the follow section.

## **1.7 PROBABLE SOURCE, TRANSPORT AND MECHANISMS OF PALLADIUM AND GOLD DEPOSITION IN JACUTINGA**

Palladium-gold mineralization and the development of D1-structures were probably coeval with the peak of metamorphism which attained temperatures of at least 600° C (Olivo et al., 1994). Oxygen fugacities during transport and deposition of these noble metals in the iron-formation were probably high, i.e., in the hematite stability field ( $fO_2$  higher than  $10^{-14}$  at 600° C; Lindsley, 1976), consistent with the hematitic composition of the host lithology. Under these conditions, Au and Pd may be transported as chloride complexes (Henley, 1973; Seward, 1984; Mountain and Wood, 1988; Gammons et al., 1992).

If palladium and gold were transported as chloride complexes, the deposition of the metals may have occurred in response to an increase in pH (Seward, 1984; Wood and Mountain, 1991). This phenomenon may have resulted of the reaction of mineralizing fluids with the jacutinga, representing possibly an altered dolomitic

itabirite (Dorr and Barbosa, 1963; Olivo et al., 1994). Because carbonate is dissolved by hydrothermal fluids (r-1), H<sup>+</sup> is consumed causing an increase in pH. The Mg liberated by dissolution of the carbonates reacted with quartz and k-feldspar to form respectively talc and phlogopite (r-2 and r-3). The decrease in ΣCl content caused by the incorporation of Cl in the phlogopite may have also accounted for the deposition of these metals (Seward, 1984; Olivo et al., 1994). In addition, Pd deposition occurred due to the formation of insoluble minerals such as selenides (Mountain and Wood, 1988; Wilde et al., 1989; Gammons et al., 1992; Olivo et al., 1994).

The rocks of the Archean Rio das Velhas Supergroup host important gold deposits and Pd contents in metamorphosed basic to ultrabasic rocks ranges up to 125 ppb and in massive sulfide ore up to 150 ppb (Ladeira, 1991; Roeser et al., 1993). Because of their Au and Pd enrichment, Roeser et al. (1993) suggested as these rocks are the most probable sources of palladium and gold hydrothermally concentrated in jacutinga.

## 1.8 COMPARISON OF THE CAUÊ GOLD DEPOSIT WITH ARCHEAN-IRON-FORMATION-HOSTED GOLD DEPOSITS

Gold deposits hosted in Algoma-type iron-formation are of importance worldwide. Some of the better known examples include the Homestake mine (Rye and Rye, 1974) and the Morro Velho mine (Ladeira, 1991), as well as other examples in

Western Australia (Phillips et al., 1984; Groves et al., 1987), Southern Africa (Fripp, 1976; Oberthur, 1990), India (Hamilton and Hodgson, 1986), Canada (MacDonald, 1983; Lhotka and Nesbitt, 1989; Gibbins et al., 1991), and Brazil (Ladeira, 1991; Vieira, 1991). Some of these deposits have been interpreted as syngenetic with later remobilization (e.g. Homestake and Morro Velho mines), while others are interpreted as epigenetic (e.g. Western Australia deposits).

Although the Cauê gold orebodies are hosted in iron-formation, they have features differing from those of Archean gold deposits hosted by iron-formation. First, the gold is hosted by a Lake Superior-type iron-formation in an early Proterozoic platform-facies sequence. In contrast, most of the Archean gold deposits are hosted by Algoma-type iron-formation in a volcano-sedimentary pile (Fripp, 1976; Groves et al., 1987; Lhotka and Nesbitt, 1989; Ladeira, 1991). Second, syngenetic and/or epigenetic iron sulfides are commonly associated with Archean gold deposits (Fripp, 1976; Groves et al., 1987), whereas in the Cauê mine there is no sulfide in the iron-formation sequence and hematite is the most important iron-bearing mineral. The occurrence of preserved sulfides in the amphibolites which are intrusives or tectonically imbricated with the iron-formation preclude the hypothesis of leaching sulfides during weathering processes. Third, most of the Archean deposits pre-date (Fripp, 1976; Ladeira, 1991) or post-date (Phillips et al., 1984; Groves et al., 1987; Lhotka and Nesbitt, 1989; Vieira, 1991) the regional deformation and the peak of thermal metamorphism. In the Cauê mine the main mineralizing event was

synchronous with S1-mylonitic foliation, which may be coeval with the peak of the thermal metamorphism. Finally, the gold grains from the Cauê mine are palladium-bearing; however, in most of the Archean deposits, gold grains are commonly silver-bearing and no palladium-bearing gold has yet been reported.

Consequently, we suggest that the palladium-bearing Cauê gold deposit should be referred as a new type of iron-formation-hosted gold deposit, formed by hydrothermal fluids circulating in shear zones reacting with Proterozoic, Lake Superior-type, carbonate-bearing oxide-facies iron-formation (dolomitic itabirite) during the peak of thermal metamorphism and under high oxygen fugacities.

## 1.9 REGIONAL IMPLICATIONS

Other gold deposits hosted by Proterozoic, Lake Superior-type iron-formation in the southern São Francisco Craton, such as the Congo Soco, Maquiné, Pitangui, and Conceição deposits, have similarities with the Cauê deposit: 1) they are close to the faulted contact between the Minas Supergroup and the underlying units in the southern São Francisco Craton (Fig. 1.1); 2) they are hosted by jacutinga; 3) they are structurally controlled by the approximately east-trending elongation lineation; and 4) they are palladium-bearing.

These similarities suggest that the gold-palladium concentration in these deposits may have occurred as a result of the same mechanism and possibly during the same deformational event. Therefore, it is proposed that the eastern border along the southern part of the São Francisco Craton hosting highly-sheared Lake Superior-type iron-formation is an exceptionally favourable geological environment for this type of deposit.

## 1.10 CONCLUSIONS

In this paper a new type of stratabound gold deposit is proposed, which is called "Palladium-bearing gold deposit hosted by highly-sheared, metamorphosed, Lake-Superior type iron-formation". The singularity of this type of deposit is characterized by: (1) the peculiar hydrothermal assemblage of jacutinga, which is dominated by hematite, quartz, talc, and phlogopite, with minor amounts of tourmaline, monazite, apatite, palladian gold, palladium-copper oxide, palladium and palladseite; (2) the synchronization of main mineralizing event with the peak of thermal metamorphism and the D1-shearing and thrusting event in the Corpo Y, Corpo X, Central, and Aba Leste orebodies; although in the Aba Norte orebody, the mineralizing event was synchronous with progressive D2-deformation; and (3) the physico-chemical conditions of the hydrothermal fluid, characterized by high temperatures and oxygen fugacities.

The proposed genesis of this new type of deposit may be summarized as follows. The high-strain ductile shear deformational event induced the percolation of high-temperature, high-oxygen-fugacity hydrothermal fluids in the iron-formation sequence. Under these physico-chemical conditions, Pd and Au were transported as chloride complexes and were deposited when the fluids reached the dolomitic itabirite layer. Palladium and gold were precipitated mainly as a result of changes in pH due to the formation of talc and phlogopite, generating the jacutinga rock-type. The continuous shearing event rotated and stretched the palladium-gold orebodies subparallel to the direction of tectonic transport. During progressive D2-deformation, the Corpo Y, Corpo X, Central and Aba Leste orebodies were folded and the Aba Norte orebody was formed and boudinaged. The Archean Rio das Velhas volcano-sedimentary sequence is suggested as the most probable source of Au and Pd.

The similarities between other palladium-bearing gold deposits in the São Francisco Craton hosted by jacutinga horizons and the Cauê mine suggest that the eastern border of southern portion of the São Francisco Craton which contains highly-sheared Lake Superior-type iron-formation is an exceptionally favourable geological environment for this type of deposit.

## REFERENCES

- Abreu, A. S., Diniz, H. B., Prado, M. G. B. and Santos , S. P., 1988, Mina de ouro de Sao Bento, Santa Barbara, Minas Gerais: Principais Depósitos minerais do Brasil: Departamento Nacional de Produção Mineral, Brasília, v. 3, p. 393-411.
- Babinski, M., Chemale, F., Jr., and Schmus, W. R., 1993, A idade das formações ferríferas bandadas do supergrupo Minas e sua correlação com aquelas da África do Sul e Austrália: Simpósio do Cráton do São Francisco, 2<sup>nd</sup>, Salvador, Brazil, August 23-26, 1993, Proceedings, p. 152-153
- Babinski, M., Van Schmus, W. R., Chemale, F., Jr., 1991, Pb/Pb Geocronology of Carbonate Rocks of Minas Supergroup, Quadrilátero Ferrífero, Minas Gerais, Brazil [abs.]: A Geophysical Union Fall Meeting Abstract with Programs, December 9-13, 1991, p. 53
- Bell, T. H., 1978, Progressive deformation and reorientation of fold axes in a ductile mylonite zone: the Woodroffe thrust: Tectonophysics, v. 44, p. 285-320.
- Bell, T. H., and Hammond, R. L., 1984, On the internal geometry of mylonite zones: Journal of Geology, v. 92, p. 667-686.
- Belo de Oliveira, O. A., 1986, As falhas de Empurrao e suas implicações na Estratigrafia e Metalogenia do Quadrilátero Ferrífero: Congresso Brasileiro Geologia, 35<sup>th</sup> , Goiânia, Brazil, v. 5, p. 15.
- Belo Oliveira, O. A., and Teixeira, W., 1990, Evidências de uma tectônica tangencial Proterozóica no Quadrilátero Ferrífero: Congresso Brasileiro de Geologia, 36<sup>th</sup>, Natal, 1990, Proceedings, v. 6, p. 2589-2604.
- Bensusan, J. A., 1929, Auriferous Jacutinga Deposits: Institute of Mining and Metallurgy Bulletin, nº 300, v. 8, p.
- Berthé, D., and Brun, J. P., 1980, Evolution of folds during progressive shear in the South Armorican Shear zone, France: Journal of Structural Geology, v. 2, p. 127-133.
- Berthé, D., Choukroune, P., and Jegouzo, P., 1979, Orthogneiss, mylonite and non-coaxial deformation of granites: the example of the South Armorican shear zone: Journal of Structural Geology, v. 1, p. 31-42.

- Boulter, C. A., Fotios, M. G., and Phillips, G. N., 1987, The Golden Mile, Kalgoorlie: A Giant gold Deposit Localized in Ductile Shear Zones by Structurally Induced Infiltration of an Auriferous Metamorphic Fluid: *Economic Geology*, v. 82, p. 1661-1876.
- Boyer, S. E., and Elliott, D., 1982, Thrust Systems: *American Association of Petroleum Geologists Bulletin.*, v. 66, p. 1196-1230.
- Cabri , L. J., Clark, A. M., Chen, T. T., 1977, Arsenopalladinite from Itabira, Brazil, and from the Stillwater Complex, Montana: *Canadian Mineralogist*, v. 15, p. 70-73.
- Chemale F., Jr., and Quade, H., 1986, Estratigrafia e Geologia Estrutural do Distrito Ferrífero de Itabira: *Congresso Brasileiro de Geologia*, 34<sup>th</sup>, Goiânia, 1986, Proceedings, v. 2, p. 987-998.
- Clark, A. M., Criddle, A. J., and Fejer, E. E., 1974, Palladium arsenide-antimonides from Itabira, Minas Gerais, Brazil: *Mineralogical Magazine*, v. 39, p. 528-543.
- Cobbold, P. R., and Quinquis, H., 1980, Development of sheath folds in shear regime: *Journal of Structural Geology*, v. 2, p. 119-126.
- Davis, R. J., Clark, A. M., Criddle, A. J., 1977, Palladseite, a new mineral from Itabira, Minas Gerais, Brazil: *Mineralogical Magazine*, v. 41, p. 123.
- Dorr, J. V. N. II, 1965, High-grade hematite ores of Brazil: *Economic Geology*, v. 60, p. 2-46.
- Dorr, J. V. N. II, 1969, Physiographic, stratigraphic and structural development of Quadrilatero Ferrifero, Minas Gerais, Brazil: U. S. Geological Survey Professional Paper, 641: 1-110.
- Dorr, J. V. N. II, 1973, Iron Formation in South America: *Economic Geology*, v. 68, p. 1005-1022.
- Dorr, J. V. N. II, and Barbosa, A. L. M., 1963, Geology and ore deposits of the Itabira district, Minas Gerais, Brazil: U. S. Geological Survey Professional Paper, 341-C, 110 p.
- Dossin, I. A., Dossin, T. M., Charvet, J., Cocherie, A., Rossi, P., 1993, Single-zircon dating by step-wise Pb-evaporation of Middle Proterozoic magmatism in the Espinhaço range, Southeastern Sao Francisco Craton (Minas Gerais, Brasil): *Simpósio do Craton do Sao Francisco*, 2<sup>nd</sup>, Salvador, Brazil, August 23-26, 1993, Proceedings, p. 39-42.

- Fleischer, R. and Routhier, P., 1973, The "Consanguineous" origin of tourmaline-bearing gold deposit: Passagem de Mariana (Brazil): Economic Geology, v. 68, p. 11-22.
- Fleischer, R., and Vial, S. S., 1991, Underground geological field trip to the Passagem de Mariana Gold Deposit, Quadrilátero Ferrífero, Minas Gerais, Brazil: Field and Mine Trip to Quadrilátero Ferrífero, Minas Gerais, Brazil, Field guide book of Brazil Gold'91: An International Symposium on the Geology of Gold. Belo Horizonte, p. 23-36.
- Fripp, R. E. P., 1976, Stratabound gold deposit in Archean banded iron-formation, Rhodesia: Economic Geology, v. 71, p. 58-75.
- Fryer, B. J., 1977. Rare-earth evidence in iron-formation for changing Precambrian oxidation states. *Geochimica et Cosmochimica Acta*, v. 41, p. 361-367.
- Gammons, C. H., Bloom, M. S. and Yu, Y., 1992, Experimental investigations of the hydrothermal geochemistry of platinum and palladium: I. Solubility of platinum and palladium sulfide minerals in NaCl/H<sub>2</sub>SO<sub>4</sub> solutions at 300° C. *Geochimica et Cosmochimica Acta*, v. 56, p. 3881-3894.
- Gibbins, W. A., Padgham, W. A., Atkinson, S., Brophy, J. A., and Gault, D., 1991, The Central Iron Formation Zone, Slave Structural Province, Northwest Territories, Canada - a gold rich Archean metallotect: Brazil Gold'91: An International Symposium on the Geology of Gold, Belo Horizonte, A. A. Balkema, 1991, Proceedings, p. 11-30.
- Goscombe, B., 1991, Intense non-coaxial shear and the development of mega-scale sheath folds in the Arunta Block, Central Australia: *Journal of Structural Geology*, v. 13, p. 299-318.
- Gross, G. A. , 1988, Gold content and geochemistry of iron-formation in Canada. Geological Survey of Canada Paper, 86-19, 54p.
- Groves, D. I., Phillips, G. N., Falconer, L. J., Houstoun, S. M., Ho, S. E., Browning, P., Dahl, N., and Mcnaughton, N. J., 1987, Evidence for an epigenetic origin for BIF-hosted gold deposits in the greenstone belts of Yilgarn Block, Western Australia: Recent Advances in Understanding Precambrian Gold Deposits, Department and University Extension, University of Western Australia, publication n° 11, p. 167-179.
- Hamilton, J. V., and Hodgson, C. J., 1986, Mineralization and structure of the Kolar gold field, India: Gold'86, an international symposium on the geology of gold deposits, Toronto, 1986, Proceedings, p. 270-283.

- Hanmer, S., Passchier, C., 1991, Shear-sense indicators: a review: Geological Survey of Canada, paper n° 90-17, 72 p.
- Henley, R. W., 1973, Solubility of gold in hydrothermal chloride solutions: Chemical Geology, v. 11, p. 73-87.
- Hoefs, J., Muller, G., and Schuster, A. K., 1982, Polymetamorphic Relations in Iron Ores from Iron Quadrangle, Brazil: The Correlation of Oxygen Isotope Variations with Deformation History: Contributions to Mineralogy and Petrology, v. 79, p. 241-251.
- Hoppe, A., Shobbenhaus, C., Walde, D. H. G., 1987, Precambrian Iron Formation in Brazil: Precambrian Iron-Formations: Athens, Theophrastus Publications S.A., p. 347-390.
- Lacassin, R., and Mattauer, M., 1985, Kilometre-scale sheath fold at Mattmark and implications for transport direction in the Alps: Nature, v. 315, p. 739-742.
- Ladeira, E. A., 1988, Metalogenia dos Depósitos de ouro do Quadrilátero Ferrífero, Minas Gerais: Principais Depósitos Minerais do Brasil, Departamento Nacional de Produção Mineral, Brasília, v. 3, p. 301-375.
- Ladeira, E. A., 1991, Genesis of gold in Quadrilatero Ferrifero: a remarkable case of permanency, recycling and inheritance- A tribute to Djalma Guimaraes, Pierre Routhier and Hans Ramberg: Brazil Gold'91: An International Symposium on the Geology of Gold, Belo Horizonte, 1991, A. A. Balkema, Proceedings, p. 11-30.
- Leao de Sá, E., and Andrade, L. P., 1990, A experiência da CVRD na lavra seletiva de minério aurífero nos itabiritos [abs.]: Int. Gold Symposium, 6<sup>th</sup>, Rio de Janeiro, August 13-14, Abstracts with program, p. 2.
- Leao de Sá, E., and Borges, N. R. A., 1991, Gold mineralization in Cauê and Conceição iron ore mines - Itabira- MG: Field and Mine trip to Quadrilátero Ferrífero, Minas Gerais, Brazil, Field guide book of Brazil Gold'91: An International Symposium on the Geology of Gold, Belo Horizonte, p. 74-85.
- Lhotka, P. G., and Nesbitt, B. E., 1989, Geology of unmineralized and gold-bearing iron formation, Contwoyto Lake - Pont Lake region, Northwest Territories, Canada: Canadian Journal of Earth Sciences, v. 26, p.46-64.
- Lindsley, D. H., 1976, Experimental studies of oxide minerals. Mineralogical Society of America short course notes, v. 3, p. L61-L88.

- Lister, G. S., and Price, G. P., 1978, Fabric development in a quartz-feldspar mylonite: *Tectonophysics*, v. 49, p. 37-78.
- Macdonald, A. J., 1983, The iron formation-gold association: evidence from the Geraldton Area: Ontario Geological Survey Miscellaneous Paper n° 110, p.75-83.
- Machado, N., Noce, C. M., Ladeira, E. A., Belo de Oliveira, O., 1992, U-Pb Geocronology of Archean magmatism and Proterozoic metamorphism in the Quadrilatero Ferrífero, southern São Francisco craton, Brazil: *Geological Society of America Bulletin*, v. 104, p. 1221-1227.
- McClay, K. R., and Insley, M. W., 1986, Duplex structures in the Lewis thrust sheet, Crowsnest Pass, Rocky Mountains, Alberta, Canada: *Journal of Structural Geology*, v. 8, p. 911-922.
- Melo, M. T. V., Borba, R. R., and Coelho, W. A, 1986, O Distrito ferrífero de Itabira, Minas do Cauê, Conceição, Dois Córregos, Periquito, Onça, Chacrinha e Esmeril: Principais Depósitos Minerais do Brasil, Departamento Nacional de Produção Mineral, Brasília, v. 2, p. 7-28.
- Minnigh, L. D., 1979, Structural analysis of sheath-folds in a meta-chert from the Western Italian Alps: *Journal of Structural Geology*, v. 1, p. 275-282.
- Mountain, B. W., and Wood, S. A., 1988, Chemical controls on the solubility, transport, and deposition of platinum and palladium in hydrothermal solutions: a thermodynamic approach: *Economic Geology*, v. 81, p. 1272-1277.
- Muller, G., Schuster, A., and Hoefs, J., 1982, Oxygen isotope variations in polymetamorphic iron ores from the Quadrilátero Ferrífero, Brazil: *Revista Brasileira Geociências*, v. 12, p. 348-355.
- Oberthür, T. S., Saager, R., and Tomschi, H. P., 1990, Geological, mineralogical and geochemical aspects of Archean banded iron-formation-hosted gold deposits: some examples from Southern Africa. *Mineralium Deposita*, v. 25: S125-S135.
- Olivo, G. R., Gauthier, M., Bardoux, M., 1994, Palladian gold from the Cauê iron mine, Itabira District, Minas Gerais, Brazil: *Mineralogical Magazine* (in press).
- Olivo, G. R., Gauthier, M., Bardoux, M., Leao de Sá, E., Borges, N., and Santana, F. C., 1993, Palladium-bearing gold deposits hosted by a Proterozoic Lake Superior-type iron-formation, Itabira Iron District, Minas Gerais, Southeast Brazil [abs.]: *Geological Association of Canada - Mineralogical Association of Canada*, Edmonton, May 1993, Program with Abstracts, p. A-79.

- Phillips, G. N., Groves, D. I., and Martyn, J. E., 1984, An epigenetic origin for Archean banded iron formation hosted gold deposits: *Economic Geology*, v. 79, p. 162-171.
- Polônia, J. C., and Souza, A. M. S., 1988, O comportamento em Microescala do Ouro no Minério de Ferro de Itabira, Minas Gerais: *Congresso Brasileiro de Geologia*, 35<sup>th</sup>, Belém, Proceedings, p. 58-69.
- Quinquis, H., Audren, C., Brun, J. P. and Cobbold, P., 1978, Intense progressive shear in Ile de Groix blueschists and compatibility with subduction or obduction: *Nature* v. 273, p. 43-45.
- Ramsay, J. G., 1967, *Folding and Fractures Rocks*: New York, McGraw-Hill, 568 p.
- Roeser, H., Schurmann, K., Tobschall, H-J and Jordt-Evangelista, H., 1993, Palladium in the Quadrilátero Ferrífero, Minas Gerais, Brazil: Brazilian Meeting on Platinum-Group Element, 1<sup>st</sup>, Brasília, 1993, Extended Abstracts volume, p. 52-54.
- Rosière, C. A., 1981, Strukturelle und texturelle Untersuchungen in der Eisenerzlagerstätte Pico de Itabira bei Itabirito, Minas Gerais, Brasilien: Unpub. Ph.D. thesis, Univ. Clausthal, 303 p.
- Rye, D. M., and Rye, R. O., 1974. Homestake gold mine, South Dakota: I stable isotope studies: *Economic Geology*, v. 69, p. 293-317.
- Schorscher, H. D., 1975, Entwicklung des polymetamorphen präkambrischen raumes Itabira, Minas Gerais, Brasilien: Umpub. Ph.D. thesis, University of Heidelberg, 302p.
- Schorscher, H. D., Santana, F. C., Polônia, J. C., and Moreira, J. M. P., 1982, Rio das Velhas Greenstone Belt and Proterozoic rocks, Quadrilatero Ferrifero, Minas Gerais State: International Symposium on Archaean and Early Proterozoic Geological Evolution and Metallogenesis, Sociedade Brasileira de Geologia, Salvador, September 3-11, Excursion annex p. 1-25.
- Seward, T. M., 1984, The transport and deposition of gold in hydrothermal systems: Gold'82: the geology, geochemistry and genesis of gold deposits, 1982, A. A. Balkema, Proceedings, p. 165-181.
- Skjernaa, L., 1980, Rotation and deformation of randomly oriented planar and linear structures in progressive simple shear: *Journal of Structural Geology*, v. 2, p. 101-109.

- Skjernaa, L., 1989, Tabular folds and sheath folds: definitions and conceptual models for their development, with examples from the Grapesvare area, northern Sweden: *Journal of Structural Geology*, v. 11, p. 689-703.
- Souza Filho, C. R., Rodrigues, L. C. R., Chemale, F., Jr., and Alkimim, F. F., 1989, Aspectos deformacionais e relações litoestratigráficas na Mina de Conceicao, Distrito Ferrífero de Itabira, Minas Gerais: Simpósio de Geologia, 5<sup>th</sup>, Núcleo Minas Gerais, Simpósio de Geologia, 1, Núcleo Brasília. Sociedade Brasileira de Geologia, Belo Horizonte, Proceedings, p. 16-20.
- Thiessen, R., 1986, Two-dimensional refold interference patterns: *Journal of Structural Geology*, v. 8, p. 563-573.
- Vial, D. S., 1988, Mina de ouro da Passagem , Mariana, Minas Gerais: Principais Depósitos Minerais do Brasil, Departamento Nacional de Produção Mineral, Brasília, v. 3, p. 421-430.
- Vieira, F. W. R., 1991, Textures and processes of hydrothermal alteration and mineralization in the Nova Lima Group, Minas Gerais, Brazil: Brazil Gold'91: An International Symposium on the geology of gold. Belo Horizonte, 1991, A. A. Balkema, Proceedings, p. 319-325.
- Vieira, F. W. R., and Oliveira, G. A. I., 1988, Geologia do Distrito Aurífero de Nova Lima, Minas Gerais: Depósitos Minerais do Brasil, Departamento Nacional de Produção Mineral, Brasília, v. 3, p. 377-391.
- Walde, D. H. G., 1986, Geologia do Ferro: Principais Depósitos Minerais do Brasil, Departamento Nacional de Produção Mineral, Brasília, v. 2, p. 3-6.
- Wilde, A. R., Bloom, A. S., and Wall, V. J., 1989, Transport and deposition of gold, uranium and platinum-group elements in unconformity-related uranium deposits: *Economic Geology Monograph*, n° 6, p. 637-660.
- Wood, S. A. and Mountain, B. W., 1991, Hydrothermal solubility of palladium in chloride solutions form 300° C to 700° C: preliminary experimental results - a discussion: *Economic Geology*, v. 86, p. 1562-1563.

## **CHAPTER II**

**PALLADIAN GOLD FROM THE CAUÊ IRON MINE,  
ITABIRA DISTRICT, MINAS GERAIS - BRAZIL**

## 1.1 INTRODUCTION

It is known that some native gold and gold-copper alloys contain palladium (Cabri, 1981). This relationship has been documented for samples from the Stillwater Complex, Montana, United States (Cabri and Laflamme, 1974), the Lac des Iles deposit, Ontario, Canada (Cabri and Laflamme, 1979), the Noril'sk and Talnakh deposits, Russia (Cabri, 1981), Hope's Nose, in Devon, England (Clark and Criddle, 1982); and in Brazil from the Serra Pelada deposit, in Pará State (Meireles and Silva, 1988), and the Congo Soco and Maquiné mines (Bensusan, 1929), the Taquaril and Porpez showings (Cabri, 1981), and the Cauê and Conceição mines (Leao de Sá and Borges, 1991; Olivo and Gauthier, 1993; Olivo et al., 1993), all in Minas Gerais State.

The palladian gold occurrences in Minas Gerais, Brazil, discussed in this paper are commonly hosted by with jacutinga, a hydrothermally-altered Lake Superior-type oxide-facies iron-formation (Bensusan, 1929; Dorr and Barbosa, 1963; Polônia and Souza, 1988; Ladeira, 1991; Leao de Sá and Borges, 1991; Olivo and Gauthier, 1993; Olivo et al., 1993). Despite the fact that the Minas Gerais deposits have been

mined since the eighteenth century, the composition and textures of their palladian gold have not been studied in detail. Although most of these mines are presently inactive, gold and palladium are still mined as by-products in the Cauê and occasionally in the Conceição iron mines (both mines, separated by approximately 7 km, are located in the Itabira Iron District). In the Conceição mine, palladium contents in gold grains are distinctly lower than at the Cauê mine (Leao de Sá and Borges, 1991).

Palladium-bearing high-grade gold ore of the Cauê mine provides a rare opportunity to study textures and compositions of palladian gold in primary ore. In this paper textural details and analytical data for palladian gold from the Cauê mine are reported and discussed in terms of the genesis of this special type of mineralization.

## 1.2 CAUÊ IRON MINE

### 1.2.1 Geologic Units

At the Cauê mine, four geologic units metamorphosed to amphibolite facies have been identified (Fig. 2.1, Olivo et al., in preparation): (1) a volcano-sedimentary sequence correlated with the Archean Rio das Velhas Supergroup; (2) an iron-formation unit comprised of itabirite (e.g. metamorphosed banded siliceous ironstone

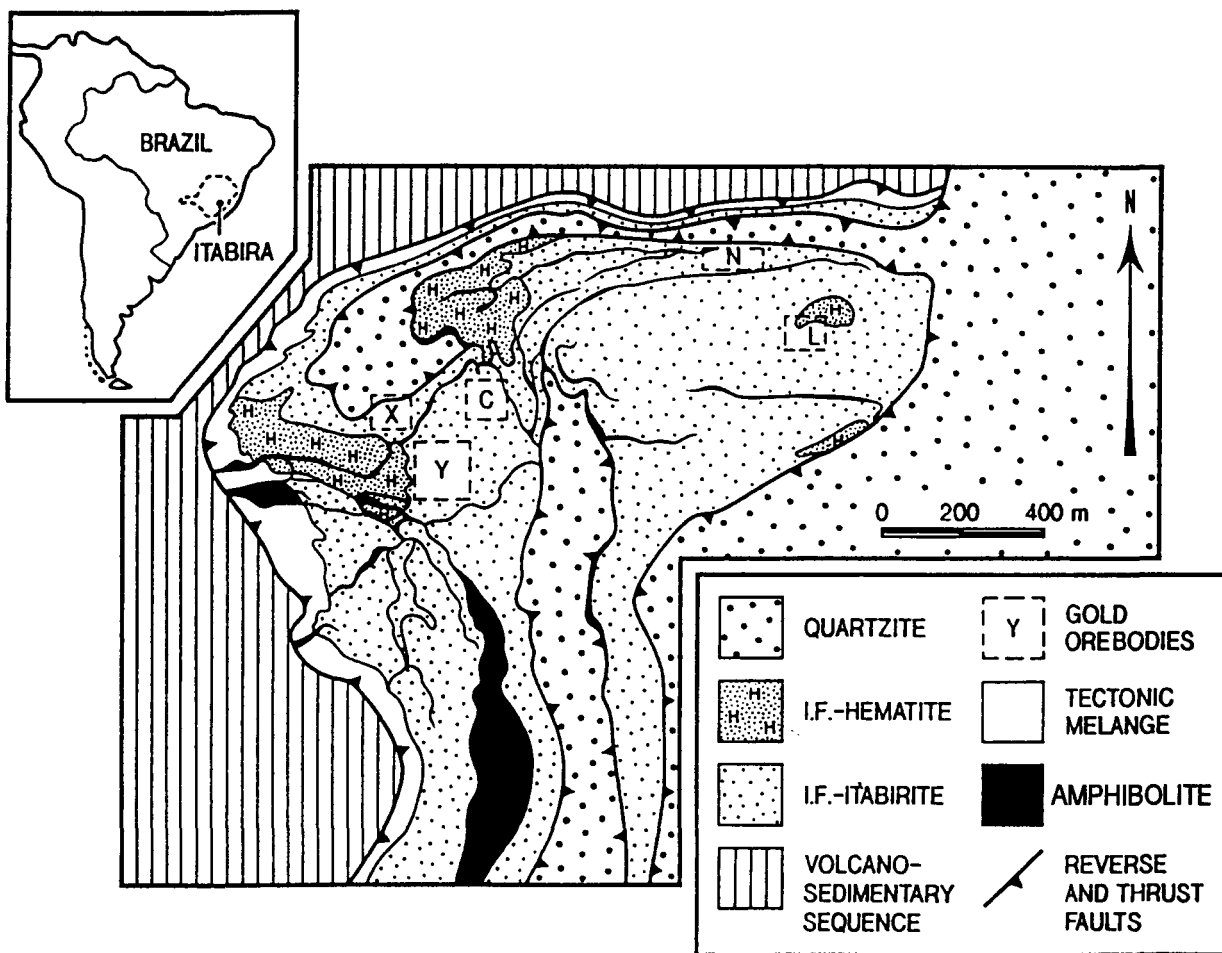


Figure 2.1. Simplified geologic map of the Cauê iron mine, Itabira District, Minas Gerais State, Brazil, showing the gold orebodies (C= Central; L= Aba Leste; N= Aba Norte; X= Corpo X; Y= Corpo Y). Modified after Leao de Sá and Borges (1991).

consisting of interlayered quartz-hematite-magnetite), massive hematite, and jacutinga which is part of the Early Proterozoic, Lake Superior-type iron-formation of the Itabira Group, Minas Supergroup; (3) a quartzite unit, correlated with the Early Proterozoic Piracicaba Group, Minas Supergroup; and (4) mafic intrusive rocks.

### **2.2.2 Structure**

These rocks were affected by three phases of folding, as well as boudinage and reverse and thrust faulting (Olivo et al, in preparation). D1-structures are represented by tight and isoclinal folds becoming sheath folds where the ENE elongation lineation (Le) and mylonitic foliation (S1) are well developed. D2-structures also include tight folds with associated parasitic fold axes and a transposing foliation (S2). D3 structures are characterized by open folds with an associated crenulation cleavage.

Millimetric to decametric boudins occur in S1 or S2 foliation planes. Reverse and thrust faults created imbricated sheets that are interpreted as synchronous with D1 deformation. Reactivation of these faults occurred during D2 deformation.

### **2.2.3 Gold Orebodies**

To date, five gold orebodies have been mined in the Cauê mine: Corpo Y, Corpo X, Central, Aba Leste, and Aba Norte (Fig. 2.1, Olivo et al., in preparation). All

orebodies are hosted by jacutinga. High gold grades (up to 1000 g/t) are associated with quartz- and hematite-rich bands parallel to the S1 mylonitic foliation and/or stretched parallel to the ENE elongation lineation.

The Corpo Y, Corpo X, Central and Aba Leste orebodies are palladium bearing, whereas in the Aba Norte orebody, gold grains have trace contents of rhodium. The Central and the Aba Norte orebodies are not discussed in this paper because gold from Aba Norte is not palladium bearing, and although palladium contents in gold from the Central orebody reach up to 20% (Andrade, oral communication), no gold-bearing polished sections were available for textural studies.

### 2.3 ELECTRON-MICROPROBE (EMP) AND SCANNING ELECTRON MICROSCOPE (SEM) ANALYTICAL TECHNIQUES

Analyses of polished sections were carried out using the Cameca Camebax automated wavelength-dispersive electron-microprobe (EMP) at McGill University. Calibration for the analyses performed at McGill was done using pure metals, at 20 kV and 20nA, and analytical precision is better than 0.2%. Energy-dispersive system (EDS) analyses were done for disaggregated gold grains that could not be polished.

Textural and compositional studies were undertaken with the Hitachi S-2300 scanning electron microscope, using a backscattered-electron detector and energy-

dispersive spectrometer (EDS) at the Université du Québec à Montréal. Elemental abundances stated here are all in weight percent.

## 2.4 OCCURRENCES OF PALLADIAN GOLD

### 2.4.1 Corpo Y

Palladian gold from the Corpo Y orebody is hosted by jacutinga which comprises millimetric to centimetric bands of various concentrations of quartz (+/- feldspar), hematite (+/- goethite) and white phyllosilicates, with minor amounts of tourmaline, apatite, and monazite. Carbonate is common as inclusions in quartz grains.

Palladian gold in jacutinga occurs as: (1) free grains and inclusions in rotated tourmaline (Fig. 2.2) hosted by hematite bands located in the core of dismembered sheath folds; (2) free grains in S1 mylonitic foliation planes of hematite bands (Fig. 2.3); (3) grains stretched parallel to the ENE elongation lineation (Fig. 2.4); (4) free grains or inclusions in boudinaged quartz bands; and (5) transposed free grains in S2 foliation planes.

SEM and EMP analyses of gold grains from polished sections of jacutinga show that the palladium contents range from 1 to 5% (Table 2.1) and that the highest concentrations are associated with small (commonly smaller than 10 µm) inclusions

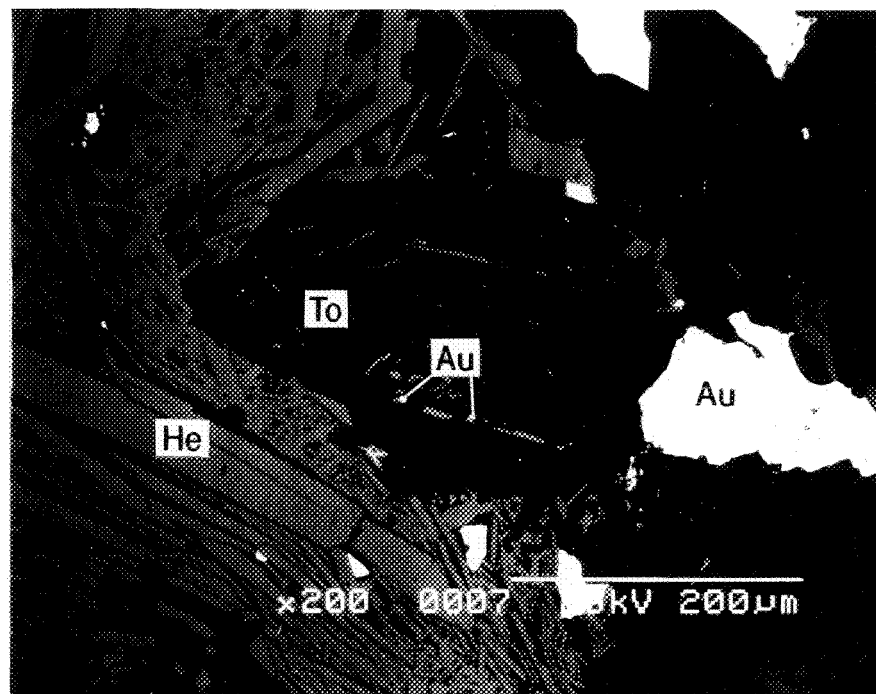


Figure 2.2. Back-scattered electron image showing gold (Au) as free grains or inclusions in rotated tourmaline (To) in the core of a dismembered sheath fold. He=hematite.

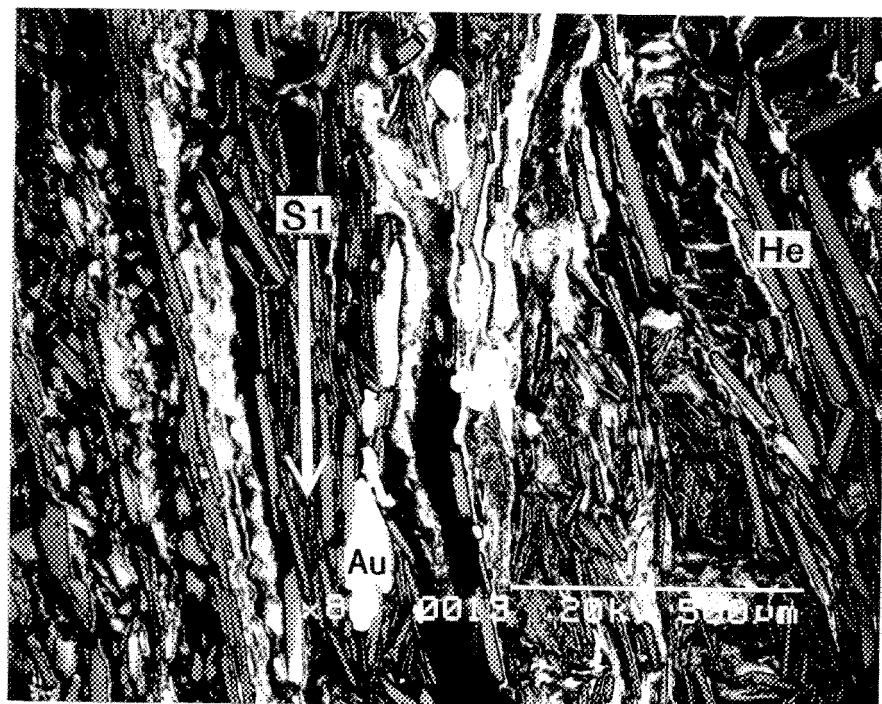


Figure 2.3. Back-scattered electron image showing gold (Au) in hematite (He) bands parallel to the S1 mylonitic foliation (from Corpo Y).

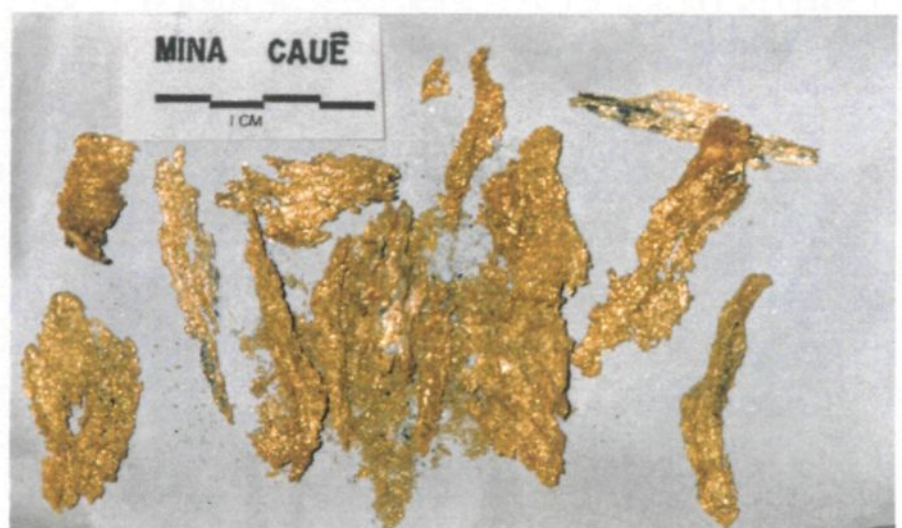


Figure 2.4. Gold grains form the *Corpo Y* elongated parallel to the elongation lineation

SAMPLE	Au	Pd	Cu	Ag	TOTAL %
Cau1 (%) (atomic proportion)	97,36 0,9584	1,92 0,0349	0,06 0,0018	0,27 0,0049	99,61
Cau2a (%) (atomic proportion)	90,33 0,8348	4,54 0,0777	2,75 0,0788	0,51 0,0087	98,13
Cau2b (%) (atomic proportion)	90,39 0,8271	4,61 0,0781	2,98 0,0846	0,59 0,0099	98,6
Cau2c (%) (atomic proportion)	84,37 0,7029	5,24 0,0808	8,28 0,2139	0,14 0,0021	98,03
Cau5 (%) (atomic proportion)	92,43 0,8451	1,83 0,0309	4,07 0,1153	0,52 0,0087	98,85
B2 (%) (atomic proportion)	94,37 0,8744	1,02 0,0176	3,1 0,0891	1,12 0,019	99,61
B3 (%) (atomic proportion)	96,11 0,9409	1,97 0,0357	0,37 0,0111	0,69 0,0123	98,14
Bpa1 (%) (atomic proportion)	99,12 0,9761	1,16 0,212	0,04 0,0011	0,09 0,0016	100,41
Bpa3 (%) (atomic proportion)	97,93 0,9664	1,2 0,0219	0,31 0,0094	0,1 0,0018	99,54
Bau1 (%) (atomic proportion)	97,39 0,9656	1,45 0,0265	0,11 0,0034	0,24 0,0043	99,19
Bau2 (%) (atomic proportion)	97,76 0,97761	1,47 0,0266	0,35 0,0105	0,38 0,0069	99,96
Bau3 (%) (atomic proportion)	97,35 0,9596	1,4 0,0256	0,3 0,0091	0,31 0,0057	99,36
Bau4 (%) (atomic proportion)	97,06 0,9517	1,23 0,0223	0,58 0,0177	0,47 0,0083	99,34
Bau5 (%) (atomic proportion)	93,35 0,8587	1,14 0,0193	3,81 0,1086	0,79 0,0133	99,09
Bau6 (%) (atomic proportion)	97,52 0,965	1,26 0,0231	0,17 0,0053	0,37 0,0067	99,32
Bau8 (%) (atomic proportion)	98 0,9707	1,25 0,0228	0,1 0,0031	0,19 0,0034	99,54

Table 2.1. Wavelength-dispersive electron microprobe analyses of palladian gold from polished sections of jacutinga, Corpo Y orebody.

of Pd-Cu oxides, showing island-mainland and replacement (relict) textures (Figs. 2.5, 2.6, and 2.7), as defined by Ineson (1989). Some disaggregated gold grains were analyzed using an energy-dispersive spectrometer (EDS), revealing palladium contents of up to 20%. Although copper is predominantly concentrated in palladium inclusions, it also occurs directly in gold (Fig. 2.7), and may reach total contents of 8% (Table 2.1). Gold grains also contain trace amounts of Ag (commonly less than 1%, Table 2.1) and enclose euhedral inclusions of hematite and tourmaline.

Disaggregated gold grains with high Pd concentrations have a whitish color and reduced malleability and ductility relative to pure gold.

#### 2.4.2 Corpo X

Palladian gold from the Corpo X orebody occurs in medium-to-coarse-grained yellow quartz concentrations hosted by 100-250 cm-wide, hematite-rich bands in the jacutinga. Some gold grains, obtained by gravimetric concentration of disaggregated primary ore, are flattened or bent, and contain Pd-Cu-oxide inclusions (Figs. 2.8 and 2.9). Although copper is more concentrated in palladium inclusions, as in Corpo Y, it is also independently alloyed with gold (Fig. 2.9). Semi-quantitative analyses using the EDS gave Pd contents of up to 10 %. Inclusions of Cr-bearing hematite and aluminosilicates are observed in a few gold grains.

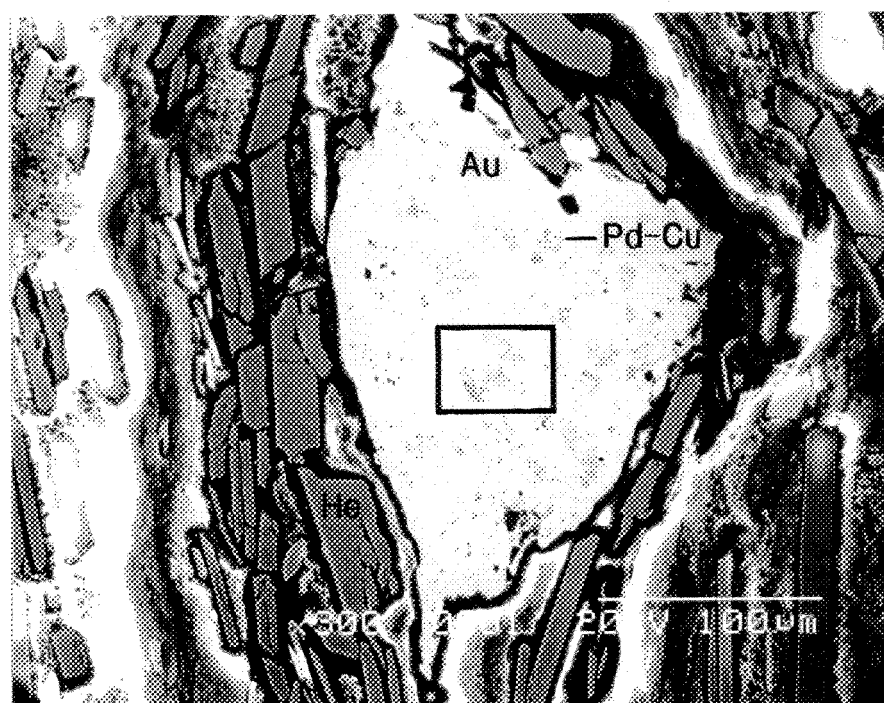


Figure 2.5. Back-scattered electron image of gold with small inclusions of Pd-Cu oxides, showing island-mainland and replacement (relict) textures (from Corpo Y).

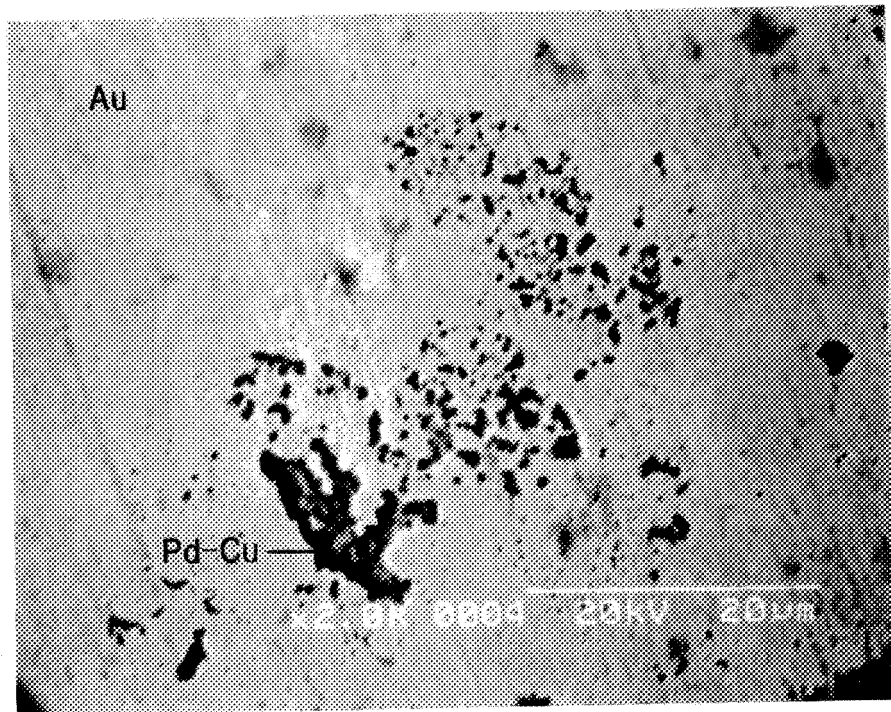


Figure 2.6. Enlargement of area outlined in Figure 2.5 showing Pd-Cu-oxide inclusions in the gold grain.

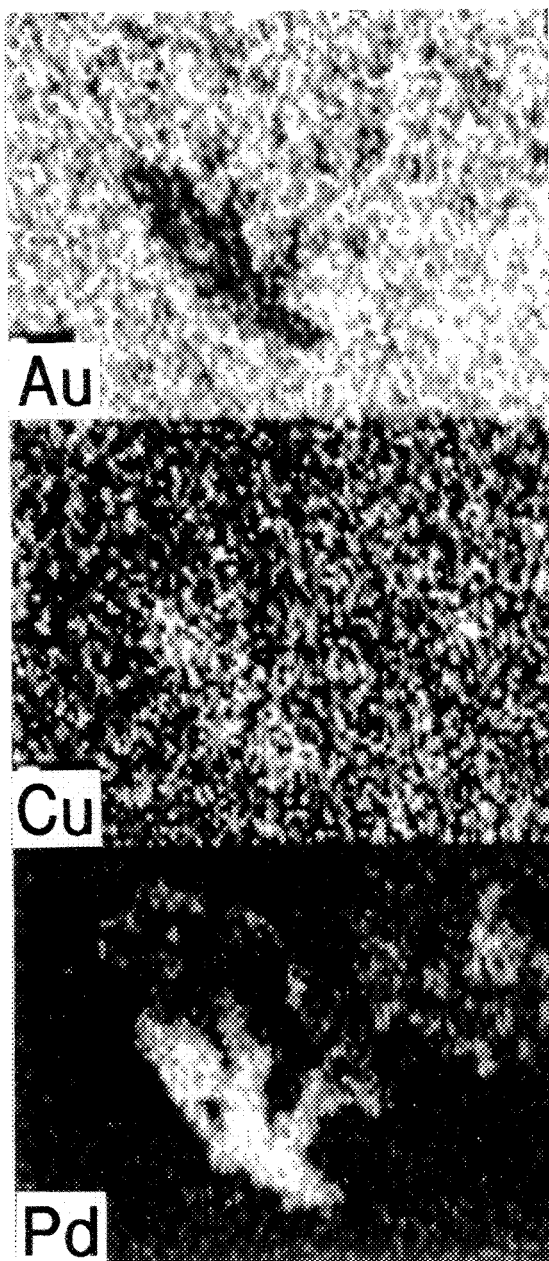


Figure 2.7. Single-element scans for Pd, Cu, and Au in the area analyzed (enclosed in box) in Figure 2.6.

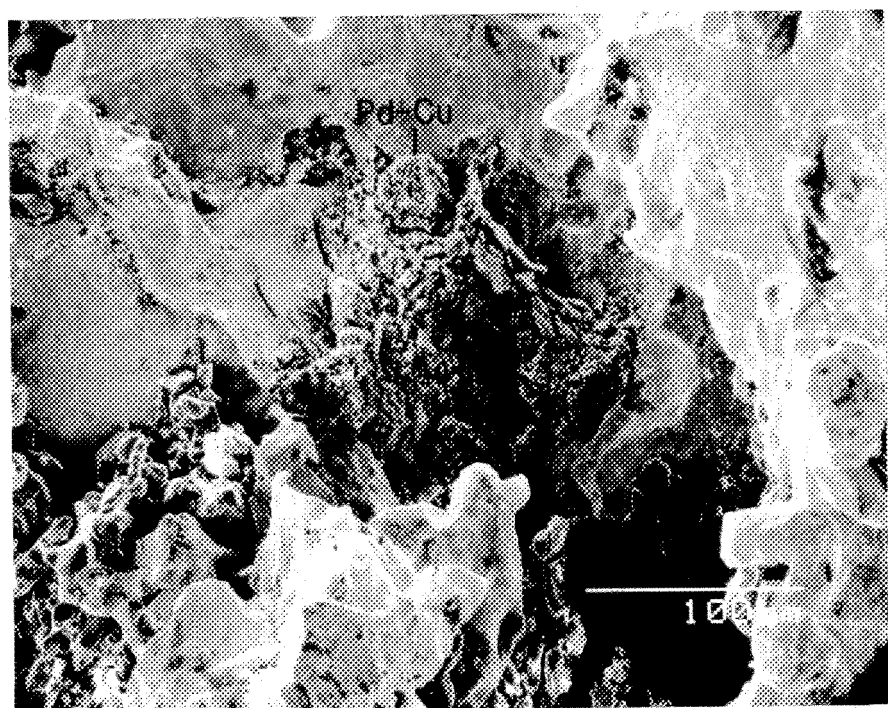


Figure 2.8. Scanning electron micrograph of gold grain from Corpo X orebody with a Pd-Cu-oxide inclusion.

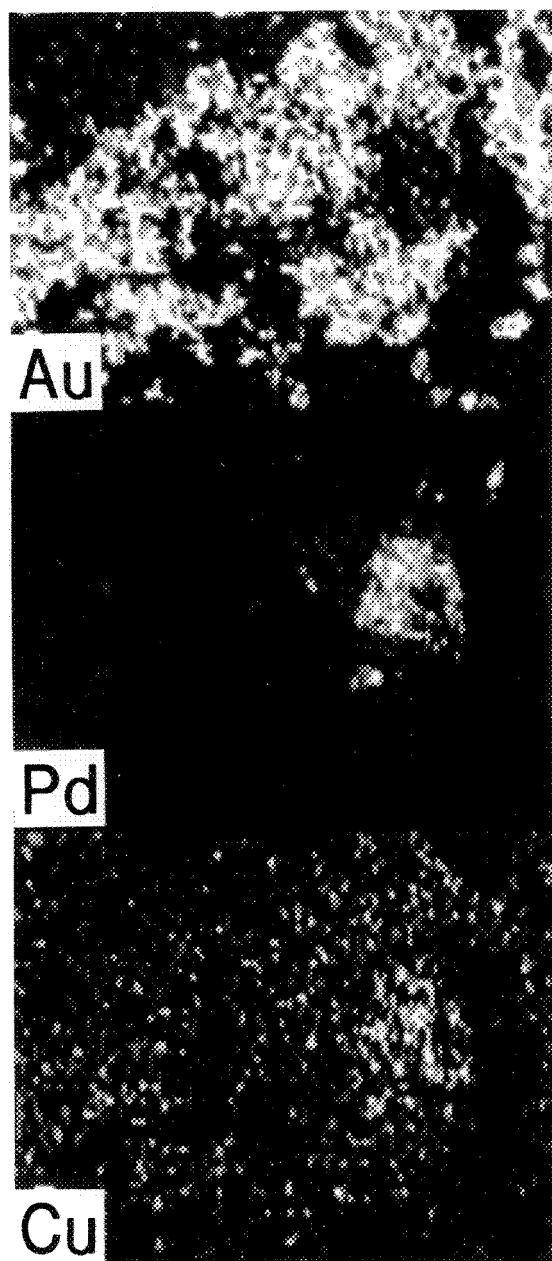


Figure 2.9. Single-element scans for Au, Pd, and Cu of the gold grain close to the Pd-Cu- oxide inclusion in Figure 2.8.

#### **2.4.3 Aba Leste**

Palladian gold from Aba Leste occurs in jacutinga composed of hematite and white phyllosilicates. In polished thin sections, only grains smaller than 20 µm were found. They occur as inclusions in S1-oriented hematite and as free grains in S1 surfaces. Regrettably, the quality of polish was inadequate for quantitative analysis of these grains. Palladian gold grains obtained by gravimetric concentration of disaggregated, rich primary ore are flat (Fig. 2.10) and contain up to 7% Pd (estimated by EDS). Palladium in these gold grains is not related to local concentrations of small inclusions; rather, it is homogeneously distributed throughout the gold grains (Fig. 2.11) a few of which contain Cr-bearing-hematite and tourmaline inclusions.

### **2.5 DISCUSSION**

#### **2.5.1 Timing of Palladium-Gold Mineralization**

In the three orebodies, palladium-gold mineralization was synchronous with the development of D1-structures.

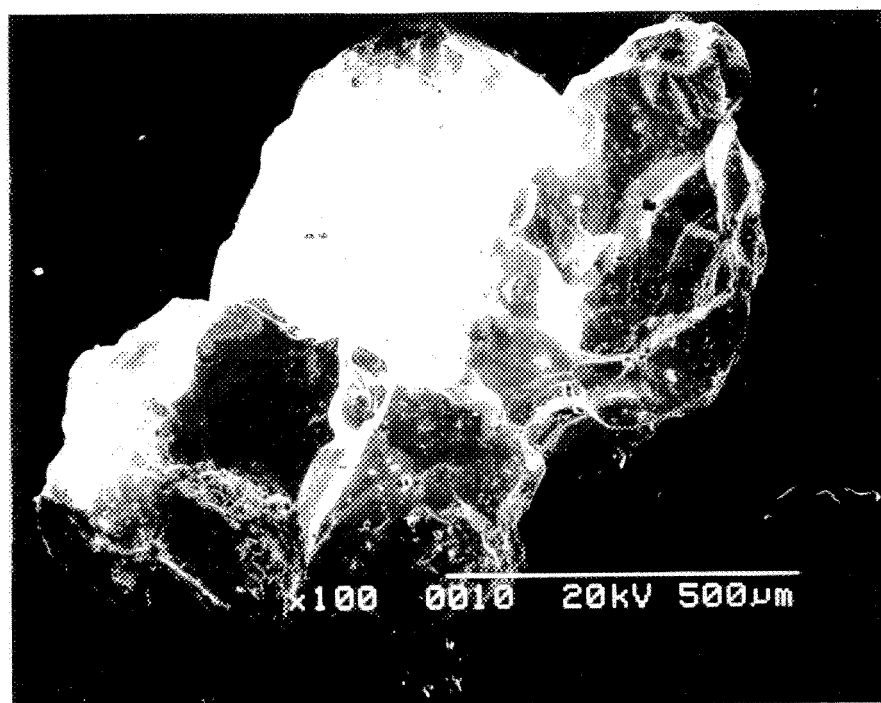


Figure 2.10. Scanning electron micrograph of a palladian gold grain from Aba Leste.

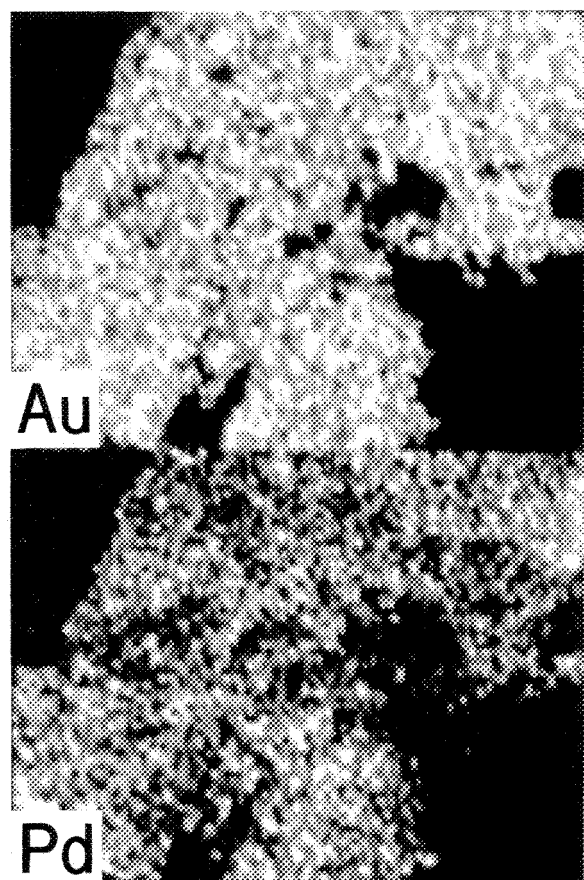


Figure 2.11. Single-element scans for Au and Pd of the gold grain in Figure 2.10.

In Corpo Y, Pd-Cu oxides may have been deposited early during the generation of the S1-mylonitic foliation. They may also have been replaced by gold during progressive deformation: an interpretation based on the presence of small inclusions of Pd-Cu oxides (1) in gold grains stretched parallel to S1, showing island-mainland and replacement (relict) textures; and (2) on slightly stretched gold grains in S1-planes showing replacement textures (Figs. 2.5 and 2.6). The second piece of evidence suggests that replacement in these grains occurred late during the creation of S1 because, if the replacement of Pd-Cu oxides by gold had occurred in the early stages of S1 generation, the gold would have been stretched due to its high ductility.

In Corpo X, replacement of Pd-Cu minerals may also have been synchronous with development of the S1-mylonitic foliation, as indicated by Pd-Cu oxide inclusions in flattened and bent gold grains.

In Aba Leste, palladium is homogeneously distributed in gold grains, suggesting that palladium and gold were deposited contemporaneously during the generation of the S1-mylonitic foliation.

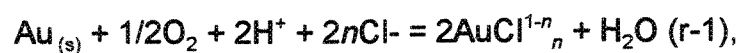
### **2.5.2 Temperature and oxygen fugacity conditions**

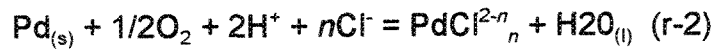
Generation of the S1 mylonitic foliation was probably synchronous with the regional peak of thermal metamorphism which, based on oxygen isotope studies of hematite and quartz (Hoefs et al., 1982), reached approximately 600° C. If the palladium-gold mineralization and the development of D1-structures were coeval, these metals were probably transported at temperatures of at least 600° C and deposited at temperatures of up to 600° C in the iron-formation unit.

Oxygen fugacities during transport and deposition of these noble metals in the iron-formation were probably high, i.e., in the hematite stability field ( $fO_2$  higher than  $10^{-14}$  at 600° C; Lindsley, 1976), consistent with the hematitic composition of the host lithology.

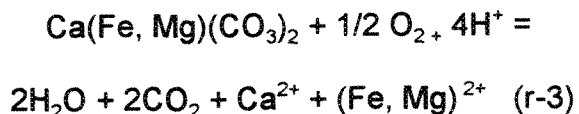
### **2.5.3 Transport and probable mechanisms of deposition of palladium and gold in jacutinga**

At high temperatures and oxygen fugacities, Au and Pd may be transported as chloride complexes (Henley, 1973; Seward, 1984; Mountain and Wood, 1988; Gammons et al., 1992), and the dissolution of Au and Pd as chloride complexes may be generalized, respectively as:





In the Cauê mine, high oxygen fugacities and temperatures, as noted by Hoefs et al. (1982) and in this study, probably provided favorable conditions for transporting palladium and gold as chloride complexes as discussed above. In this case, deposition of the metals may have occurred in response to an increase in pH (Seward, 1984; Wood and Mountain, 1991). This phenomenon may have occurred as a result of mineralizing fluids reacting with the jacutinga, representing possibly an altered dolomitic itabirite (Dorr and Barbosa, 1963). The presence of (Ca-Fe-Mg-bearing) carbonate inclusions in quartz within the jacutinga may indicate that carbonate was present in the rock matrix and might have reacted with acidic mineralizing fluids, causing an increase in pH according to:



According to Wood and Mountain (1991) and Gammons et al. (1992), palladium concentrations must decrease by two orders of magnitude for each unit increase in the actual pH if the dominant solution species are chloride complexes (see r-2). The same effect can be applied to gold (see r-1). Consequently, a pH increase caused by mineralizing fluids reacting with carbonate-bearing horizons may have been an effective mechanism for depositing gold and palladium. Another mechanism that may also account for the deposition of these metals is the decrease in  $\Sigma\text{Cl}$  content caused

by the incorporation of Cl in phlogopite formed by fluids reacting with host rocks (Olivo et al., in preparation). In addition, Pd deposition occurred due to saturation with insoluble minerals such as Se-minerals (Mountain and Wood, 1988; Wilde et al., 1989; Gammons et al., 1992). This last mechanism could explain why Pd was deposited earlier than gold, in agreement with the presence of the Pd-Se mineral, palladseite coated by gold, in bands parallel to S1 (Olivo and Gauthier, 1993).

## 2.6 CONCLUSIONS

Although palladian gold occurs in several geological environments, palladium-bearing high-grade gold ore of the Cauê mine provides an excellent opportunity to compare the precious metal mineralogy with the various mechanisms that have been postulated for the genesis of this special type of deposit. From this study, we may conclude that:

- (1) palladium and gold mineralization was synchronous with the development of intense D1-strain features. In Corpo Y and Corpo X, palladium may have been deposited early during the formation of the S1-mylonitic foliation, and replaced by gold during progressive deformation. This conclusion is based on the presence of small inclusions of Pd-Cu oxides in gold grains slightly to completely stretched parallel to S1, showing island-mainland and replacement (relict) textures. In Aba Leste, palladium and gold may have been deposited simultaneously as suggested by the homogeneously distribution of Pd in gold grains; and

(2) at high oxygen fugacities (hematite stability field) and high temperatures (up to 600° C), as indicated by the oxygen isotope studies and mineralogical assemblage in the auriferous iron-formation, Pd and Au may have been transported as chloride complexes and deposited mainly as a result of changes in pH. Dilution of Cl concentrations may have been a complementary mechanism of Pd and Au deposition, and the deposition of Pd as selenide minerals may have taken place early during the generation of S1-mylonitic foliation.

## REFERENCES

- Bensusan, A. J. (1929) Auriferous jacutinga deposits. *Institution of Mining and Metallurgy Bulletin*, Vol. 8, 300, 1-25.
- Cabri, L. J. (1981) Analyses of Minerals containing platinum-group elements. In *Platinum-Group Elements: Mineralogy, Geology, Recovery* (Cabri, L. J. ed.). Canad. Inst. Mining. Metall. Spec. Vol. 23, 151-173
- Cabri, L. J. and Laflamme, J. H. G. (1974) Rhodium, platinum, and gold alloys from the Stillwater complex. *Canadian Mineralogist*, 12, 399-403.
- Cabri, L. J. and Laflamme, J. H. G. (1979) Mineralogy of samples from the Lac-des-iles area, Ontario. *Canada Centre for Mineral and Energy Technology, report*, 79-27, 20 pp.
- Clark, A. M. and Criddle, A. J. (1982) Palladium minerals from Hope's Nose, Torquay, Devon. *Mineralogical Magazine*, 46, 371-377.
- Dorr, J. V. N., II, and Barbosa, A. L. M. (1963) Geology and ore deposits of the Itabira district, Minas Gerais, Brazil. *United States Geological Survey professional paper*, 341C, 110p.
- Gammons, C. H., Bloom, M. S. and Yu, Y. (1992) Experimental investigations of the hydrothermal geochemistry of platinum and palladium: I. Solubility of platinum and palladium sulfide minerals in NaCl/H<sub>2</sub>SO<sub>4</sub> solutions at 300 ° C. *Geochim. Cosmochim Acta*, 56, 3881-3894.
- Henley, R. W. (1973) Solubility of gold in hydrothermal chloride solutions. *Chemical Geology*, 11, 73-87.
- Hoefs, J., Muller, G., and Schuster, A. K. (1982) Polymetamorphic relations in iron ores from Iron Quadrangle, Brazil: the correlation of oxygen isotope variations with deformation history. *Contrib. Mineral. Petrol.*, 79, 241-251.
- Ineson, P. R. (1989) Introduction to practical ore microscopy. Longman Earth Science Series, John Wiley & Sons, Inc., New York, 181 pp.
- Ladeira, E. A. (1991) Genesis of gold in Quadrilátero Ferrífero: a remarkable case of permanency, recycling and inheritance - a tribute to Djalma Guimaraes, Pierre Routhier and Hans Ramberg. In *Proceedings of Brazil Gold'91: an international*

symposium on the geology of gold (Ladeira, E. A., ed.), A. A. Balkema, Rotterdam, pp. 11-30

Leao de Sá, E. and Borges, N. R. A. (1991) Gold mineralization in Cauê and Conceição iron ore mines, Itabira-MG. Field guide book of Brazil Gold'91: An international symposium on the geology of gold. (Fleisher, R., Grossi Sad, J.H., Fuzikawa, K., Ladeira, E. A. eds.), pp. 74-85.

Lindsley, D. H. (1976) Experimental studies of oxide minerals. In *Mineralogical Society of America short course notes* (Rumble, D., III, ed.), vol 3, L61-L88

Meireles, E. M. and Silva, A. R. B. (1988) Depósito de ouro de Serra Pelada, Marabá, Pará. In *Depósitos Minerais do Brasil* (Schobbenhaus, C. and Coelho, C.E.S., eds.), Vol. 3, 547-557.

Mountain, B. W. and Wood, S. A. (1988) Chemical controls on the solubility, transport, and deposition of platinum and palladium in hydrothermal solutions: a thermodynamic approach. *Econ. Geol.*, 83, 492-510.

Olivo, G. R. and Gauthier, M. (1993) Mineralogy of the palladium-bearing gold deposit hosted by a Lake Superior type iron-formation, Cauê Mine, São Francisco Craton, Brazil. In *Geological Society of America Annual Meeting, Boston, MA, October 25-28- Abstracts with Programs*, pp. A-276.

Olivo, G. R., Gauthier, M., Bardoux, M., Leao de Sá, L., Borges, N., and Santana, F. C. (1993) Palladium-bearing gold deposits hosted by a Proterozoic Lake Superior-type iron-formation, Itabira Iron District, Minas Gerais, southeast Brazil. *Geological Association of Canada and Mineralogical Association of Canada Joint Annual Meeting, May 17-19, Edmonton. Program and Abstracts*, pp. A-79.

Polônia, J. C. and Souza, A. M. S. (1988) O comportamento em microescala do ouro no minério de ferro de Itabira, Minas Gerais. In *Anais do Congresso Brasileiro de Geologia*, 35, 58-69.

Seward, T. M. (1984) The transport and deposition of gold in hydrothermal systems. In *Proceedings of the Symposium Gold'82: the geology, geochemistry and genesis of gold deposits*. (Foster, R. P., ed.). A. A. Balkema, Rotterdam, pp. 165-181.

Wilde, A. R., Bloom, A. S., and Wall, V. J. (1989) Transport and deposition of gold, uranium and platinum-group elements in unconformity-related uranium deposits. *Econ. Geol. Monogr.* 6, 637-660.

Wood, S. A., Mountain, B. W. (1991) Hydrothermal solubility of palladium in chloride solutions from 300° C to 700 ° C: preliminary experimental results - a discussion. *Econ. Geol.*, **86**, 1562-1563.

## **CHAPTER III**

**PALLADIUM MINERALS FROM THE CAUÊ IRON MINE,  
ITABIRA DISTRICT, MINAS GERAIS - BRAZIL.**

### 3.1 INTRODUCTION

Palladium minerals in the Itabira region were first described by Clark et al. (1974). These minerals were recovered from 4 g of residual concentrates from the gold washing in Itabira and consist of various quantities of three palladium arsenide-antimonides. The principal phase is arsenopalladinite ( $\text{Pd}_5(\text{As},\text{Sb})_2$ ), later recalculated to  $\text{Pd}_8(\text{As},\text{Sb})_3$  by Cabri et al. (1977), followed by minor quantities of isomertieite,  $(\text{Pd},\text{Cu})_5(\text{Sb},\text{As})_2$ , atheneite,  $(\text{Pd},\text{Hg})_3\text{As}$ , and a palladium selenide, later identified as palladseite ( $\text{Pd}_{17}\text{Se}_{15}$ ), Davis et al., 1977). Recently, Jedwab et al. (1993) reported the presence of palladium oxides (palladinite) in museum samples (rocks and concentrates) from Itabira.

These previous studies described the crystallographic and mineralogical characteristics of the minerals, but as most of them where found in concentrates, not in host-rock, textural features and a genetic interpretations were not provided. This is reviewed here, where textural details and analytical data for palladium minerals

found in the primary palladium-bearing gold ore of the Cauê iron mine, Itabira District, Brazil, are reported and discussed in terms of their genesis.

### 3.2 GEOLOGICAL SETTING

The Cauê iron mine is situated in the northeastern part of the Itabira Iron District, in the southern São Francisco craton (Fig. 3.1). At the Cauê mine, four geologic units metamorphosed to amphibolite facies have been identified (Fig. 3.2, Olivo et al. *in press*). They are commonly correlated with units of the Quadrilátero Ferrífero, also in the southern São Francisco Craton. The four geologic units are, from the bottom to the top:

- (1) a volcano-sedimentary sequence correlated with the Archean Rio das Velhas Supergroup;
- (2) a Lake Superior-type iron-formation unit composed of itabirite (e.g. metamorphosed banded siliceous ironstone consisting of interlayered quartz-hematite-magnetite), massive hematite and jacutinga (e.g hydrothermally-altered carbonate-bearing oxide-facies iron-formation hosting gold and palladium mineralization) which is part of the Early Proterozoic, Lake Superior-type iron-formation of the Itabira Group, Minas Gerais Supergroup;
- (3) a quartzite unit, correlated with the Early Proterozoic Piracicaba group, Minas Gerais Supergroup; and

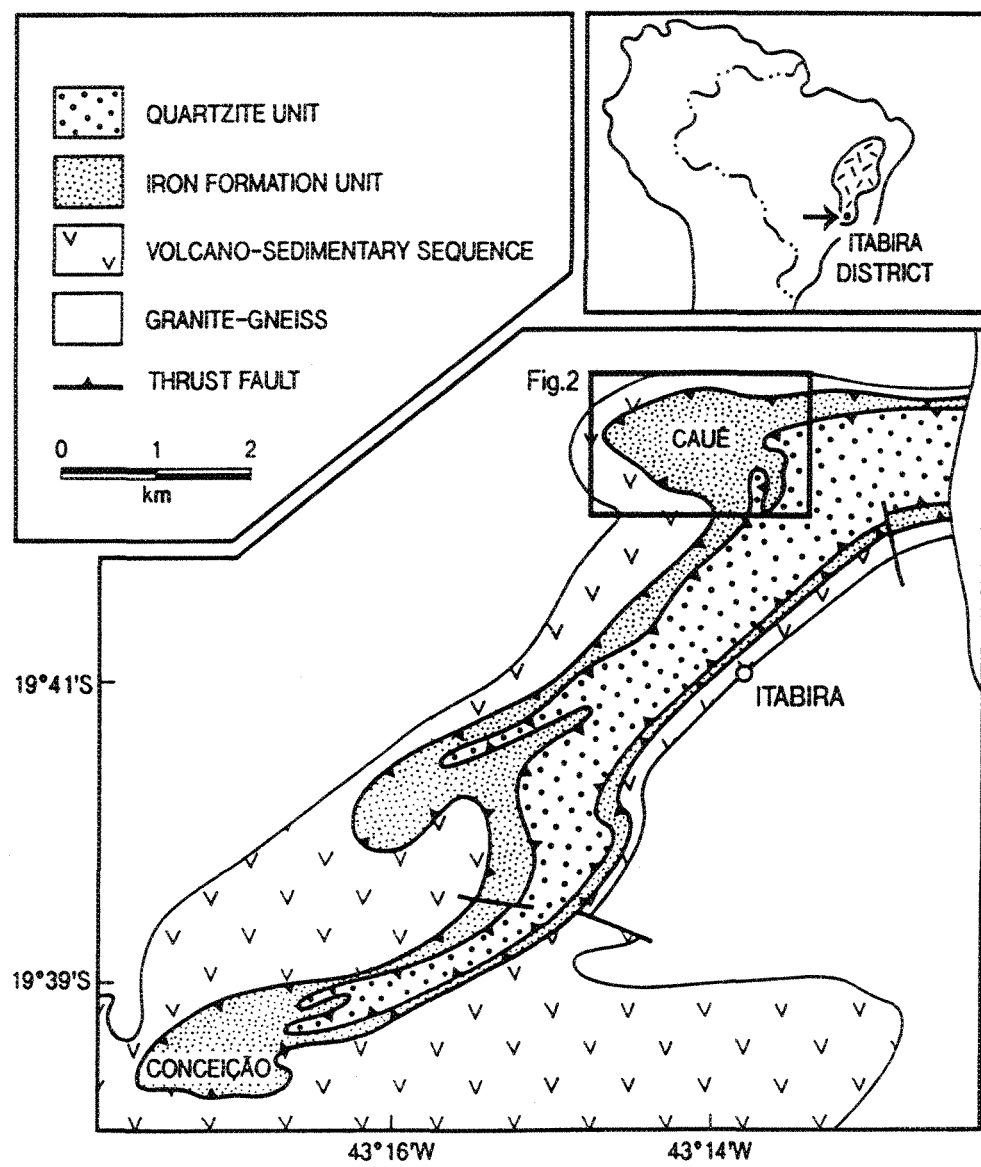


Figure 3.1. Simplified map of the Itabira District (after Olivo et. al., in press).

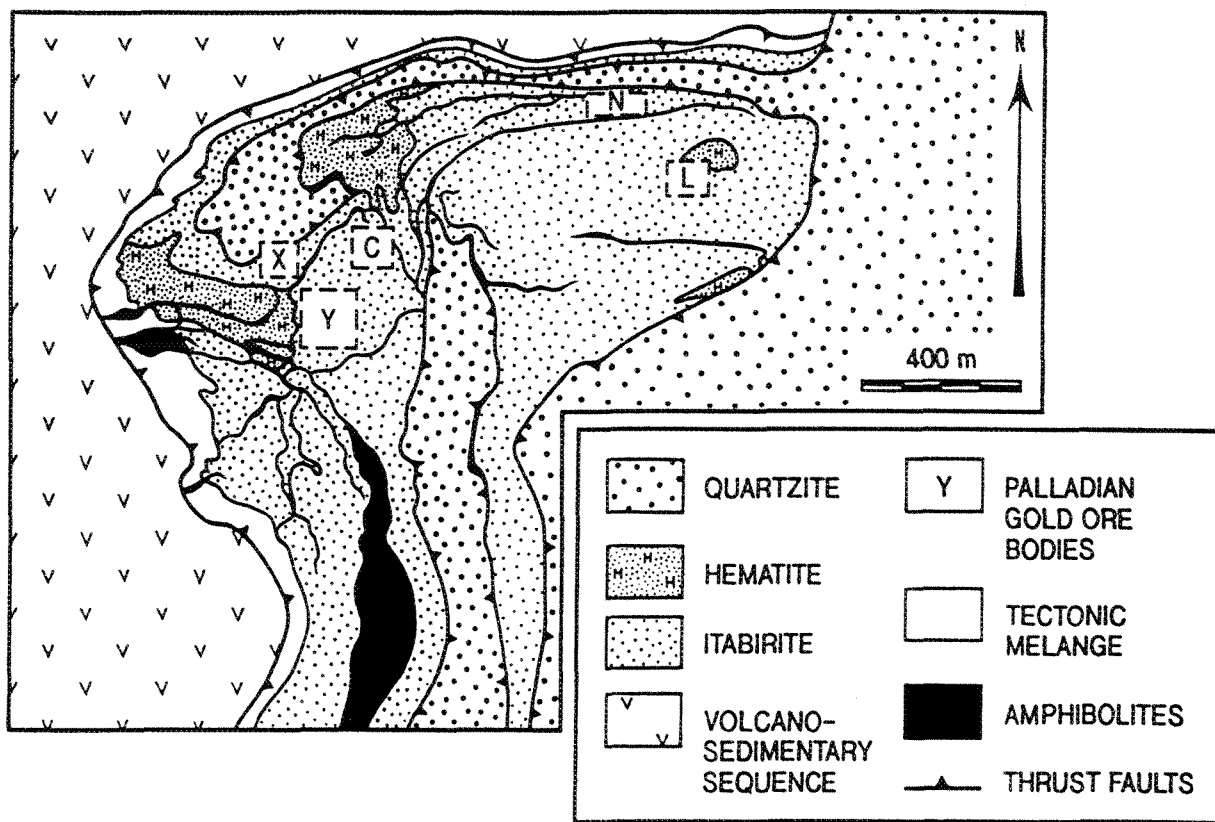


Figure 3.2. Simplified geologic map of the Cauê iron mine, Itabira District, Minas Gerais State, Brazil, showing the palladian gold orebodies (C= Central; L= Aba Leste; N= Aba Norte; X= Corpo X; Y= Corpo Y). Modified after Leao de Sá and Borges (1991).

- (4) Archean tectonic slices and Proterozoic dikes of mafic intrusive rocks (amphibolites).

These rocks were affected by three phases of folding, boudinage and thrust faulting (Olivo et al., in press). D1-structures are tight to isoclinal folds becoming sheath folds where the ENE elongation lineation (Le) and mylonitic foliation (S1) are well developed. S1-foliation is contemporaneous with the peak of thermal metamorphism (Hoefs et al., 1982). D2-structures also include tight folds associated parasitic fold axes and the S2 transposition foliation. D3 structures are characterized by open folds and are associated with a crenulation cleavage.

Millimetric to decametric boudins occur in S1 and S2 foliation planes. Reverse and thrust faulting created imbricated sheets that are interpreted as synchronous with Proterozoic D1 deformation (Olivo et. al., in press). Reactivation of these faults occurred during D2 and D3 deformation events.

### **3.3. ELECTRON-MICROSCOPE (EMP) AND SCANNING ELECTRON MICROSCOPE (SEM) ANALYTICAL TECHNIQUES**

Analyses were carried out using the Cameca Camebax and JEOL JXA- 8900L automated wavelength-dispersive electron-microprobe (EMP) at McGill University. Calibration for the analyses was done using pure metals, except mercury for which

the synthetic standard Cabri-451 ( $\text{Pd}_3\text{HgTe}_3$ ) was used at 20 kv and 15 kv and 20 nA. The analytical precision is better than 2%. The presence of oxygen was estimated using hematite and cassiterite standards and energy dispersive spectrometry analysis.

Textural and compositional studies were undertaken with the Hitachi S-2300 scanning electron microscope (SEM), using a back-scattered-electron detector and energy-dispersive spectrometry (EDS) at the Université du Québec à Montréal. Elemental abundances stated here are all in weight percent, and the microprobe standards and polished sections were freshly polished before analysis.

### 3.4. PALLADIUM MINERALS: OCCURRENCES AND CHEMICAL COMPOSITIONS

In the Cauê iron mine, gold and palladium have been mined as by-products in five orebodies (Fig. 3.2; Corpo Y, Corpo X, Central, Aba Leste, and Aba Norte; Olivo et al., in preparation) hosted by jacutinga. Palladium-bearing high-grade gold ores (up to 1000 g/t Au and 20 g/t Pd, L. Andrade, oral communication, 1993) are hosted by quartz- and hematite-rich bands parallel to the S1 mylonitic foliation and/or elongated parallel to the ENE elongation lineation.

Palladium-bearing minerals are observed in polished sections and in gravimetric concentrates of gold-rich jacutinga from the Corpo Y orebody. In this

orebody, jacutinga comprises millimetric to centimetric bands of various concentrations of quartz (+/- feldspar), hematite (+/- goethite) and white phyllosilicates (talc +/- phlogopite +/- kaolin), with minor amounts of zoned tourmaline and monazite. Ankerite is common as inclusions in quartz grains. The palladium minerals occur in gold-rich bands parallel to the S1-foliation.

### 3.4.1 Palladium and palladseite

Four palladium grains occur in quartz and white phyllosilicate-rich boudins parallel to the S1 mylonitic foliation. These grains do not exceed 100 µm, and are commonly coated with films of gold. In plane polarized light, palladium is creamy yellow in air and very light grey in oil immersion and is isotropic. Unfortunately, it does not polish well. The best analysis obtained for palladium is reported in Table 3.1, revealing that it is alloyed with small quantities of Au, Cu, and Fe (less than 2%).

One grain of palladium in a white phyllosilicate boudin has a core of palladseite (Table 3.1, Figs. 3.3 and 3.4) which polishes well in comparison with palladium. Palladseite is whitish cream in air and light grey in oil, and is isotropic. EMP analyses of palladseite obtained in this study are shown in Table 3.1. In addition to trace amounts of Fe and Au, it has lower Se and Cu contents and higher Hg contents than the values reported by Davis et al. (1977).

	Palladium	Palladseite	Palladseite	Palladseite *	Palladseite Davis et al. (1977)
Pd	91,99	54,50	55,70	60,03	55,77
Cu	1,31	2,95	3,08	2,45	3,99
Hg	n.d.	3,02	3,08	3,78	1,66
Se	n.d.	36,95	34,19	33,60	38,59
Au	1,98	0,08	0,06	n.d	n.d
Fe	1,31	0,48	0,66	n.d	n.d
TOTAL	96,65	97,98	96,77	99,85	100,01

Table 3.1: Wavelength-dispersive system analyses by electron-microprobe of palladium and palladseite, shown in Figures 3.3 and 3.4, from jacutinga of the Corpo Y orebody. Data reported by Davis et al. (1977) and an average of 4 analyses obtained by energy-dispersive system analyses (\*, with 0.15% Mn) are given for comparison.

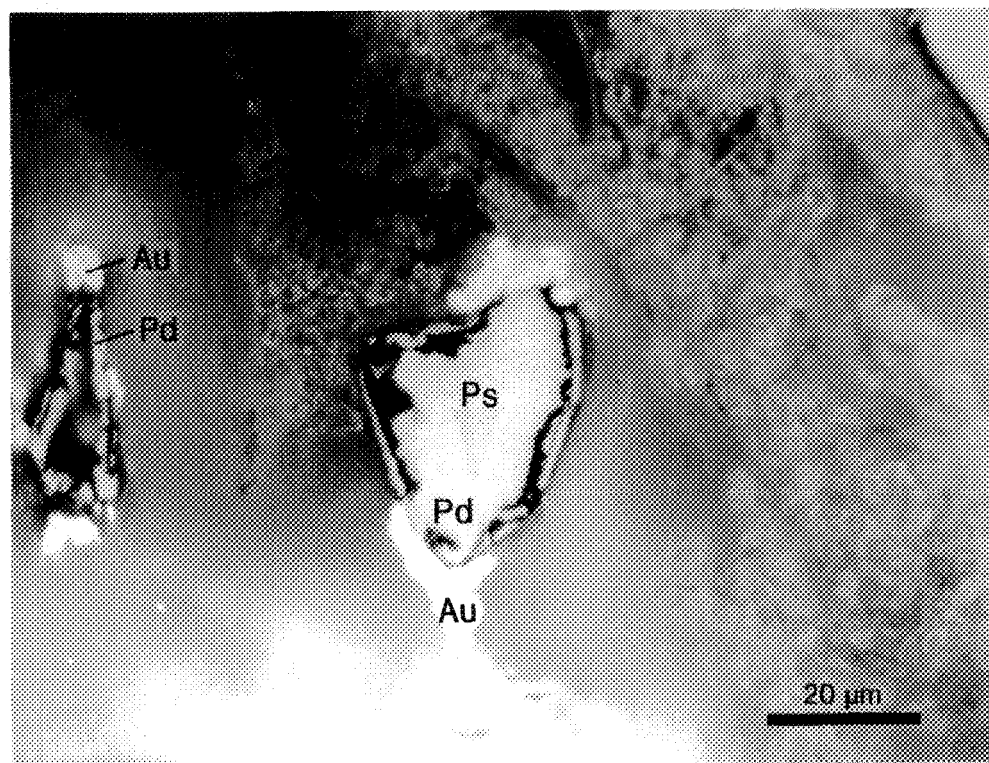


Figure 3.3. Photomicrograph of two palladium grains (Pd) coated with gold (Au) in a phyllosilicate-rich boudin parallel to S1; The large grain has a core of palladseite (Ps), and in the small grain, only the rim is preserved. He= hematite.

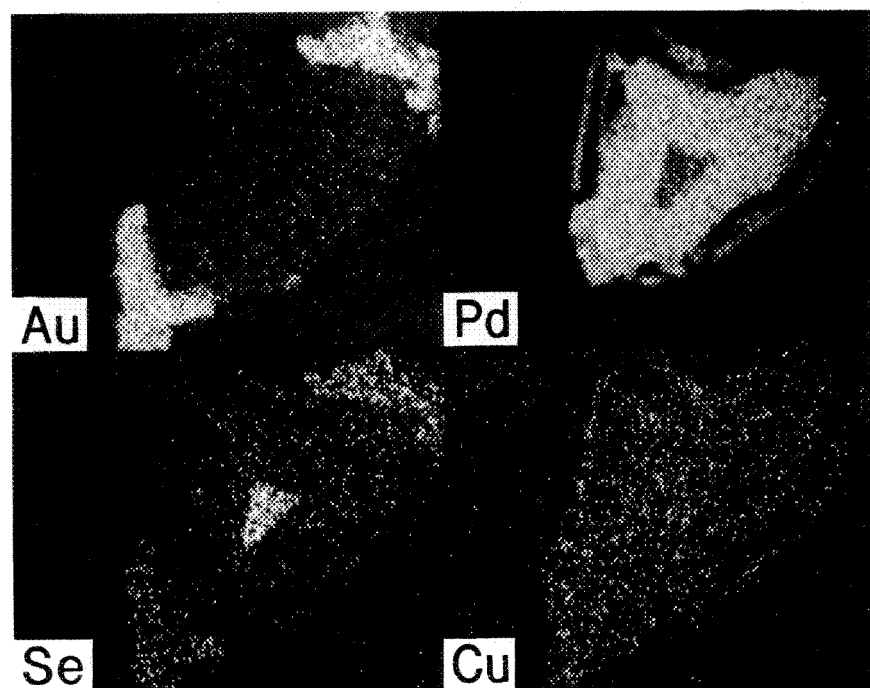


Figure 3.4. Single-element scans of Pd, Cu, Au, and Se for the large palladium grain of Figure 3.3 showing a core of palladseite.

### 3.4.2 Palladium-copper oxide

Nine palladium-copper oxide occurs in hematite bands as free grains stretched parallel to the elongation lineation  $L_e$  (Fig. 3.5) and in quartz and white phyllosilicate boudins (Figs. 3.6 and 3.7) parallel to the  $S_1$ -foliation. In plane polarized light in air or oil immersion, the palladium-oxide grains are medium-to-dark grey (darker than hematite), slightly anisotropic and without internal reflections. They show the same optical properties described for palladinite ( $PdO$ , Jedwab et al., 1993). The grains are euhedral, finely zoned, coated with films of gold, and commonly do not exceed 100  $\mu m$  (Figs. 3.5 and 3.6). The grain shown in Figure 3.5 has a wide gold coating in the pressure-shadow regions, and this coating is slightly stretched along the  $S_1$  foliation plane.

Zoning in these minerals is characterized by the alternation of dark coloured zones (high  $Pd/Cu$  ratios) with light areas (low  $Pd/Cu$  ratios). This variation is most evident in grains with relatively coarse zonation (see Fig. 3.5 and Table 3.2). In the grains observed in Figures 3.5 and 3.6, the Hg contents are high in the cores (up to 1.42%) and diminish toward the edges of the grains where the Hg contents are less than 0.1%. Se and Sb contents are low (less than 0.1%) and vary independently of the band colour and position in the grain (core or rim). Some palladium-copper-oxide grains also contain fine inclusions of gold oblique to the compositional bands (Fig. 3.7).

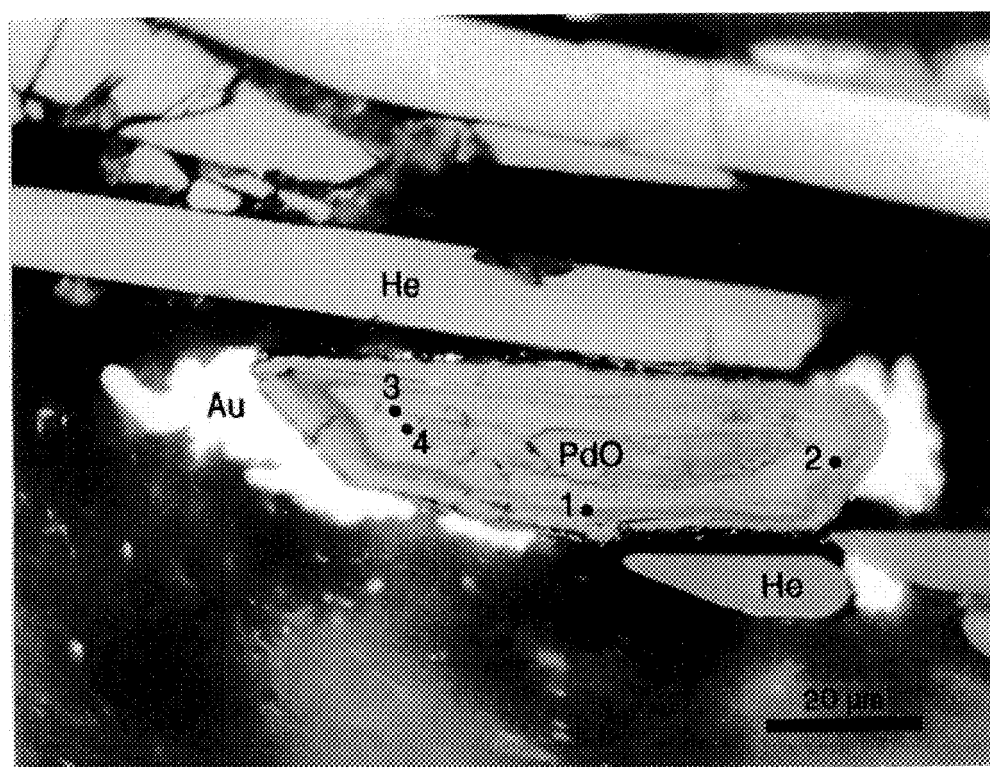


Figure 3.5. Photomicrograph of palladium-copper oxide (PdO) coated with gold (Au) in a hematite (He) band parallel to the S1 mylonitic foliation and stretched parallel to the elongation lineation. Zoning is characterized by the alternation of dark colored zones (high Pd/Cu ratios) with light zones (low Pd/Cu ratios). Arabic numbers correspond to analyzed points referred to in Table 3.2.

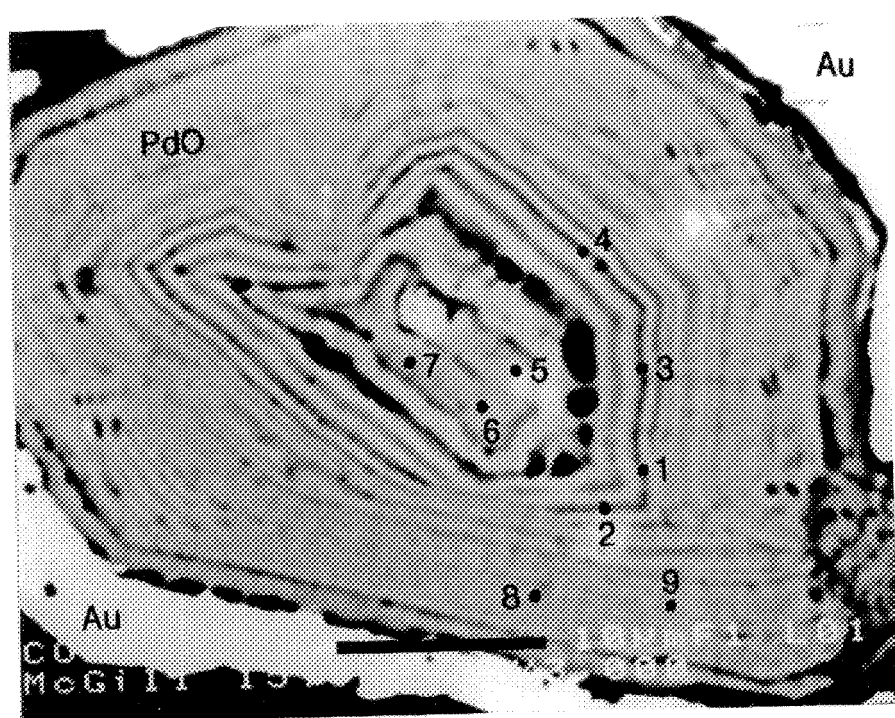


Figure 3.6 Back-scattered electron image showing finely zoned palladium-copper oxide (PdO) coated with gold occurring in white phyllosilicate band parallel to the S1 mylonitic foliation. Arabic numbers correspond to analyzed points referred to in Table 3.2.



Figure. 3.7. Back-scattered electron image showing a finely zoned palladium-copper-oxide grain (PdO) in a white phyllosilicate band parallel to the S1 mylonitic foliation. The oxide grain was coated with gold which was removed by repeated polishing, and contains fine inclusions of gold oblique to the compositional bands (Au). Arabic numbers correspond to the analyzed points referred to in Table 3.2.

Grain	I				II									III				IV		V
	1	2	3	4	1	2	3	4	5	6	7	8	9	1	2	3	4			
PdO	95,81	90,30	90,38	87,88	93,60	90,37	89,45	90,76	93,30	88,06	89,07	88,72	88,69	91,51	89,71	87,67	88,90	87,87	91,51	
CuO	4,51	5,47	7,06	6,74	7,40	7,41	8,04	7,78	7,37	8,40	8,40	8,03	7,76	7,25	7,51	6,87	7,58	8,27	7,93	
HgO	0,46	0,05	1,05	1,20	0,82	0,67	0,91	0,80	1,21	1,42	1,35	0,56	0,36	1,56	1,57	1,48	1,55	1,34	1,49	
AuO	0,53	0,35	0,47	0,14	0,07	0,10	n.d.	0,08	0,16	0,47	0,26	0,39	0,05	0,09	n.d.	n.d.	0,09	0,29	0,16	
Fe <sub>2</sub> O <sub>3</sub>	1,28	1,10	0,89	0,75	0,38	0,40	0,35	0,34	0,30	0,32	0,29	0,38	0,39	0,71	n.d.	0,77	0,60	0,25	0,34	
SeO <sub>2</sub>	0,07	0,08	0,02	0,04	n.d.	0,04	0,03	0,01	n.d.	0,09	0,10	0,09	0,04	n.d.	n.d.	n.d.	n.d.	n.d.	n.d.	
Sb <sub>2</sub> O <sub>5</sub>	0,02	0,05	0,03	0,04	n.d.	0,01	n.d.	n.d.	n.d.	0,03	n.d.	0,03	0,01	n.d.	n.d.	n.d.	n.d.	n.d.	n.d.	
TOTAL	102,68	97,40	99,90	96,79	102,27	99,00	98,78	99,77	102,34	98,79	99,47	98,20	97,30	101,12	98,78	96,79	98,72	98,00	101,43	
Pd	79,84	75,24	75,35	73,26	78,00	75,33	74,57	75,67	77,75	73,43	74,28	73,97	73,93	76,26	74,76	73,08	74,14	73,27	76,26	
Cu	3,41	4,13	5,33	5,08	5,58	5,59	6,07	5,87	5,56	6,34	6,34	6,06	5,86	5,47	5,69	5,17	5,74	6,24	6,01	
Hg	0,41	0,04	0,93	1,07	0,73	0,60	0,81	0,72	1,07	1,26	1,20	0,50	0,32	1,38	1,39	1,32	1,37	1,19	1,33	
Au	0,47	0,32	0,60	0,12	0,06	0,09	n.d.	0,07	0,15	0,42	0,23	0,34	0,04	0,08	n.d.	n.d.	0,08	0,22	0,23	
Fe	0,85	0,73	0,42	0,50	0,25	0,27	0,24	0,23	0,20	0,22	0,19	0,25	0,26	0,47	n.d.	0,51	0,40	0,19	0,14	
Se	0,05	0,06	0,01	0,03	n.d.	0,03	0,02	0,01	n.d.	0,06	0,07	0,06	0,03	n.d.	n.d.	n.d.	0,51	n.d.	n.d.	
Sb	0,01	0,03	0,02	0,03	n.d.	0,01	n.d.	n.d.	n.d.	0,02	n.d.	n.d.	0,01	n.d.	n.d.	n.d.	n.d.	n.d.	n.d.	
Pd/Cu	23,41	18,21	14,13	14,42	13,97	13,47	12,29	12,89	13,96	11,58	11,71	12,21	12,61	13,94	11,13	14,13	12,92	11,74	12,69	

Table 3.2. Wavelength-dispersive analyses by electron-microprobe of palladium-copper oxide from jacutinga of Corpo Y orebody. Arabic numbers correspond to the analyses plotted in Figures 3.5 (grain I), 3.6 (grain II) and 3.7 (grain III).

Small inclusions of Pd-Cu oxide ( $< 20\mu$ ) showing island-mainland and replacement (relict) textures (Fig. 3.8), as defined by Ineson (1989), were also observed in gold grains that are parallel to the S1-foliation and slightly to highly stretched parallel to the elongation lineation (Olivo et al., 1994).

### 3.4.3 Arsenopalladinite

One grain of arsenopalladinite was recovered from a mechanically disaggregated jacutinga sample. This grain contains inclusions of palladium-copper oxide (Figs. 3.9 and 3.10). Regrettably, it was not physically possible to mount this grain in a polished section due to its small size. However, energy-dispersive spectrometer (EDS) analyses indicate average contents of 77.59% Pd, 17.08% As, and 5.33% Sb.

The occurrence of arsenopalladinite and palladseite in jacutinga raises the question about the genetic link between the palladium minerals in the gold washings previously described by Clark et al. (1974) and the palladium minerals found in the auriferous Cauê iron-formation. We suggest that jacutinga is the most probable source of these palladium minerals because (1) we found in jacutinga two of the four minerals, arsenopalladinite and palladseite, described by Clark et al. (1974), and (2) the minerals described by these authors contain inclusions of palladium-oxide and hematite which also occur in jacutinga.

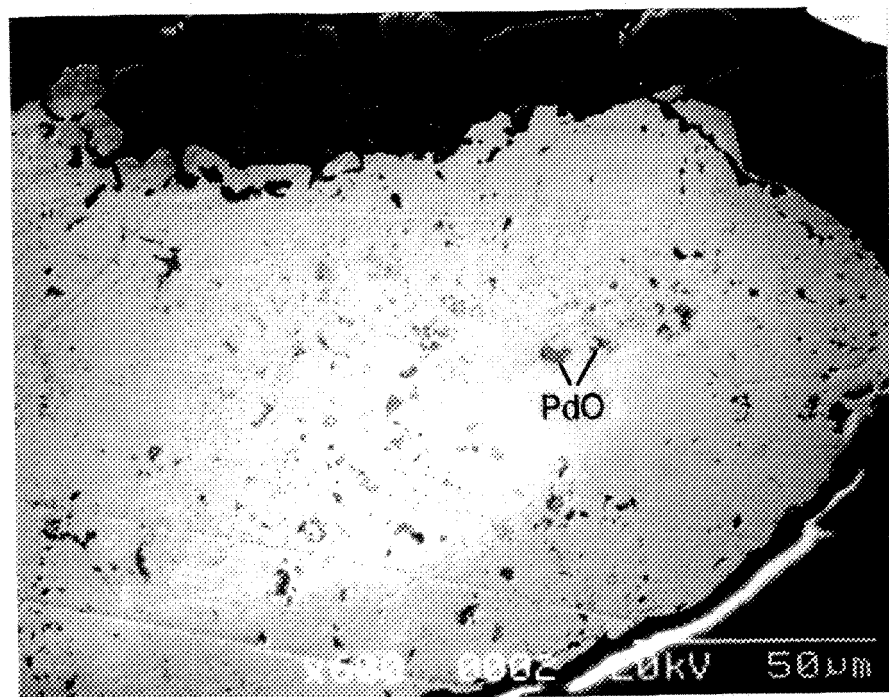


Figure 3.8. Back-scattered electron image of stretched gold with small inclusions of Pd-Cu oxides (PdO), showing island-mainland and replacement (relict) textures (from Corpo Y). He= hematite

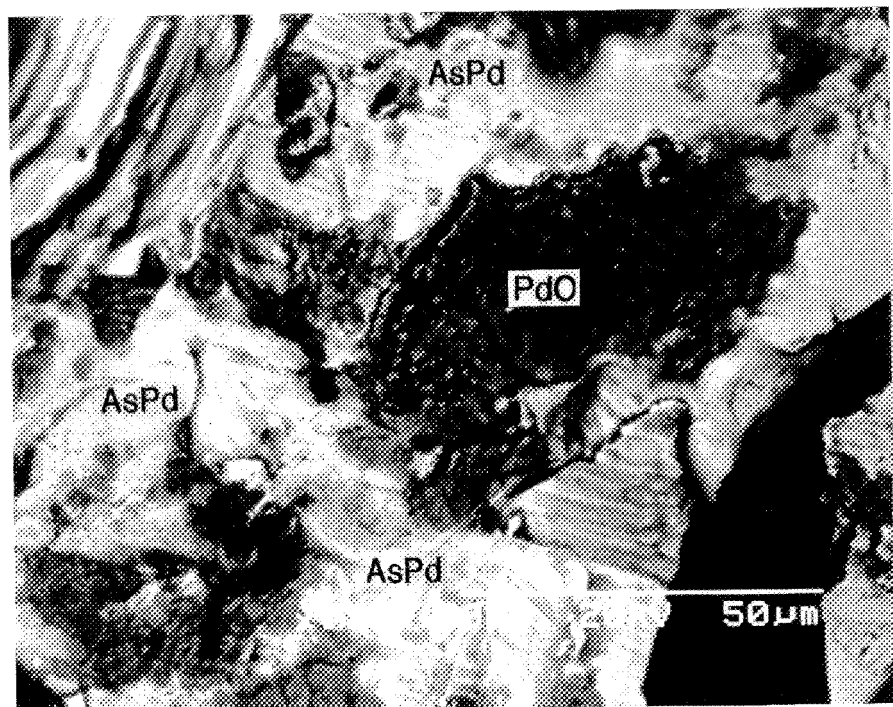


Figure 3.9. Back-scattered electron image of arsenopalladinite (AsPd) with inclusions of palladium-copper oxide (PdO).

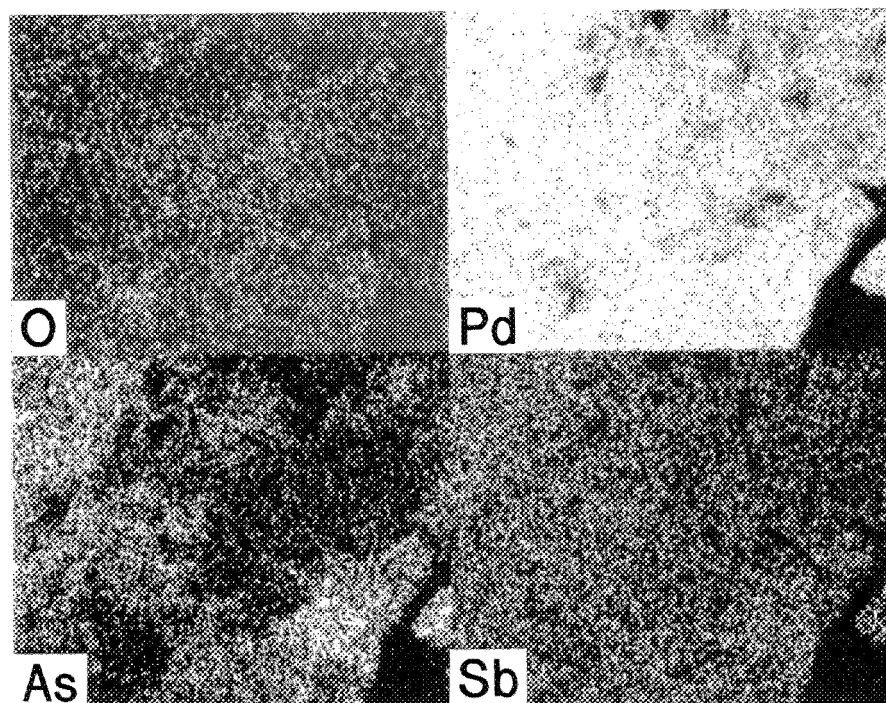


Figure 3.10. Single-element scans of Pd, As, Sb, and O for the area shown in Figure 3.9.

### 3.5 DISCUSSION

The palladium mineralization of the Corpo Y orebody in the Cauê iron mine was synchronous with the development of D1-structures. This interpretation is based on the presence of:

- (a) palladium-copper oxide in hematite bands stretched parallel to the ENE elongation lineation in the plane of S1-mylonitic foliation;
- (b) palladium-copper-oxide and palladium grains in quartz and white phyllosilicate boudins parallel to the S1-mylonitic foliation; and
- (c) palladium-copper oxide inclusions in gold strongly to weakly stretched parallel to the ENE elongation lineation.

The generation of the S1 mylonitic foliation was synchronous with the peak of thermal metamorphism at about 600° C. This temperature is based on oxygen isotope studies in hematite and quartz (Hoefs et al., 1982) and is in agreement with the metamorphic assemblages in the country rocks. The oxygen fugacities during the hydrothermal event, coeval with the peak of metamorphism, were as high as values equivalent to the hematite stability field; this finding is consistent with the hematitic composition of the iron-formation (itabirite, massive bodies of hematite, and jacutinga). Under these conditions, Pd and Au are readily transported as chloride complexes (Henley, 1973; Seward, 1984; Mountain and Wood, 1988; Gammons et al., 1992). The deposition of these metals may have occurred in response to an

increase in pH, resulting from mineralizing fluids reacting with the dolimitic itabirite host rock to produce jacutinga (Olivo et al., 1994). A complementary mechanism of Pd deposition may have been the saturation of Pd with selenide and arsenide-antimonide (Mountain and Wood, 1988, Wilde et al., 1989; Gammons et al., 1992). This would explain the palladium grain with a palladseite core and the occurrence of arsenopalladinite in jacutinga.

The physico-chemical conditions may have oscillated during the D1-shearing event. This interpretation is based on (1) the presence of Pd-Cu oxide occurring as inclusions with replacement (relict) textures in gold grains stretched parallel to S1 foliation and as gold-coated grains (without replacement textures) stretched parallel to the S1 foliation and (2) the presence of zoned palladium and the other hydrothermal minerals (e.g. tourmaline and monazite).

The occurrence of gold, either with palladium inclusions showing replacement textures, or as coatings on palladium minerals, could be tentatively explained as follows. Gold probably replaced palladium minerals during the oxidation of a previous palladium phase in response to local changes in the physico-chemical conditions. If this occurred, the palladium, replaced by gold, may have been reprecipitated as palladium-copper oxide or palladium close to the site of replacement, and gold was probably deposited as a coating on the new palladium minerals. In Figure 3.5, the gold coating around the stretched palladium oxide grain is wide in the pressure

shadow regions, suggesting that the gold coating, as well as the palladium minerals, was deposited during the formation of the S1-mylonitic foliation.

The above features also suggest that palladium-copper oxide formed during the shear-related hydrothermal mineralizing event and not by oxidation of earlier palladium minerals as result of weathering processes.

### 3.6 CONCLUSIONS

Palladium minerals in the jacutinga samples (palladium, palladseite, and palladium-copper oxide) are parallel to the S1 mylonitic foliation and/or the elongation lineation. They are commonly coated with films of gold and textural features suggested that they were deposited during the same deformational event. The S1-mylonitic foliation was synchronous with the peak of thermal metamorphism (approximately 600 C), and the oxygen fugacities during this event were as high as the hematite stability field. Under these conditions, palladium and gold are favourably transported as chloride complexes. Deposition of these metals may have been prompted by an increase of pH due to mineralizing fluids reacting with dolomitic itabirite. Pd may also have been deposited following saturation with insoluble Pd-selenide and arsenide-antimonides (as indicated by the presence of palladseite and arsenopalladinite).

Textural and compositional studies of palladium and other hydrothermal minerals suggest that oscillations in the physico-chemical conditions of hydrothermal fluids occurred during the mineralizing event. Finally, the occurrence of arsenopalladinite and palladseite in jacutinga suggests that this rock is the most probable source of palladium minerals found in residual concentrates from the gold washing at Itabira reported by Cabri et al. (1974).

## REFERENCES

- Cabri, L. J., Clark, A. M., Chen, T. T. (1977). Arsenopalladinite from Itabira, Brazil, and from the Stillwater Complex, Montana. *Canadian Mineralogist* Vol. 15, 70-73.
- Clark, A. M., Criddle, A. J., and Fejer, E. E. (1974). Palladium arsenide-antimonides from Itabira, Minas Gerais, Brazil. *Mineralogical Magazine*, vol. 39, 528-543.
- Davis, R. J., Clark, A. M., Criddle, A. J. (1977). Palladseïte, a new mineral from Itabira, Minas Gerais, Brazil. *Mineralogical Magazine*, vol. 41, 123.
- Gammons, C. H., Bloom, M. S. and Yu, Y. (1992) Experimental investigations of the hydrothermal geochemistry of platinum and palladium: I. Solubility of platinum and palladium sulfide minerals in NaCl/H<sub>2</sub>SO<sub>4</sub> solutions at 300 ° C. *Geochim. Cosmochim Acta*, 56, 3881-3894.
- Henley, R. W. (1973) Solubility of gold in hydrothermal chloride solutions. *Chemical Geology*, 11, 73-87.
- Hoefs, J., Muller, G., and Schuster, A. K. (1982) Polymetamorphic relations in iron ores from Iron Quadrangle, Brazil: the correlation of oxygen isotope variations with deformation history. *Contrib. Mineral. Petrol.*, 79, 241-251.
- Ineson, P. R. (1989) Introduction to practical ore microscopy. Longman Earth Science Series, John Wiley & Sons, Inc., New York, 181 pp.
- Jedwab, J., Cassedanne, J., Criddle, A. J., Ry P., Ghysens, G., Meisser, N., Piret, P., and Stanley, C. J. (1993) Rediscovery of palladinite PdO from Itabira (Minas Gerais, Brazil) and from Ruwe (Shaba, Zaire). *Abstract Supplement n. 3, Terra Nova*, 5: p. 21
- Leao de Sá, E. and Borges, N. R. A. (1991) Gold mineralization in Cauê and Conceição iron ore mines, Itabira-MG. Field guide book of Brazil Gold'91: An international symposium on the geology of gold. (Fleisher, R., Grossi Sad, J.H., Fuzikawa, K., Ladeira, E. A. eds.), pp. 74-85.
- Mountain, B. W. and Wood, S. A. (1988) Chemical controls on the solubility, transport, and deposition of platinum and palladium in hydrothermal solutions: a thermodynamic approach. *Econ. Geol.*, 83, 492-510
- Olivo, G. R., Gauthier, M., Bardoux, M. (1994) Palladium gold from the Cauê iron mine, Itabira District, Minas Gerais- Brazil. *Mineralogical Magazine* (in press).

Olivo, G. R., Gauthier, M., Bardoux, M., Leao de Sá, E., Fonseca, J. T. F., Santana, F. C. (in press) Palladium-bearing gold deposit hosted by Proterozoic Lake Superior-type iron-formation at Cauê iron mine, Itabira district, Southern São Francisco Craton, Brazil: geologic and structural controls. *Economic Geology* (in press).

Seward, T. M. (1984) The transport and deposition of gold in hydrothermal systems. In *Proceedings of the Symposium Gold'82: the geology, geochemistry and genesis of gold deposits* (Foster, R. P., ed.). A. A. Balkema, Rotterdam, pp. 165-181.

Wilde, A. R., Bloom, A. S., and Wall, V. J. (1989) Transport and deposition of gold, uranium and platinum-group elements in unconformity-related uranium deposits. *Econ. Geol. Monogr.* 6, 637-660.

## **CHAPTER IV**

### **LEAD ISOTOPE DETERMINATIONS IN THE IRON-FORMATION AND AMPHIBOLITE OF THE CAUE MINE, ITABIRA DISTRICT, BRAZIL: TECTONIC AND METALLOGENIC IMPLICATIONS**

#### 4.1 INTRODUCTION

The Itabira District is one of the most productive Brazilian iron ore districts with an annual production of  $5.0 \times 10^6$  t of high grade ore and concentrates (Leao de Sá and Borges, 1991). In addition to iron, both gold and palladium have been selectively extracted as byproducts in the Cauê and Conceição mines. The estimated gold reserves are 100 000 t of ore at 30 g/t Au, and the annual production is approximately 500 Kg of palladium-bearing gold bullion (L.P. Andrade, pers. communication, 1993).

Due to the rarity of this type of iron-formation-hosted palladium-bearing gold deposits, little is known about their genesis. Knowledge of the timing of palladium-gold deposition, based on geological, structural and geochronological data, is of fundamental importance for understanding their genesis. In this context, Pb isotopes are a preferred tool because (a) traces of Pb are frequently present in ore-bearing minerals, and (b) traces of U in the ore-bearing minerals may allow the in situ growth of radiogenic Pb and thereby enables Pb-Pb isochrons to be defined as proposed by Carignan et al. (1993).

In this paper, the results of the Pb isotope study of the Cauê mine rocks are reported and discussed together with geological and structural data in order to determine the timing of gold-palladium deposition, and to place the mineralizing event in a regional tectonic framework.

#### 4.2 REGIONAL GEOLOGIC SETTING

The Cauê iron mine lies in the Itabira District at the northeastern end of the Quadrilátero Ferrífero in the southern São Francisco Craton (Fig. 4.1, Dorr and Barbosa, 1963; Chemale and Quade, 1986).

Four major lithostratigraphic units, which are well studied in the Quadrilátero Ferrífero sector, are present in the southern part of the São Francisco Craton (Fig. 4.1, Dorr and Barbosa, 1963; Dorr, 1969; Schorscher et al., 1982): (1) the Archean granite-gneiss complex (up to 3.28 Ga, Machado and Noce, 1993); (2) the Archean (2772 to 2776 Ma) volcano-sedimentary Rio das Velhas Supergroup (Machado et al., 1992; Machado and Noce, 1993); (3) the Early Proterozoic (2.6 to 2.4 Ga) Minas supergroup (Babinski et al., 1993), the overlying metasedimentary sequence that hosts the iron and the palladium-bearing gold deposits discussed in this paper; and (4) the Middle Proterozoic metasedimentary Espinhaço Supergroup, containing minor 1700 Ma potassic volcanic rocks (Dossin et al., 1993). All these units are cut by

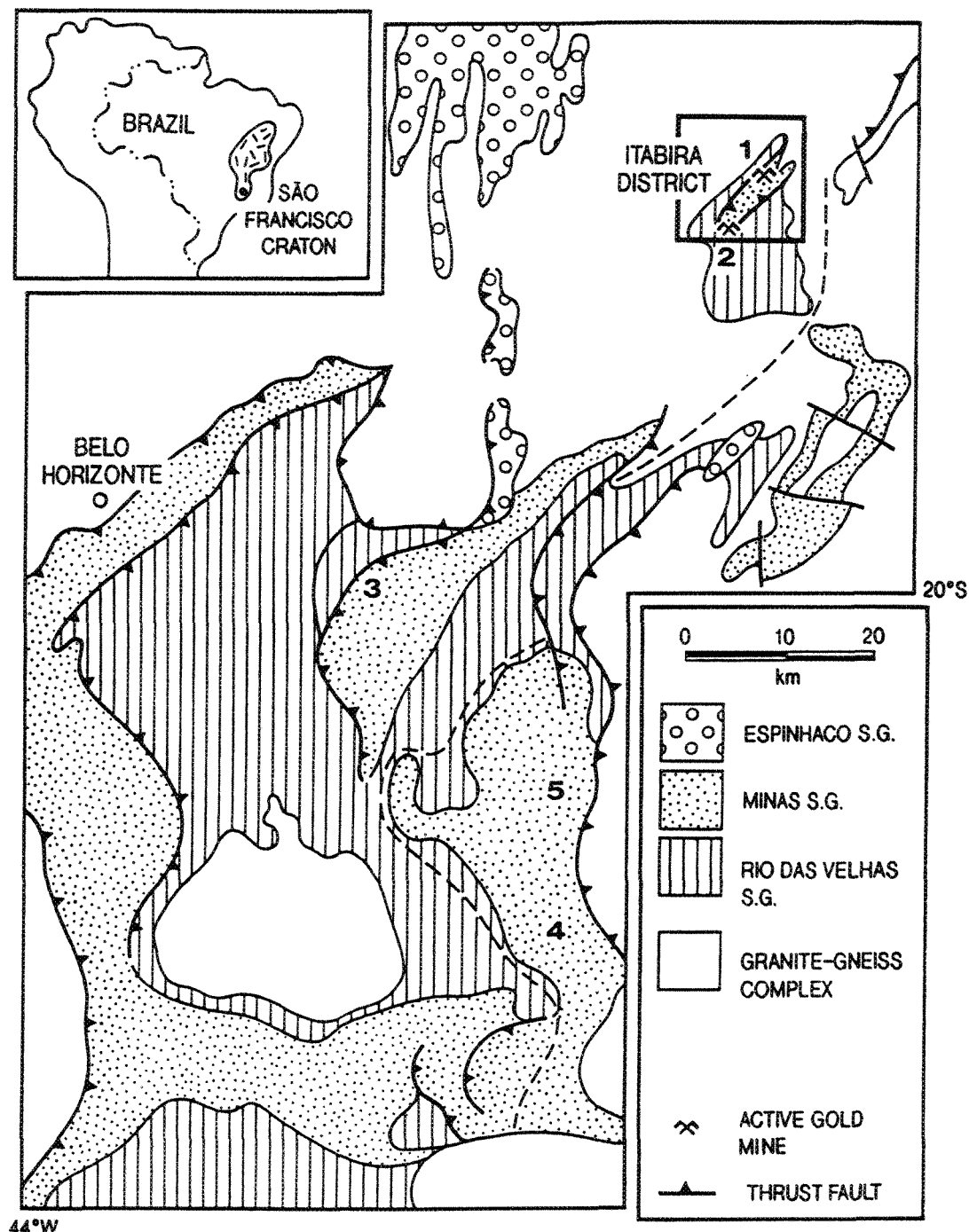


Figure 4.1. Schematic geologic map of the southern part of the São Francisco Craton (modified after Dorr and Barbosa, 1963; Schorscher et al., 1982; Dorr, 1969; Ladeira, 1991) showing the gold mines hosted by Lake Superior-type iron-formation in the Itabira District: 1= Cauê, 2= Conceição, 3= Congo Soco, 4= Maquiné, 5= Pitangui.

several types and generations of intrusive rocks ranging in age from Archean to late Proterozoic (Teixeira and Figueiredo, 1991).

According to Teixeira and Figueiredo (1991), the southern part of the Sao Francisco Craton was fully cratonized by the end of the Transamazonian Orogeny, at 1.9-1.8 Ga ago. The Transamazonian tectonic deformation affecting the western part of the southern Sao Francisco Craton produced isoclinal recumbent folds and thrust-fault imbrications (Fig. 4.1, Rosière, 1981; Hoppe et al., 1987). In the eastern portion of the Sao Francisco Craton (Fig. 4.1), parautochthonous and allochthonous nappes, comprising the Itabira District discussed herein, were thrusted towards the west and northwest (Hoefs et al., 1982; Schorscher et al., 1982; Belo de Oliveira, 1986; Belo de Oliveira and Teixeira, 1990). The relative age of these structures is not yet well established, they are considered to be Early Proterozoic by Schorscher et al. (1982) and Late Proterozoic by Belo de Oliveira and Teixeira (1990).

Metamorphic grade in southern Sao Francisco Craton increases from west to east from greenschist to granulite facies (Schorscher, 1975; Hoefs et al., 1982).

## 4.3 CAUÊ MINE GEOLOGY AND SAMPLING

### 4.3.1 Geologic Units

Three geologic units, mafic intrusive rocks, and tectonically imbricated slices of amphibolite were identified (Fig. 4.2, Olivo et al., in press): (1) a volcano-sedimentary sequence, correlated with the Archean Rio das Velhas Supergroup in the Quadrilátero Ferrífero; (2) an iron-formation unit, referred to as the Cauê Formation of the Itabira Group (part of the Early Proterozoic Minas Supergroup); and (3) a quartzite unit, correlated with the Piracicaba group of the Minas Supergroup. With the exception of intrusive contacts, all contacts between the various units are structural and coincide with thrust faults.

This study concentrates on the iron-formation unit and on the amphibolite. The latter is tectonically imbricated into the former.

The iron-formation unit comprises itabirite and jacutinga, which we analyzed in this study, and several compact hematite bodies. Itabirite is composed of alternating centimeter- to millimeter-wide bands of specular-hematite and hematite with relict magnetite, as well as quartz bands containing trace amounts of white phyllosilicates. Jacutinga, which is a hydrothermally-altered itabirite, hosts the palladium-gold mineralization.

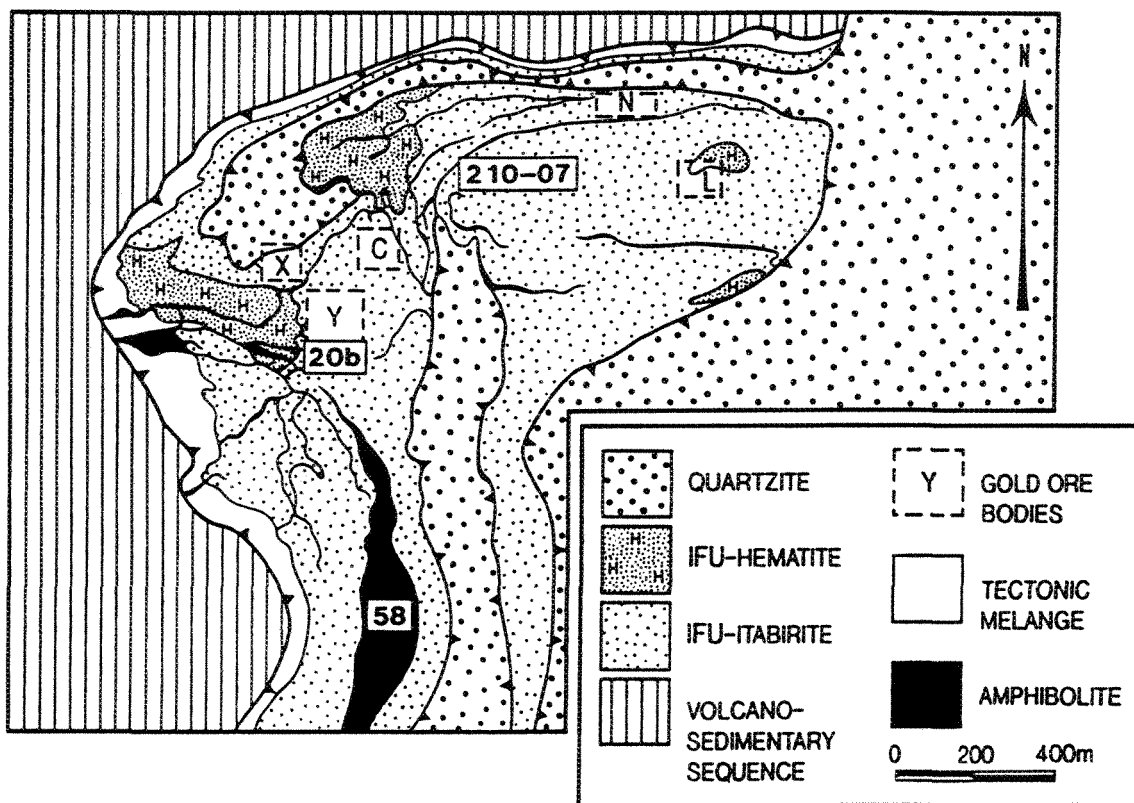


Figure 4.2 . Simplified geologic map of the Cauê mine (modified after Leao de Sá and Borges, 1991), showing the palladium-bearing gold ore bodies (Y= Corpo Y, X= Corpo X, C= Central, L= Aba Leste, and N= Aba Norte) with locations of samples analyzed in this paper. The open pit of the Cauê iron mine corresponds to itabirite and hematite (iron-formation unit) outcrop.

The tectonically imbricated slices of amphibolite are composed of hornblende, plagioclase, quartz, and ilmenite with hematite intergrowths. Close to the fractures and faults, hornblende grains are replaced by biotite, and biotite by chlorite; ilmenite is replaced by rutile. Also in these sites, plagioclase grains are partially altered to epidote, and carbonate; late muscovite and trace amounts of chalcopyrite and pyrrhotite were also noted.

#### 4.3.2 Structure

The Cauê mine rocks were affected by three phases of deformation (Olivo et al., *in press*). D1-structures are represented by tight and isoclinal folds which become sheath folds where the ENE elongation lineation (Le) and the mylonitic foliation (S1) are well developed. The specular hematite, quartz and gold samples, which were analyzed in this study, occur parallel to S1 in zone of high strain. Hornblende and ilmenite of tectonically imbricated slices of amphibolite were rotated parallel to S1. These minerals were also analyzed. D2-structures include tight folds and the S2 foliation, which was mainly developed in the northern sector. Elsewhere D2 only transposed S1 foliation without development of S2 foliation.

D3 structures are open folds (F3) with an associated N-S S3 crenulation cleavage. The L3 crenulation lineation is associated with this fold phase and trends

broadly N-S with a moderate to horizontal plunge. N-S-oriented meter- to centimeter-scale talc-hematite-quartz veins were also generated during D3 folding.

Thrust faults repeat and truncate geologic units and forms several imbricated sheets (Fig. 4.2). These faults are interpreted to be syn-D1 features (Olivo et al., in press). These structures were reactivated during D2 and D3 events as indicated by E-W and late N-S lineations on fault surfaces.

Refolding of macroscopic D1 folds by D2 folds generated complex fold interference patterns (Fig. 4.2) that have no similarity to the classical interference patterns described by Ramsay (1967) and Thiessen (1986). Instead, the D1-D2 interference patterns are more analogous to that observed in ductile shear zones that have undergone progressive non-coaxial shear (Berthé and Brun, 1980; Cobbold and Quinquis, 1980; Goscombe, 1991).

#### 4.3.3 Metamorphism

Oxygen isotope data on quartz and hematite parallel to S1 foliation from the itabirite of the Cauê mine indicate an average metamorphic temperature of 610° C. This is consistent with data obtained from similar rocks of the Conceição and Dois Córregos mines in the Itabira District (Hoefs et al., 1982), as well as from the metamorphic assemblage described in the country rocks (Schorscher et al., 1982).

The amphibolite slices exhibit in the most fresh samples mineral assemblages diagnostic of amphibolite facies.

#### 4.4.4 Palladium-bearing Gold Orebodies

At present five gold orebodies have been mined at the Cauê mine (Fig. 4.2, Olivo et al., in press). All orebodies are hosted by jacutinga. Higher gold grades (up to 1000 g/t; Leao de Sá and Borges, 1991) are associated with hematite- and quartz-rich bands parallel to S1 mylonitic foliation and/or stretched parallel to the ENE elongation lineation (Olivo et al., in press). The samples from jacutinga mentioned in this paper are from the Corpo Y orebody.

In the Corpo Y, jacutinga comprises millimetric to centimetric bands of various concentrations of quartz, specular hematite, hematite with relict magnetite (+/- goethite), and white phyllosilicates, with minor amounts of tourmaline, apatite, and monazite. Carbonate is common as inclusions in quartz grains.

Gold is palladium bearing (up to 20% Pd) and occurs as: (1) free grains and inclusions in rotated tourmaline hosted by hematite bands located in the cores of dismembered sheath folds; (2) free grains in S1 mylonitic foliation planes of hematite bands; (3) grains stretched parallel to the Le; and (4) free grains or inclusions in boudinaged quartz bands (Olivo et al., 1994).

#### 4.4 TECTONIC REGIME AND RELATIVE TIMING OF PALLADIUM-GOLD MINERALIZATION

Detailed mapping and petrographic studies of the Corpo Y palladium-bearing gold orebody suggest that the mineralizing event was contemporaneous with D1 deformation (Olivo et al., 1994). D1 deformation was ductile and non-coaxial with high bulk shear strain, and was synchronous with the peak of thermal metamorphism (Olivo et al., in preparation). During the D1 event, the iron-formation unit was detached from the underlying sequence along décollement surfaces as indicated by (a) the thrust-faulted contacts with the adjacent volcano-sedimentary sequence, and (b) the interruption of mafic intrusive bodies at the contact between the iron-formation unit and the underlying volcano-sedimentary sequence (Fig. 4.2).

The sense of tectonic transport during D1 (and probably D2) is consistently east-over-west throughout the iron-formation unit (Olivo et al., in press). This is in agreement with the regional transport of parautochthonous and allochthonous nappes of the Minas Supergroup, which were not yet dated (Schorcher et al., 1982; Belo de Oliveira and Teixeira, 1990).

#### 4.5 ANALYTICAL TECHNIQUES FOR PB ISOTOPE DETERMINATIONS

Brief descriptions of the mineralogy and locations of samples used in this study are given in Table 4.1 and Figure 4.2.

All samples were crushed and sieved to a grain size of 100 to 200 µm. Mineral separation was accomplished using heavy liquids and a magnetic separator. Approximately 200-400 mg of hornblende, ilmenite, hematite, quartz and gold were handpicked under a binocular microscope and washed with distilled water in an ultrasonic bath.

Oxide minerals were powdered in a agate mortar and some aliquots were leached with hot HCl solutions. The supernatant were recovered for Pb isotope analyses before complete dissolution of the residues. Other aliquots of oxide minerals were completely dissolved, without separation of supernatant and residues, using hot HCl-HNO<sub>3</sub> solutions. Quartz grains were washed using HCl-HNO<sub>3</sub> solutions and completely dissolved using HF-HBr solutions. One hornblende aliquot was leached with HBr and HF solutions for 5 minutes and the residue was completely dissolved in a HNO<sub>3</sub>-HF-HCl solution. Another aliquot of hornblende was completely dissolved in a HNO<sub>3</sub>-HF-HCl solution, without separation of supernatant and residues. Gold grains were dissolved in a HCl-HNO<sub>3</sub> solution.

ROCKS	SAMPLES	$^{206}\text{Pb}/^{204}\text{Pb}$	$^{207}\text{Pb}/^{204}\text{Pb}$	$^{208}\text{Pb}/^{204}\text{Pb}$
<b>Itabirite</b> <b>(210-07)</b>	Mixed hematite (B)	59,712	19,851	38,736
	Mixed hematite (R)	65,929	20,100	38,630
	Mixed hematite (L)	40,675	18,259	38,454
	Specular hematite (R)	21,882	15,906	38,290
	Specular hematite (L)	41,502	18,240	38,081
	Quartz	22,721	16,308	38,954
<b>Jacutinga</b> <b>(20b)</b>	Mixed hematite (B)	45,643	17,680	39,249
	Mixed hematite (R)	64,053	18,822	40,457
	Mixed hematite (L)	29,043	16,773	38,679
	Specular hematite (R)	19,083	15,670	38,410
	Specular hematite (L)	27,109	16,642	37,474
	Gold	20,142	15,928	37,525
<b>Amphibolite</b> <b>(-58-)</b>	Hornblende (B)	16,728	15,354	38,255
	Hornblende (R)	18,300	15,616	38,180
	Hornblende (L)	17,826	15,554	38,247
	Ilmenite (B)	17,487	15,559	40,007
	Ilmenite (R)	17,663	15,541	40,001
	Ilmenite (L)	18,167	15,686	39,006

Table 4.1 Pb isotope results on minerals from the iron-formation and amphibolite samples of the Cauê mine (B= Bulk; L=Leachate; R= Residue).

Leaching treatments have been described by Carignan and Gariépy (1993) and Carignan et al. (1993) and the purpose is to maximize the spread of the Pb ratios in the isochron diagram in order to obtain better age precision. Lead separation was done according to the technique described in Manhès et al. (1980), and the isotopic compositions were determined on a VG SECTOR thermal ionization mass spectrometer. Total blanks were at less than 50 picograms and negligible. The  $2\sigma$  uncertainties are 0.10, 0.15 and 0.20 percent for the  $^{206}\text{Pb}/^{204}\text{Pb}$ ,  $^{207}\text{Pb}/^{204}\text{Pb}$ , and  $^{208}\text{Pb}/^{204}\text{Pb}$  ratios, respectively, and the applied fractionation corrections were 0.09 and 0.24 percent  $\text{amu}^{-1}$  for the Faraday and Daly detectors, respectively. All regressions were calculated according to the method of York (1969) and the decay constants of Steiger and Jäger (1977). All errors were quoted at the 95 percent of confidence level.

## 4.6 RESULTS

### 4.6.1 Amphibolite

Leachates, residues and bulk analyses of hornblende yield  $^{206}\text{Pb}/^{204}\text{Pb}$  ratios between 16.73 to 18.30,  $^{207}\text{Pb}/^{204}\text{Pb}$  between 15.35 to 15.62, and  $^{208}\text{Pb}/^{204}\text{Pb}$  between 38.18 to 38.26 (Table 4.1). Leachates, residues and bulk analyses of ilmenite from the same sample yield comparable composition for  $^{206}\text{Pb}/^{204}\text{Pb}$  and  $^{207}\text{Pb}/^{204}\text{Pb}$  ratios,

but the  $^{208}\text{Pb}/^{204}\text{Pb}$  ratios are more radiogenic and range from 39.07 to 40.01 (Table 4.1).

The results for ilmenite and hornblende are positively correlated in the  $^{207}\text{Pb}/^{204}\text{Pb}$  vs.  $^{206}\text{Pb}/^{204}\text{Pb}$  diagram (Fig. 4.3) with a slope of  $0.1807 \pm 0.0161$  (Mean squares weighted deviation (MSWD)= 4.5), corresponding to an age of  $2.7 \pm 0.6$  Ga. The large error is due to both the small spread of the data and the deformation, metamorphism and alteration processes under which these rocks were submitted during and after their tectonic emplacement. The data are not correlated in  $^{208}\text{Pb}/^{204}\text{Pb}$  diagram, suggesting a large variation of the Th/U ratios between different minerals.

#### 4.6.2 Iron-formation

Leachates, residues and bulk analyses of hematites and quartz from itabirite yield  $^{206}\text{Pb}/^{204}\text{Pb}$  ratios varying from 21.88 to 65.93,  $^{207}\text{Pb}/^{204}\text{Pb}$  from 15.91 to 20.10, and  $^{208}\text{Pb}/^{204}\text{Pb}$  from 38.08 to 38.95 (Table 4.1). The aliquots of hematites, gold from jacutinga yield  $^{206}\text{Pb}/^{204}\text{Pb}$  and  $^{207}\text{Pb}/^{204}\text{Pb}$  ratios comparable to the itabirite samples, however  $^{208}\text{Pb}/^{204}\text{Pb}$  ratios are more radiogenic and range between 37.47 to 40.46 (Table 4.1).

The highest Pb isotopic ratios correspond to the residues and bulk analyses of mixed populations of specular hematite and hematite pseudomorphous of

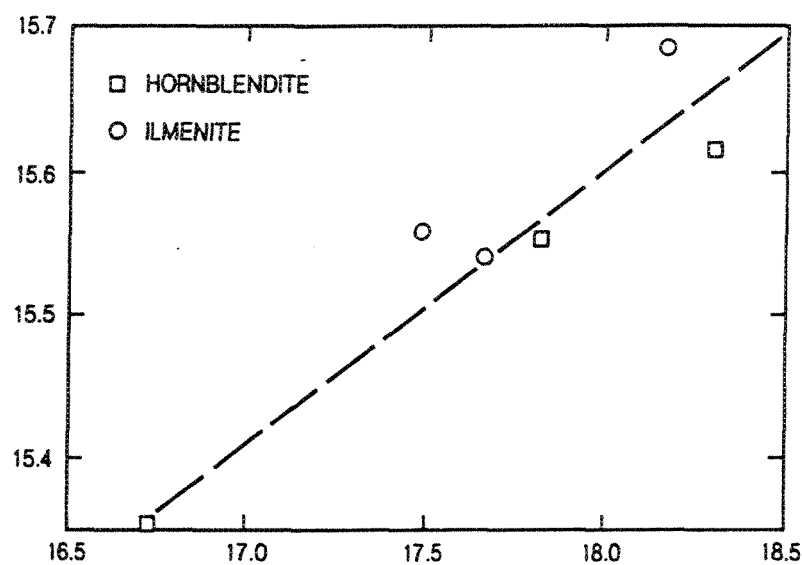


Figure 4.3.  $^{207}\text{Pb}/^{204}\text{Pb}$  vs  $^{206}\text{Pb}/^{204}\text{Pb}$  diagram showing data on minerals from amphibolite of the Cauê mine. Hornblende and ilmenite yield an age of  $2.7 \pm 0.6$  Ga.

magnetite. This mixed hematite population is also more radiogenic than the leachates of specular hematite from the same sample. This may due to the fact that hematite pseudomorphs after magnetite grains in itabirite and jacutinga samples show relicts of magnetite in polished section, which suggests that the replacement of magnetite by hematite was not completed during deformation events. Excluding these more radiogenic data from the regression calculation, the data define are collinear in the  $^{207}\text{Pb}/^{204}\text{Pb}$  vs.  $^{206}\text{Pb}/^{204}\text{Pb}$  diagram (Fig. 4.4) with a slope of  $0.1140 \pm 0.0059$ , that would correspond to an age of  $1.9 \pm 0.2$  Ga (MSWD= 0.62). The data are not correlated in the  $^{208}\text{Pb}/^{204}\text{Pb}$  diagram, probably due to the large variation of the Th/U ratios both between and within different minerals.

## 4.7 DISCUSSION AND CONCLUSIONS

### 4.7.1 Amphibolite

The ilmenite-hornblende isochron, corresponding to an age of  $2.7 \pm 0.6$  Ma, means that the amphibolite is a slice of Archean basement and precludes the possibility this rock represents a younger intrusive event as was suggested by Leao de Sá and Borges (1991). In the Itabira District, amphibolites older than the iron-formation unit have been reported by Chemale et al. (1987) as part of the volcano-sedimentary sequence which is correlated with the Archean Rio das Velhas Supergroup of the Quadrilátero Ferrífero. This is the first time that Archean rocks are

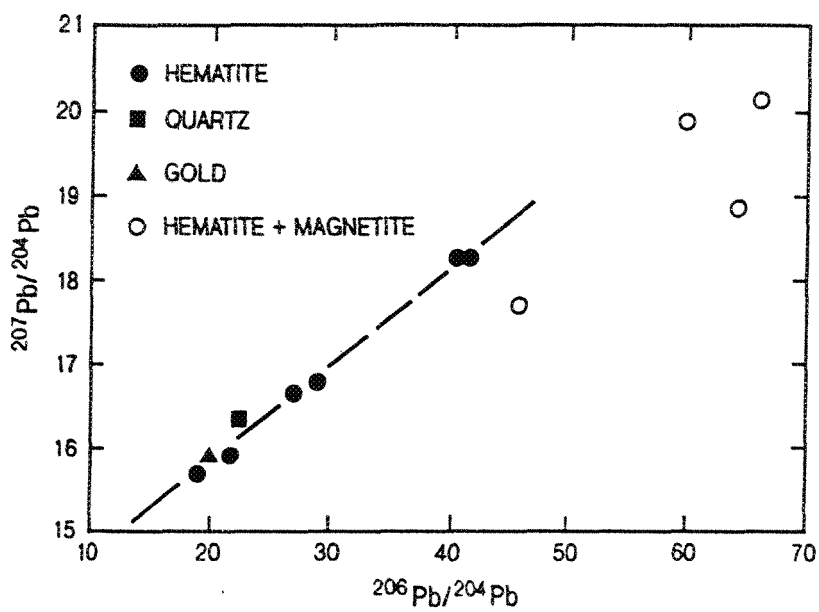


Figure 4.4.  $^{207}\text{Pb}/^{204}\text{Pb}$  vs  $^{206}\text{Pb}/^{204}\text{Pb}$  diagram showing data on minerals from the iron-formation of the Cauê mine. An age of  $1.9 \pm 0.2$  Ga is obtained for hematite, quartz and gold, when the most radiogenic residues and bulk analysis of samples with relict of magnetite are omitted from the regression.

dated in the Itabira District, and it unequivocally demonstrates the presence of Archean basement in this sector of the São Francisco Craton.

#### **4.7.2 Iron-formation and associated palladium-bearing mineralization**

The occurrence of free palladium-bearing gold grains stretched parallel to S1-foliation provided an exceptional opportunity to directly date the ore. The isochron of the  $1.9 \pm 0.2$  Ga is a good estimation of the age of palladium-bearing gold mineralization which is contemporaneous with D1-shearing and thrusting and with the peak of thermal metamorphism. This result is in agreement with the age of the metamorphism of the Minas Supergroup in the Quadrilátero Ferrífero (Babinski et al., 1991), and corresponds with the Transamazonian orogenesis in the southern part of the São Francisco Craton (Teixeira and Figueiredo, 1991; Machado and Noce, 1993). The fact that the Pb-Pb age for palladian gold quartz and hematite is younger than the age of the sedimentation of the Minas Supergroup (2.4-2.6 Ga, Babinski et al., 1993) confirms that this type of mineralization is epigenetic.

Other gold deposits hosted by the Minas Supergroup in the southern São Francisco craton, such as the Congo Soco, Maquiné, Pitangui, and Conceição deposits (Fig. 4.1, Bensusan, 1929; Ladeira, 1991; Leao de Sá and Borges, 1991), have some similarities with the Cauê mine: (1) they are close to the faulted contact between the Minas supergroup and the Archean terrains; (2) they are hosted by jacutinga; (3) they are structurally controlled by the approximately east-trending

elongation lineation; and (4) they are palladium bearing. These similarities suggest that the palladium-gold mineralization was a widespread process associated with the tectonic transport of the Minas sequence during the Transamazonian orogenesis.

Although the Late Proterozoic Brasiliano orogenesis reset K-Ar systems in micas of granitic gneiss, in this part of the Itabira District (Herz, 1970), the silicates, gold, and oxides (with exception of the relict magnetite), were able to preserve the Early Proterozoic age resulted of in situ growth of radiogenic Pb from U-decay. This observation suggests that the closure temperatures for U and Pb diffusion in these mineral species is higher than for Ar diffusion in micas.

In addition, this study highlights the importance of careful sample selection based on textural and morphological criteria in order to avoid meaningless data from multigrain analysis (e.g. mixed populations of specular hematite and hematite with relict magnetite).

## REFERENCES

- Babinski, M., Chemale, F., Jr., and Schmus, W. R., 1993, A idade das formações ferríferas bandadas do Supergrupo Minas e sua correlação com aquelas da África do sul e Austrália: In Anais do Segundo Simpósio do Cráton do São Francisco, p. 152-153
- Babinski, M., Van Schmus, W. R., Chemale, F., Jr., 1991, Pb/Pb Geochronology of Carbonate Rocks of Minas Supergroup, Quadrilátero Ferrífero, Minas Gerais, Brazil. AGU 1991 Fall Meeting Program and Abstract, December 9-13, 1991, p. 53
- Belo de Oliveira, O. A., 1986, As falhas de Empurrao e suas implicações na Estratigrafia e Metalogenia do Quadrilátero Ferrífero: Congresso Brasileiro Geologia, 35, Goiânia, v. 5, p. 15.
- Belo Oliveira, O. A., and Teixeira, W., 1990, Evidências de uma tectônica tangencial Proterozóica no Quadrilátero Ferrífero: Congresso Brasileiro de Geologia, 36, Natal, v. 6, p. 2589-2604.
- Bensusan, J. A., 1929, Auriferous Jacutinga Deposits: Institute of Mining and Metallurgy Bulletin, n. 300, v. 8, p. 1-25
- Berthé, D., and Brun, J. P., 1980, Evolution of folds during progressive shear in the South American Shear zone, France: Jour. Structural Geology, v. 2, p. 127-133.
- Carignan, J. and Gariépy, C., 1993, Pb isotope geochemistry of the Silidor and Launay gold deposits: implications for the source of Archean Au in the Abitibi subprovince: ECON. GEOL., v. 88, p. 1722-1730.
- Carignan, J., Machado, N., and Gariépy, C., 1993, Pb isotope composition of Ni-Cu-Pb ore deposits in an Archean greenstone belt: evidence for Proterozoic remobilization in the Pontiac subprovince of Canada: ECON. GEOL., v. 88, p. 709-715.
- Chemale F., Jr., and Quade, H., 1986, Estratigrafia e Geologia Estrutural do Distrito Ferrífero de Itabira: Congresso Brasileiro de Geologia, 34, Goiânia, v. 2, p. 987-998.
- Chemale, F., Quade, H., and Carbonari, F. S., 1987, Economic and structural geology of the Itabira iron district, Minas Gerais, Brazil: Zentralblatt fuer Geologie und Paläontologie; Teil I: Allgemeine Angewandte, Regionale und Historische Geologie, v. 7-8: p. 743-752.

- Cobbold, P. R., and Quinquis, H., 1980, Development of sheath folds in shear regime: *Jour. Structural Geology*, v. 2, p. 119-126.
- Dorr, J. V. N. II, 1969, Physiographic, stratigraphic and structural development of Quadrilatero Ferrifero, Minas Gerais, Brazil: U. S. Geol. Survey Prof. Paper, 641: 1-110.
- Dorr, J. V. N. II, and Barbosa, A. L. M., 1963, Geology and ore deposits of the Itabira district, Minas Gerais, Brazil: U. S. Geol. Survey Prof. Paper, 341-C, 110p.
- Dossin, T. M., Dossin, I. A., Charvet, J., Cocherie, A. and Rossi, P., 1993, Single-zircon dating by step-wise Pb-evaporation of middle Proterozoic magmatism in the Espinhaço range, southeastern São Francisco Craton (Minas Gerais, Brazil)
- Goscombe, B., 1991, Intense non-coaxial shear and the development of mega-scale sheath folds in the Arunta Block, Central Australia: *Jour. Structural Geology*, v. 13, 299-318.
- Herz, N., 1970, Gneissic and Igneous Rocks of the Quadrilátero Ferrífero, Minas Gerais, Brazil: Geol. Survey Prof. Paper 641-B, 60p.
- Hoefs, J., Muller, G., and Schuster, A. K., 1982, Polymetamorphic Relations in Iron Ores from Iron Quadrangle, Brazil: The Correlation of Oxygen Isotope Variations with Deformation History: *Contr. Mineralogy Petrology*, v. 79, p. 241-251.
- Hoppe, A., Shobbenhaus, C., Walde, D. H. G., 1987, Precambrian Iron Formation in Brazil, in Appel, P. W. U., and LaBerge, G. L., eds., *Precambrian Iron-Formations*: Athens, Theophrastus Publications S.A., p. 347-390.
- Ladeira, E. A., 1991, Genesis of gold in Quadrilatero Ferrifero: a remarkable case of permanency, recycling and inheritance- A tribute to Djalma Guimaraes, Pierre Routhier and Hans Ramberg, in Ladeira, E. A., ed., *Brazil Gold'91: An International Symposium on the Geology of Gold*, Belo Horizonte, Elsevier, p. 11-30.
- Leão de Sá, E., and Borges, N. R. A., 1991, Gold mineralization in Cauê and Conceição iron ore mines - Itabira- MG, in Fleischer, R., Grossi Sad, J. H., Fuzikara, K., and Ladeira, E. A., eds., *Field guide book of Brazil Gold'91: An International Symposium on the Geology of Gold*, Belo Horizonte, p. 74-85.
- Machado, N. and Noce, C. M., 1993, A evolução do setor sul do Cráton do São Francisco entre 3.1 e 0.5 Ga baseada em geocronologia U-Pb. In *Anais do Segundo Simpósio do Cráton São Francisco*, p. 100-102.

- Machado, N., Noce, C. M., Ladeira, E. A., Belo de Oliveira, O., 1992, U-Pb Geochronology of Archean magmatism and Proterozoic metamorphism in the Quadrilatero Ferrifero, southern Sao Francisco craton, Brazil: *Geol. Soc. America Bull.*, v. 104, p. 1221-1227.
- Manhès, G., Allègre, C. J., Dupré, B., and Hamelin, B., 1980, Lead isotope study of basic-ultrabasic layered complexes: Speculations about the age of the earth and primitive mantle characteristics : *Earth Planet. Sci. Letters*, v. 47, p. 370-382.
- Olivo, G. R., Gauthier, M. and Bardoux, M. 1994, Palladian gold from the Cauê iron mine, Itabira District, Minas Gerais-Brazil. *Mineralogical Magazine (in press)*.
- Ramsay, J. G., 1967, *Folding and Fractures Rocks*: New York, McGraw-Hill, 568 p.
- Rosière, C. A., 1981, Strukturelle und texturelle Untersuchungen in der Eisenerzlagestätte Pico de Itabira bei Itabirito, Minas Gerais, Brasilien. Unpub. Ph.D. thesis, Univ. Clausthal, 303 p.
- Schorscher, H. D., 1975, Entwicklung des polymetamorphen präkambrischen raumes Itabira, Minas Gerais, Brasilien. Umpub. Ph.D. thesis, Univ. Heidelberg, 302p.
- Schorscher, H. D., Santana, F. C., Polônia, J. C., and Moreira, J. M. P., 1982, Rio das Velhas Greenstone Belt and Proterozoic rocks, Quadrilatero Ferrifero, Minas Gerais State, in *Excursion annex of International Symposium on Archaean and Early Proterozoic Geological Evolution and Metallogenesis*: Sociedade Brasileira de Geologia, Salvador, September, 3-11, p. 1-25.
- Steiger, R. H., and Jäder, E., 1977, Subcommission of geochronology: Convention on the use of decay constants in geo- and cosmo-chronology: *Earth Planet. Sci. Letters*, v. 36, p. 359-362.
- Teixeira, W., and Figueiredo, M. C. H., 1991, An outline of Early Proterozoic crustal evolution in the Sao Francisco craton, Brazil: a review: *Precambrian Research*, v. 53, p. 1-22.
- Thiessen, R., 1986, Two-dimensional refold interference patterns: *Jour. Structural Geology*, v. 8, p. 563-573.
- York, D., 1969, Least-squares fitting of a straight line with correlated errors: *Earth Planet. Sci. Letters*, v. 5, p. 320-324.

## **CHAPTER V**

**PALLADIUM-BEARING GOLD DEPOSIT HOSTED BY LAKE SUPERIOR-TYPE  
IRON-FORMATION AT CONCEICAO IRON MINE, ITABIRA DISTRICT,  
SOUTHERN SAO FRANCISCO CRATON, BRAZIL**

## 5.1 INTRODUCTION

The Conceição iron mine is located in the southwestern sector of the Itabira District, in the extreme south of the São Francisco Craton (Figs. 5.1 and 5.2). It is one of the most productive iron mines of the Itabira District, with an annual production capacity of 25 million tons of iron ore (CVRD, 1989).

Although Conceição is presently an important iron mine, in the 18th and 19th centuries, it was gold rather than iron that was mined in the Conceição Peak by Portuguese and English companies. Little is known of the development of the gold deposit during this time, and there is no record of their total production (Dorr and Barbosa, 1963). Henwood (in Dorr and Barbosa, 1963) stated that "a single pan of material from Conceição Peak yielded 17.21 troy pounds (6.42 Kg) of gold and that in 6 years 12,295.55 pounds (4,589 kg) of gold were extracted from ore mine in the Conceição area". English and Portuguese mining stopped when the water table level was reached (Leao de Sá and Borges, 1991). In 1985, the Companhia Vale do Rio Doce (CVRD) iron mining operations reached dewatering level in the Conceição mine

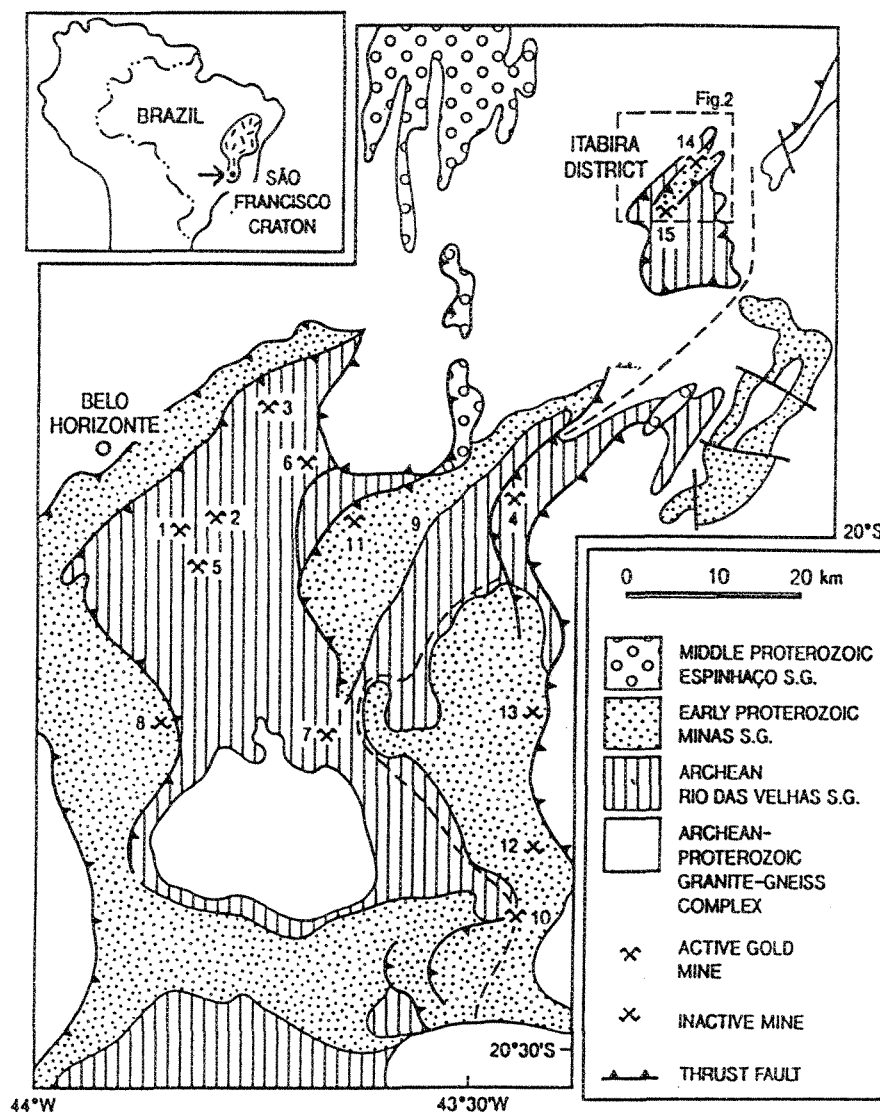


Figure 5.1 . Schematic geologic map of the southern part of the São Francisco Craton (modified after Dorr and Barbosa, 1963; Schorscher et al., 1982; Dorr, 1969; Ladeira, 1991), showing the main gold mines and occurrences hosted by: (a) Archean banded-iron-formation: 1= Morro Velho, 2= Raposos, 3=Cuiabá; 4= São Bento; (b) mylonitic Archean volcano-sedimentary rocks: 5= Bela Fama, 6= Juca Vieira, 7= Paciência; (c) Early Proterozoic Witwatersrand-type conglomerates: 8= Cata Branca, 9= Serra do Gandarela; (d) Early Proterozoic graphitic phyllite: 10= Passagem de Mariana; and (e) Lake Superior-type iron-formation: 11= Congo Soco, 12= Maquiné, 13= Pitangui, 14= Cauê, 15= Conceição. Dashed line= staurolite in isograd (modified after Hoefs et al., 1982).

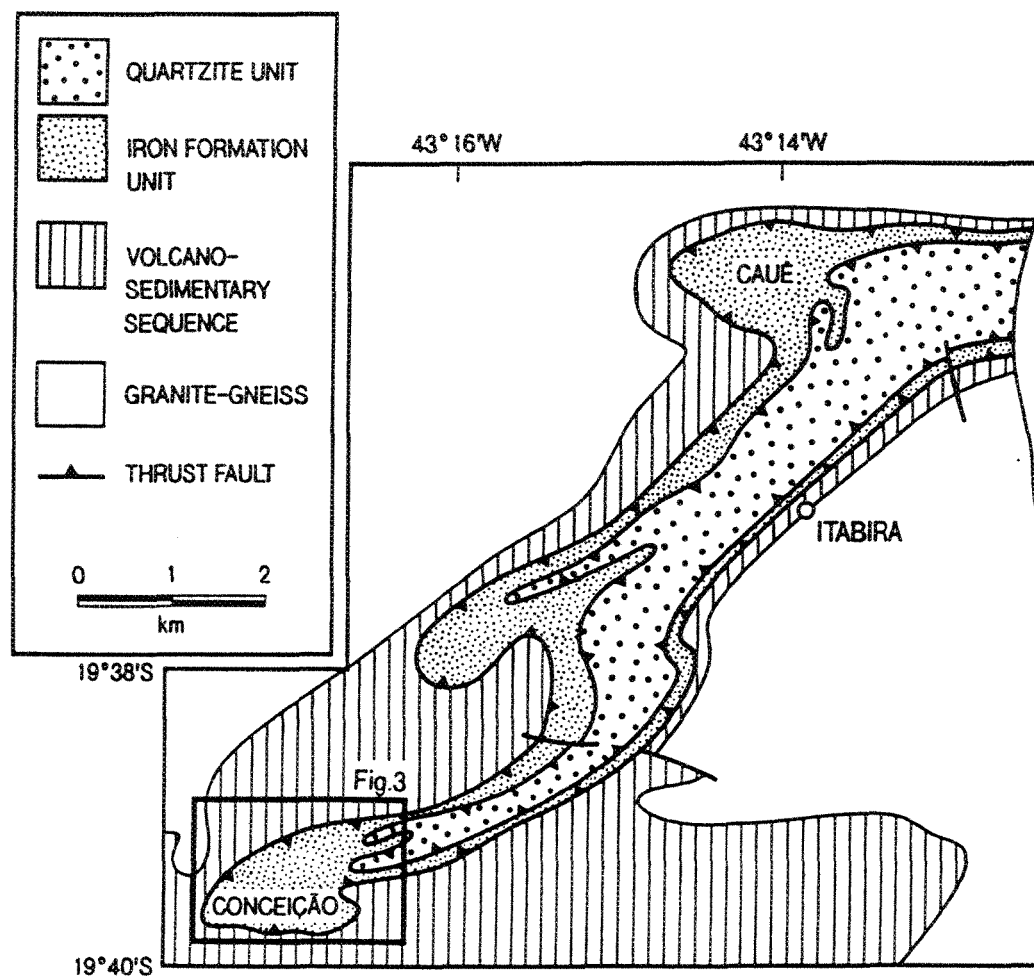


Figure 5.2. Simplified map of the Itabira District Map (modified after Dorr and Barbosa, 1963; Schorscher et al., 1982; Chemale and Quade, 1986). The iron mine open pits correspond to the northern and western sectors of the iron-formation unit which is complete outcrop.

exposing the gold orebody, which enabled its selective and intermittent extraction in the following year (Leao de Sá and Borges, 1991). Leao de Sá and Andrade (1990) reported that a total of 705 Kg of palladium-bearing gold was mined from 1987 to 1990 in the Conceição mine.

The purpose of this paper is to present the geological and structural framework, the hydrothermal alteration, the ore mineralogy, and the geochemical investigations of the Conceição palladium-bearing gold orebody for comparison to the Cauê palladium-bearing gold orebodies.

## 5.2 REGIONAL GEOLOGIC SETTING

The southern part of the São Francisco Craton comprises four major lithostratigraphic units (Fig. 5.1, Dorr and Barbosa, 1963; Dorr, 1969; Schorscher et al., 1982): (1) the Archean to Proterozoic Granite-gneiss Complex; (2) the Archean volcano-sedimentary Rio das Velhas Supergroup dated between 2772 to 2776 Ma (Machado et al., 1992); (3) the Early Proterozoic Minas Supergroup, an overlying metasedimentary sequence that hosts the Conceição gold deposit discussed in this communication; and (4) the Middle Proterozoic Espinhaço Supergroup, a metasedimentary sequence with minor metavolcanic rocks dated at 1700 Ma (Dossin et al., 1993). All these units are cut by several types and generations of intrusive rocks.

The Minas Supergroup, which hosts the gold Conceição deposit, consists of conglomerates, phyllites, Lake Superior-type iron-formations, carbonates, quartzites, and graywackes (Table 5.1; Dorr, 1969; Ladeira, 1991). Pb/Pb isochron ages for carbonates from the Gandarela Formation and the Piracicaba Group (Table 5.1; Babinski et al., 1991), and U/Pb ages (Machado et al., 1992) from the Quadrilátero Ferrífero suggest that deposition of the Minas Supergroup took place between 2.6 and 2.4 Ga (Babinski et al., 1993). The data also suggest that these rocks were metamorphosed at approximately 2.0 Ga (Babinski et al., 1991).

Metamorphic temperatures for the Minas Supergroup in the southern São Francisco Craton increase moving eastward, from 390° C to 710° C (Schorscher, 1975; Hoefs et al., 1982; Muller et al., 1982). A staurolite in/chloritoid out isograd oriented NNE-SSW has been mapped in the eastern part of this region (Fig. 5.1, Hoefs et al., 1982). Mineral reactions and oxygen isotope temperatures indicate amphibolite facies (> 600° C) transitional to granulite facies further east of the isograd (Hoefs et al., 1982).

The Transamazonic orogeny (c.a. 2 Ga) produced isoclinal recumbent folds and thrust faults causing imbrications within the Minas sequence in the western part of the São Francisco Craton (Fig. 5.1, Rosière, 1981; Hoppe et al., 1987). In the eastern part, parautochthonous and allochthonous nappes, involving the Itabira District discussed herein, were thrusted westward and northwestward (Hoefs et al.,

SUPERGROUP		FORMATION		LITHOLOGIES	ENVIRON- MENT	APPARENT THICKNESS (m)	COMMENTS
GROUP		SABARA					
MINAS		PIRACICABA		Chorite schist and phyllite, metatuff, graywacke, tilloid, conglomerate, quartzite, minor iron-formation	Molasse (?)	3,000	detrital zircon U/Pb age 2,125 +/- 4 Ma (Machado et al., 1992)
CARAÇA		ITABIRÁ		LOCAL EROSIONAL UNCONFORMITY			
MOEDA	CANDARELA	FECHO DO FUNIL	TABOES	Phyllite and graphitic phyllite	Stable shelf	150	Pb/Pb isochron age 2,050 (+/- 230) Ma (Babinski et al., 1991)
	CAUÉ	CERCADINHO	BARREIRO	Orthoquartzite	Stable shelf	125	
BATATAL				Quartzose phyllite, dolomitic phyllite, siliceous dolomite	Stable shelf	410	
				Quartzite and phyllite, minor conglomerate and dolomite	Stable shelf	600	
SABARA		LOCAL EROSIONAL UNCONFORMITY					
ITABIRÁ	CANDARELA	LOCAL EROSIONAL UNCONFORMITY		Dolomite and minor limestone, dolomitic itabirite, itabirite, dolomitic phyllite	Stable shelf	600	Pb/Pb isochron age 2,420 +/- 25 Ma (Babinski et al., 1991)
	CAUÉ	LOCAL EROSIONAL UNCONFORMITY		Itabirite (oxide-facies iron-formation), dolomitic itabirite, minor phyllite and dolomite	Stable shelf	350	Host unit of palladium-bearing gold deposits
BATATAL		LOCAL EROSIONAL UNCONFORMITY		Phyllite, slightly graphitic phyllite, minor metachert and iron-formation	Stable shelf	250	Host unit of the Passagem de Mariana Gold Deposit
	MOEDA	LOCAL EROSIONAL UNCONFORMITY		Paralic facies: orthoquartzite, conglomerate, phyllite; Blanket facies: sericitic quartzite, quartzose phyllite, quartzite	Stable shelf	1000 150	Witwatersrand-type gold deposits

Table 5.1 The stratigraphic column of the Early Proterozoic Minas Supergroup.

1982; Muller et al., 1982, Shorscher et al., 1982; Belo de Oliveira, 1986; Belo de Oliveira and Teixeira, 1990). Although the relative age of these structures is not yet established, they are considered to be Early Proterozoic by Shorscher et al. (1982) or Late Proterozoic by Belo de Oliveira and Teixeira (1990).

### 5.3 CONCEIÇÃO MINE GEOLOGY

#### 5.3.1 Geological units

The Conceição mine consists of three metamorphosed lithostratigraphic units (from bottom to top; Figs. 5.3, ): (1) a volcano-sedimentary sequence, correlated with the Archean Rio das Velhas Supergroup in the Quadrilátero Ferrífero; (2) an iron-formation unit, referred to as Cauê Formation of the Itabira Group, which is part of the Early Proterozoic Minas Supergroup; and (3) a quartzite unit, correlated with the Piracicaba Group of the Minas Supergroup. These units are cut by mafic intrusive rocks (Melo et al., 1986; Souza Filho et al., 1989), which are commonly strongly weathered. With the exception of intrusive contacts, all contacts between the various units are structural and interpreted as thrust faults (Figs 5.4 and 5.5)..

(1) Volcano-Sedimentary Sequence: This sequence of rocks comprises quartz-chlorite schist, carbonate-chlorite schist, biotite schist, magnetite-talc schist, lenticular bodies of magnetite and hematite quartzite, and intraformational conglomerate. This

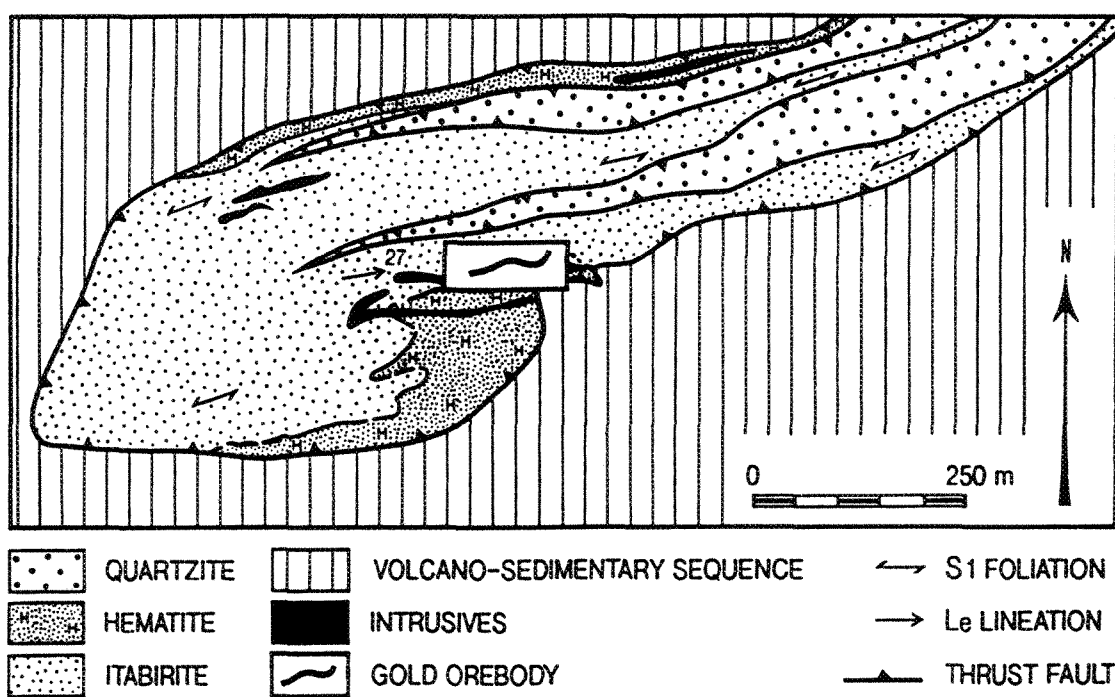


Figure 5.3. Simplified geologic map of the Conceição mine (modified after Leao de Sá and Borges, 1991).



Figure 5.4. Picture of the southern part of Conceição-iron-mine open pit, showing (a) the tectonic contact between the volcano-sedimentary sequence (Vs), iron-formation uint, and quartzite unit (Qz), indicated by thrust fault symbol, as in figure 5.3; (b) the intrusive rocks indicated by "i"; and (c) the location of the Conceição orebody, indicated by "CG".

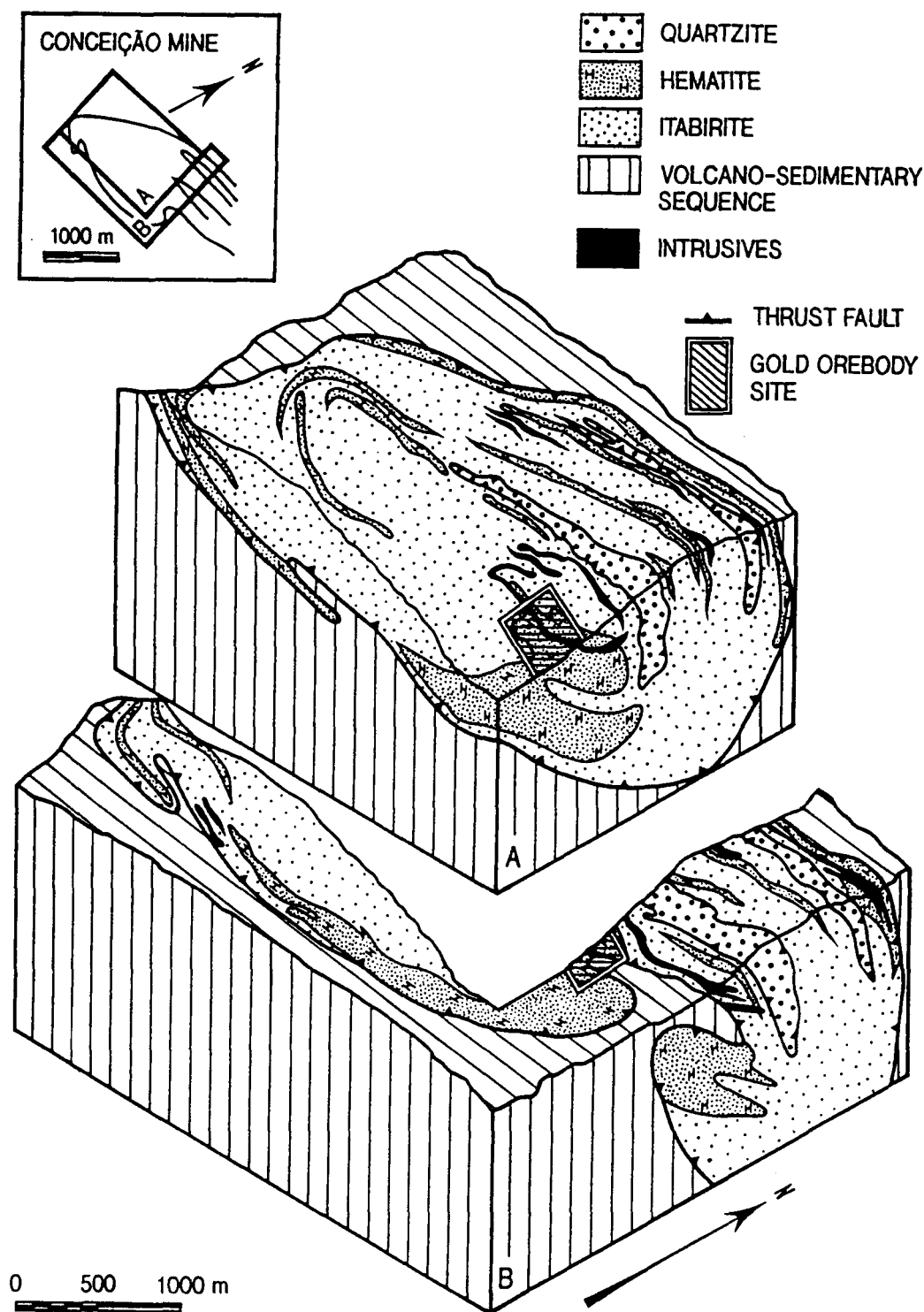


Figure 5.5. Block diagram of the Conceição open pit based on mapping and drill log information of CVRD.

sequence structurally underlies the iron-formation unit and outcrops southwest of Conceição Peak. Outcrop exposure gives more than thousand meters (Fig. 5.2 and Dorr and Barbosa, 1963).

(2) Iron-formation Unit: With an apparent thickness of five hundred meters (Dorr and Barbosa, 1963), this unit is composed of itabirite, talc-kaolin-bearing hematite schists, pure hematite bodies, and the auriferous iron-formation called jacutinga. Itabirite is composed of alternating centimetric to millimetric layers of either specular hematite, hematite pseudomorphous of magnetite octahedrons, or quartz. The hematite bodies are more concentrated in the southern part of the Conceição mine (Figs. 5.3 and 5.5). This unit is referred to as a Lake superior-type iron-formation (Hoppe et al., 1987).

(3) Quartzite unit: This unit comprises ferruginous quartzite, muscovite quartzite and subordinate carbonaceous muscovite-quartz schist.

The basal unit of the Minas Supergroup, the Caraça Group, that was described by Dorr and Barbosa (1963) and Leao de Sá and Borges (1991) was not recognized during this research. Souza Filho et al. (1989) also did not observe this basal unit.

### 5.3.2 Structure

The rocks were subjected to three phases of folding. The first folding phase, D1, is characterized by tight asymmetric (Fig. 5.6) and isoclinal folds, which develop progressively and locally into sheath folds. The D1 fabrics are the S1 foliation and the elongation lineation (Figs. 5.6 and 5.7). S1 is a penetrative C-S foliation, interpreted as mylonitic foliation in agreement with the observations of Souza Filho et al. (1989). This foliation is defined by the preferred shape orientation of specular hematite and becomes coplanar in highly deformed sites. The elongation lineation (Le) is defined by elongate hematite grains in the S1 plane and has also been referred to as mineral lineation (Fig. 5.7, Souza Filho et al., 1989). The Le plunges 30-40 towards N70-80E and is broadly parallel to the D1-fold axis. The D1 folding is contemporaneous with the ENE-WSW thrust faults, which segment the lithological units (Souza filho et al., 1989).

The second folding phase is characterized by large-scale tight folds and associated parasitic folds. Locally this folding event developed a axial planar foliation which transposed S1. The axes of D2 folds plunge 30-45 towards N65-70E, being broadly parallel to Le. The third phase of folding is characterized by open folds with an associated broadly N-S crenulation cleavage with a moderate dip.



Figure 5.6 D1 asymmetric tight fold, showing the sense of shearing during D1 and the S1-mylonitic foliation.

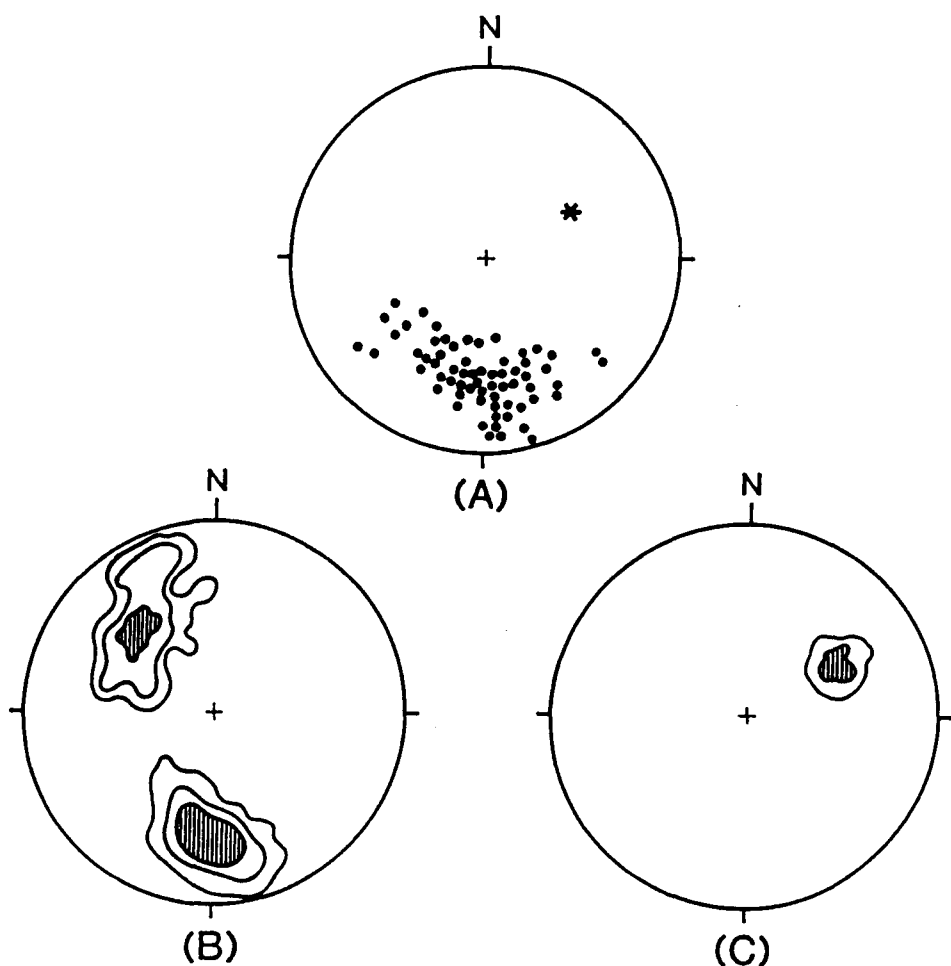


Figure 5.7. Lower hemisphere, equal-area, stereographic projections of structural data from the Conceição mine. A. Poles to the S1 foliation (open circles); Le (star); measured in this work. B. Kamb contour of Poles to the S1 foliation (Souza Filho, 1989). C. Kamb contour of mineral lineation (Souza Filho et al., 1989).

Based on the presence of C/S fabrics (Berthé et al., 1979) and sheath folds (Cobbold and Quinquis, 1980; Lacassin and Mattauer, 1985; Goscombe, 1991), the D1 deformation in the Conceição mine is interpreted to have been generated by a simple shear regime. The sense of shear during the D1 folding phase has been determined in the field from asymmetrical folds (Fig. 5.6) by using the criteria of Hanmer and Passchier (1991). The sense of shear is east-over-west, consistent with the tectonic transport during D1 as determined in the Cauê mine (Olivo et al., in press). Souza Filho et al. (1989) suggested that the three folding phases in Conceição area are associated with a single progressive folding event with a tectonic transport from ENE to WSW.

The intrusive bodies in the iron-formation unit are both discordant and concordant with the S1 foliation and are folded by the D2 phase (Fig. 5.5), suggesting that these bodies are syn- to late-D1 folding phase. The truncation of these intrusive bodies at the contact of the iron-formation unit and the underlying volcano-sedimentary sequence is the fundamental evidence that the iron-formation unit was detached from the underlying sequence during the D1 folding phase.

The structures and textures of the Conceição mine are very similar to those of Cauê mine, suggesting that the nature of D1 and D2 deformations in both mines are the same. According to Olivo et al. (in press), D1 and D2 deformations have been

generated by a progressive simple shear regime with high bulk shear strain (Olivo et al., in preparation).

### **5.3.3 Metamorphism**

The oxygen isotope data on hematite and quartz grains found in the S1 planes from the itabirite in the Conceição mine indicate a metamorphic temperature up to 660° C (Hoefs et al., 1982). This temperature is consistent with data obtained from similar rocks in the Cauê and Dois Córregos mines (Hoefs et al., 1982), and with the metamorphic assemblage in the quartzite unit, which suggest amphibolite facies conditions (Yardley, 1989). In the volcano-sedimentary sequence, the mineral assemblages denote retrograde metamorphism to biotite and chlorite zones of greenschist facies.

## **5.4 PALLADIUM-BEARING OREBODY OF THE CONCEIÇÃO MINE**

In the Conceição mine, only one gold orebody has been intermittently mined since 1987 (Leao de Sá and Borges, 1991). The orebody, which is located in the southern end of the Conceição mine (Figs. 5.3, 5.4, and 5.5), is hosted by jacutinga in the iron-formation unit. Jacutinga is a hydrothermally altered ironstone consisting of interlayered bands of quartz (+/- feldspar), hematite (+/- magnetite, +/- goethite) and white phyllosilicates (talc, phlogopite and kaolin), with minor amounts of

tourmaline. Ankerite grains are common as inclusions in quartz grains. Monazite and apatite, which were identified in the Cauê jacutinga, were not found at Conceição. In addition, rutile and zircon, which have been described as trace minerals in Conceição jacutinga by CVRD geologists, were not found during the present investigation. The jacutinga aspect in outcrops is characterized by a light to dark brown layer with abundant white phyllosilicate and yellow dismembered quartz veins. It clearly contrasts with the barren iron-formation which is grey to black and homogeneous in composition (Fig. 5.8). The mineral abundances for Conceição jacutinga samples and barren iron-formation samples are showed in the Table 5.2.

#### **5.4.1 Geometry and structural controls**

The Conceição gold orebody is parallel to the S1 mylonitic foliation in the limb of macroscopic D1 and D2 folds (Figs. 5.3, 5.4, 5.5, 5.8 and 5.9). This orebody varies from 0.5 meters to 0.1 meters in thickness and extends for at least 400 meters on mine surface. It extends 100 meters down dip in the direction of the elongation lineation (Leao de Sá and Borges, 1991). This gold vein was dismembered by the progressive shear deformation (Fig. 5.9) and folded during D2 (Fig. 5.8). The general attitude of the auriferous quartz vein is WSW plunging 50-75 towards the NW (Fig. 5.9).

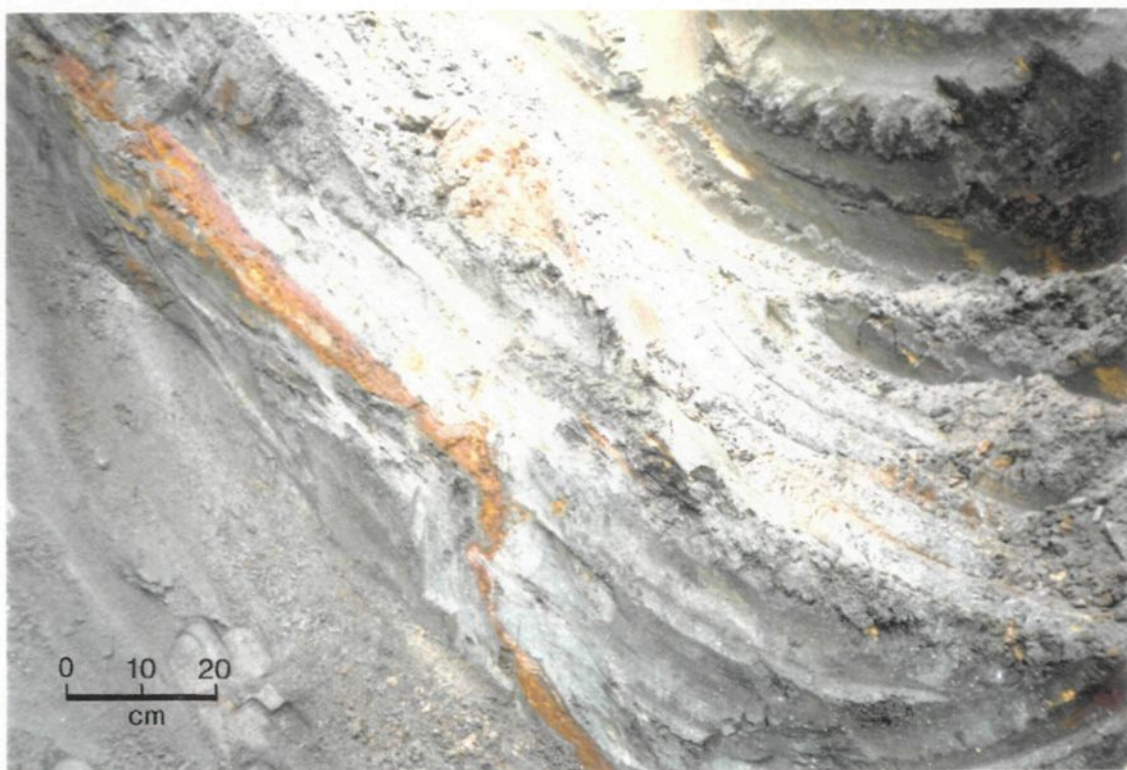


Figure 5.8. Vertical section of the Conceição gold orebody (yellow to dark brown vein) folded by parasitic D2-fold.

MINERALS	JACUTINGA	ITABIRITE	HEMATITE BODIES
Hematite	40-70%	35-65%	95-100%
Quartz	5-20%	35-65%	trace
Magnetite	trace	trace	trace
Goethite	3-10%	trace	trace
Kaolin	25-35%	trace	0-5%
Phlogopite	5-15%		
Talc	trace		
Feldspar	trace	trace	
Tourmaline	trace		
Carbonate	trace	trace	

Table 5.2 Mineral abundances of jacutinga, itabirite and compact hematite body of the Conceição mine

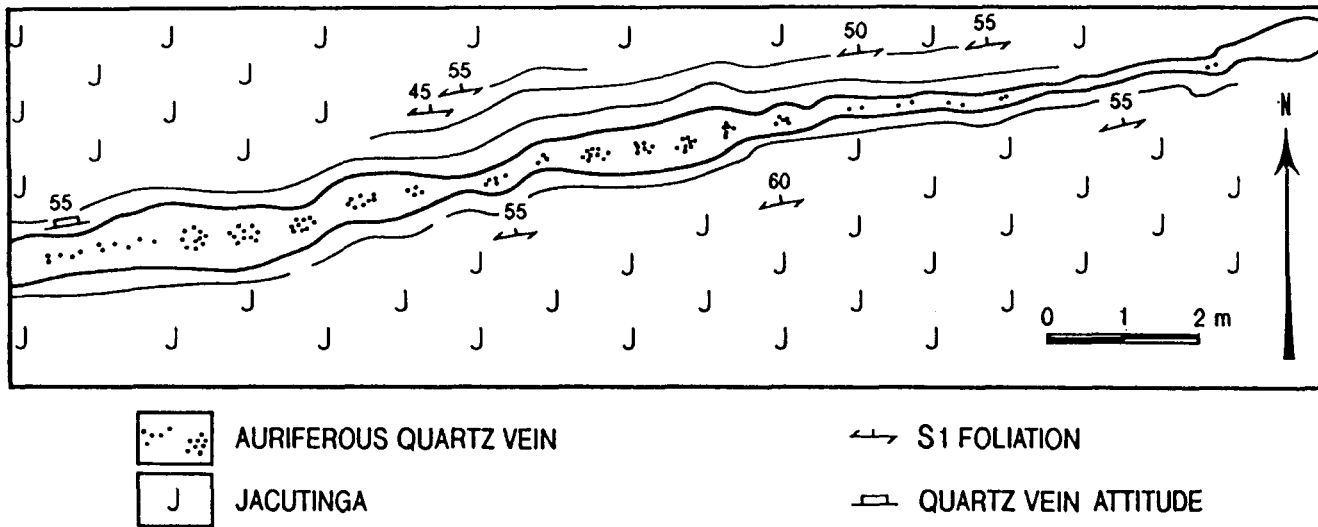


Figure 5.9 Geological map of the level 901 of the Conceição orebody

#### **5.4.2 Hydrothermal alteration and effects of weathering in jacutinga**

In the Conceição mine, the main hydrothermal-metamorphic phases (i.e., phlogopite, talc, quartz, hematite and tourmaline) are all parallel to the S1 foliation. The white phyllosilicates indicate pervasive alteration in the jacutinga and are more abundant adjacent to the vein. Hematite enrichment is also observed along the border of the auriferous quartz vein (Fig. 5.10). Tourmaline occurs throughout the jacutinga.

Weathering in the Conceição mine is more pronounced than in the Cauê mine. The main weathering minerals are kaolinite and goethite. The kaolinite is pseudomorphous after phlogopite and talc, and goethite replaces magnetized magnetite. Leao de Sá and Borges (1991) suggested that goethite may also replace hydrothermal carbonates.

#### **5.4.3 Ore mineralogy**

Gold grains occurring in the jacutinga may be primary, associated with the hydrothermal event, or secondary, as the result of weathering. The primary gold grains have been described by Leao de Sá and Borges (1991) as platy grains oriented parallel to the jacutinga foliation and elongated along the Le direction. In this study, we also observed primary gold grains as inclusions in specular hematite, tourmaline and quartz grains. But most of the Conceição gold grains are very fine,



Figure 5.10. Detail of the Conceição auriferous vein, showing the dismembered yellow quartz vein with a border of goethitic and hematitic alteration.

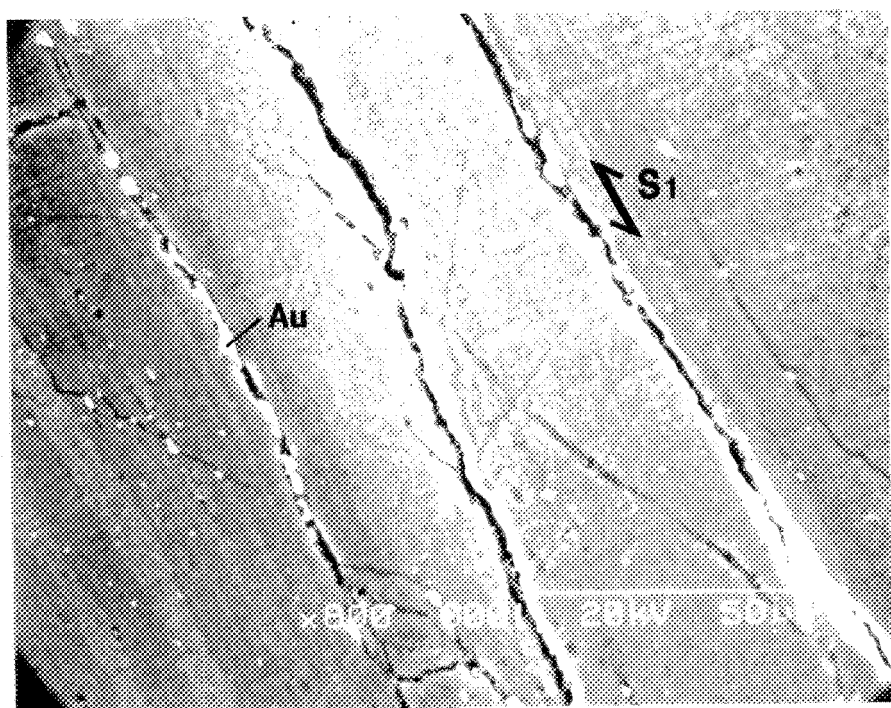


Figure 5.11. Back-scattered electron image showing gold grains in open spaces parallel to S1-foliation in goethite-rich band.

smaller than 0.0030 mm, and are associated with goethitic bands (Fig. 5.11) that may have resulted from the weathering of carbonates (Leao de Sá and Borges, 1991). In addition, some octahedral gold crystals, with a diameter greater than 3.5 cm (Fig. 5.12), were recovered from the weathered jacutinga. It is not clear if they were formed during the hydrothermal event or during weathering. In general, the Conceição gold grains are darker yellow than the Cauê grains.

Electron microprobe energy-dispersive spectrometry analyses of three bent gold grains and one gold crystal (Table 5.3) revealed that the Pd content in the bent grains may reach up to 0.8 %, whereas Pd was not detected in the octahedral crystal. Silver (up to 2%), Fe (up to 4%) and Cu (up to 3%) are alloyed with gold in both the grains and the crystal. Inclusions of hematite and Mn oxides, and trace amounts of Rh, Ru, and Te were also found in the bent gold grains.

#### 5.4.4 Whole rock geochemical investigations

Four hand samples from the mineralized zone were selected for whole rock analysis. In addition one sample of drill core of non-auriferous iron-formation from the southern part of the Conceição mine was also analyzed for comparison. In all samples, major elements and Ag, Sc, V, Cr, Co, Ni, Cu, Zn, Cd, Sn, Sb, Ba, and Pb, were analyzed by Inductively coupled plasma (ICP). For 41a, 41c and Fau-06-07 samples, As was analyzed using ICP, and for samples 41d and 41g, As was also



Figure 5.12. Octahedral gold grains of the Conceição orebody.

	CO-1 a	CO-1 b	CO-1 c	CO-2 a	CO-2 b	CO-2 c	CO-3 a	CO-3 b	CO-3 c
Au	97,57	93,77	89,45	96,54	91,69	95,33	94,79	94,42	96,02
Pd	n.d	n.d	0,47	n.d	n.d	0,77	n.d	n.d	n.d
Ag	2,36	1,47	1,43	0,61	0,57	1,66	2,04	2,09	1,24
Cu	0,87	0,76	2,66	n.d	n.d	0,91	0,73	1,77	1,00
Fe	1,20	1,40	3,98	2,58	1,67	0,41	2,25	1,71	1,53
Rh	n.d	n.d	0,71	n.d	n.d	0,92	n.d	n.d	n.d
Ru	n.d	n.d	0,91	n.d	n.d	n.d	n.d	n.d	n.d
Te	n.d	0,30	n.d	0,27	0,25	n.d	n.d	n.d	n.d
Mn	n.d	n.d	n.d	n.d	5,52	n.d	0,19	n.d	0,21
Cl	n.d	2,39	0,39	n.d	n.d	n.d	n.d	n.d	n.d

Table 5.3. Electron microprobe energy dispersive system analyses of gold grains of the Conceição orebody. CO-3 is an octahedral crystal; the other gold grains are bent (value en wt%).

analyzed by atomic absorption. Rare earth elements, platinum-group elements and Au were determined in the 41a, 41c and Fau-06-07 samples by instrumental neutron activation analysis (INAA). For the other samples, La was determined by ICP and Ce by INAA and Au, Pd, and Pt were analyzed by fire-assay-DCP techniques. The results are listed in Table 5.4.

Results reported here are only qualitative, due to the substantial weathering of itabirite and jacutinga. Results reflect the effect of alteration from both the hydrothermal and weathering processes. Jacutinga is much richer in Fe<sub>tot</sub>, Ni, Cr, V, La and Ce contents than the average values for Lake Superior-type oxide-facies iron-formation as reported in Fryer (1977) and Gross (1988).

Samples 41a, 41c, and fau-06-07 were analyzed for platinum group elements, but only Pd and Pt were detected, yielding values up to 220 ppb and 130 ppb, respectively. The gold grade in the hand samples ranges up to 4900 ppb, which is much lower than the average grade of the Conceição gold ore as shown in Table 5.5 (Andrade, 1991, pers. communication). This observation may be explained by the heterogeneous gold distribution (nugget effect) in the jacutinga unit.

	41a	41c	41d	41g	Fau 06-07
SiO <sub>2</sub> (%)	12,89		3,07	6,12	
Fe <sub>2</sub> O <sub>3</sub> (%)	80,01		95,00	86,77	
Al <sub>2</sub> O <sub>3</sub> (%)	0,99		0,77	3,06	
MnO (%)	0,57		0,88	0,11	
TiO <sub>2</sub> (%)	0,03		0,05	0,09	
MgO (%)	0,10		0,06	0,15	
Na <sub>2</sub> O (%)	0,02		0,01	0,12	
K <sub>2</sub> O (%)	0,02		n.d.	n.d.	
CaO (%)	n.d.		0,10	0,06	
LOI (%)	4,09		0,49	2,29	
<b>TOTAL</b>	<b>98,91</b>		<b>100,43</b>	<b>98,77</b>	
Au (ppb)	4900	130	69	177	3,7
Pd (ppb)	220	31	47	8	n.d
Pt (ppb)	n.d.	130	7	n.d	n.d
Ag ppm	1,2	1,2	0,8	0,9	1,8
Cu (ppm)	34	9	10	6	103
Ni (ppm)	56	36	21	28	43
Cr (ppm)	377	107	119	87	547
V (ppm)	177	27	6	6	41
As (ppm)	40	18	2,49	1,43	24
Sb (ppm)	n.d.	6	0,48	0,48	8
Zn (ppm)	81	72	33	16	16
Pb (ppm)	7	4	n.d	n.d	16
Cd (ppm)	5,1	7,4	2,9	2,2	2,6
Sn (ppm)	24	55	n.d	n.d	42
Ba (ppm)	112	123	71	10	13
La (ppm)	10	14	34	32	7
Ce (ppm)	23	18	10	6,3	12
Nd (ppm)	10	11			n.d
Sm (ppm)	2,8	2,7			1,9
Eu (ppm)	0,9	1			n.d

Table 5.4. Major elements, and trace and precious metal contents of Conceição iron-formation specimens (41a= dismembered auriferous quartz vein with hematitic alteration border; 41c and 41g= jacutinga from the hanging wall of the auriferous quartz vein; 41d= jacutinga from the footwall of the auriferous quartz vein; FAU-06-07= itabirite).

LEVEL (m)	ORE PRODUCTION (t)	TOTAL Au CONTENT (g)	AVERAGE GRADE (g/t)
942,5	293	3 495	11,9
940,5	136	45 082	331,5
938,5	1146	42 375	35
935	1047	8 042	7,7
931,5	817	246 768	302
928	1042	233 371	224
924	995	18 594	18,7
920	1016	18 914	18,6
915	660	46 805	70,9
911	513	6 429	12,5
908	496	34 078	68,7
904,5	360	1 460	4,1
<b>TOTAL</b>	<b>8521</b>	<b>705 413</b>	<b>82,8</b>

Table 5.5. Tonnage, metal content and average gold grade of Conceição gold orebody from different levels mined between 1987 to 1990 (Andrade, 1991, pers. communication)

## 5.5 COMPARISON OF THE CONCEIÇAO GOLD DEPOSIT WITH THE CAUÊ DEPOSITS

The Conceição palladium-bearing orebody has some similarities with the Cauê orebodies described as follows:

- (a) In both mines, palladium-bearing orebodies are hosted by jacutinga in the iron-formation unit which tectonically overlies the volcano-sedimentary sequence;
- (b) The Conceição and Cauê orebodies are structurally controlled by the S1-mylonitic foliation and Le elongation lineation, coeval with thrust faulting and the peak of thermal metamorphism;
- (c) The hydrothermal alterations are similar, consisting of talc and phlogopite formation, hematite enrichment, and tourmalinization.
- (d) Both orebodies contain palladium gold; and
- (e) The jacutinga from both mines has higher Ni, Cr, V, La and Ce contents than the averages values reported in Fryer, (1977) and Gross (1988) for Lake Superior-type oxide-facies iron-formation.

The main differences between the Conceição and Cauê orebodies are the morphologies and chemical composition of gold grains and the average gold grade. In the Conceição orebody, the largest gold grains are in form of octahedral crystals rather than stretched grains, whereas the reverse is true for the Cauê mine (especially Corpo Y orebody). In addition, the PGE contents in gold grains are quite

different: (a) In the Conceição grains, Pd contents are not greater than 0.77 %; in contrast, the Pd contents in the Cauê gold grains may attain 20% (Olivo et al., 1994); (b) The Conceição gold grains have Rh and Ru contents greater than 0.9 %; in the Cauê mine, Rh contents (up to 1%) were detected only in the syn-D2 Aba Norte orebody, and Ru contents were not detected in any orebody (Olivo et al. in press). Furthermore, the Cu contents in the Conceição gold grains (up to 2.7%) are lower than in the Cauê gold grains (up to 8.3%; Olivo et al., 1994). Regarding the average gold grade, the Conceição ore is higher (82.3 g/t) than Cauê ore (24.4 g/t) (Andrade, 1991, pers. communication).

The different trace element concentrations in gold grains from Conceição and Cauê is directly reflected in the composition of the gold bullion produced by both mines. In Conceição, the gold bullion averages 96.48% Au, 2.83% Pd, 0.63% Ag and 0.24% Cu, and in the Cauê mine the bullion averages 91.21% Au, 6.27% Pd, 0.96% Ag and 0.85% Cu (Leao de Sá and Borges, 1991).

The compositional and textural differences in the Cauê and Conceição gold ores may be related to both hydrothermal and weathering processes. The most pure gold grains are commonly associated with the most weathered rocks.

## 5.6 CONCLUSIONS

The similarities between the Conceição and Cauê palladium-bearing gold deposits suggest that the palladium-gold concentrations in both deposits may have occurred as a result of the same processes during the D1 deformational event. The Conceição orebody is another example of a "Palladium-bearing gold deposit hosted by highly-sheared, metamorphosed, Lake Superior-type iron-formation" as defined in Olivo et al. (in press). The proposed genesis of this type of deposit may be summarized as follows: During the tectonic transport of the iron-formation unit, the high-strain ductile shear event (D1) may have induced the percolation of high-temperature, high-oxygen-fugacity hydrothermal fluids through this unit. Under these physico-chemical conditions, Pd and Au may have been transported as chloride complexes and then deposited when the fluids reached the dolomitic itabirite layer (Olivo et al., in press). Palladium and gold may have been precipitated mainly as a result of changes in pH due to the formation of talc and phlogopite, during the development of the jacutinga rock-type. The gold vein was subsequently dismembered and folded during the progressive shear deformation D2.

The similarities between the Cauê and Conceição deposits suggest that the Itabira District is an exceptionally favourable geological environment for palladium-bearing gold deposits hosted by Lake Superior-type iron-formation.

## REFERENCES

- Babinski, M., Chemale, F., Jr., and Schmus, W. R., 1993, A idade das formações ferríferas bandadas do supergrupo Minas e sua correlação com aquelas da África do Sul e Austrália: Simpósio do Cráton do São Francisco, 2<sup>nd</sup>, Salvador, Brazil, August 23-26, 1993, Proceedings, p. 152-153
- Babinski, M., Van Schmus, W. R., Chemale, F., Jr., 1991, Pb/Pb Geocronology of Carbonate Rocks of Minas Supergroup, Quadrilátero Ferrífero, Minas Gerais, Brazil [abs.]: A Geophysical Union Fall Meeting Abstract with Programs, December 9-13, 1991, p. 53
- Belo de Oliveira, O. A., 1986, As falhas de Empurrao e suas implicações na Estratigrafia e Metalogenia do Quadrilatero Ferrífero: Congresso Brasileiro Geologia, 35<sup>th</sup>, Goiânia, Brazil, v. 5, p. 15.
- Belo Oliveira, O. A., and Teixeira, W., 1990, Evidências de uma tectônica tangencial Proterozóica no Quadrilatero Ferrífero: Congresso Brasileiro de Geologia, 36<sup>th</sup>, Natal, 1990, Proceedings, v. 6, p. 2589-2604.
- Berthé, D., Choukroune, P., and Jegouzo, P., 1979, Orthogneiss, mylonite and non-coaxial deformation of granites: the example of the South Armorican shear zone: Journal of Structural Geology, v. 1, p. 31-42.
- Chemale, F., Fr. and Quade, H., 1986, Estratigrafia e Geologia Estrutural do Distrito Ferrífero de Itabira: Congresso Brasileiro de Geologia, 34<sup>th</sup>, Goiânia, Proceedings, v. 2, p. 987-998.
- Cobbold, P. R., and Quinquis, H., 1980, Development of sheath folds in shear regime: Journal of Structural Geology, v. 2, p. 119-126.
- CVRD, 1989, Mining: Itabira-Timbopeba. Companhia Vale do Rio Doce Edition, Rio de Janeiro, 31 p.
- Dorr, J. V. N. II, 1969, Physiographic, stratigraphic and structural development of Quadrilatero Ferrífero, Minas Gerais, Brazil: U. S. Geological Survey Professional Paper, 641: 1-110.
- Dorr, J. V. N. II, and Barbosa, A. L. M., 1963, Geology and ore deposits of the Itabira district, Minas Gerais, Brazil: U. S. Geological Survey Professional Paper, 341-C, 110 p.

- Dossin, I. A., Dossin, T. M., Charvet, J., Cocherie, A., Rossi, P., 1993, Single-zircon dating by step-wise Pb-evaporation of Middle Proterozoic magmatism in the Espinhaço range, Southeastern São Francisco Craton (Minas Gerais, Brasil): Simpósio do Craton do São Francisco, 2<sup>nd</sup>, Salvador, Brazil, August 23-26, 1993, Proceedings, p. 39-42.
- Fryer, B. J., 1977. Rare-earth evidence in iron-formation for changing Precambrian oxidation states. *Geochimica et Cosmochimica Acta*, v. 41, p. 361-367.
- Goscombe, B., 1991, Intense non-coaxial shear and the development of mega-scale sheath folds in the Arunta Block, Central Australia: *Journal of Structural Geology*, v. 13, p. 299-318.
- Gross, G. A., 1988, Gold content and geochemistry of iron-formation in Canada: Geological Survey of Canada Paper n° 86-19, 54p.
- Hanmer, S., Passchier, C., 1991, Shear-sense indicators: a review: *Geological Survey of Canada*, paper n° 90-17, 72 p.
- Hoefs, J., Muller, G., and Schuster, A. K., 1982, Polymetamorphic Relations in Iron Ores from Iron Quadrangle, Brazil: The Correlation of Oxygen Isotope Variations with Deformation History: Contributions to Mineralogy and Petrology, v. 79, p. 241-251.
- Hoppe, A., Shobbenhaus, C., Walde, D. H. G., 1987, Precambrian Iron Formation in Brazil: Precambrian Iron-Formations: Athens, Theophrastus Publications S.A., p. 347-390.
- Lacassin, R., and Mattauer, M., 1985, Kilometre-scale sheath fold at Mattmark and implications for transport direction in the Alps: *Nature*, v. 315, p. 739-742.
- Ladeira, E. A., 1991, Genesis of gold in Quadrilatero Ferrífero: a remarkable case of permanency, recycling and inheritance- A tribute to Djalma Guimaraes, Pierre Routhier and Hans Ramberg: Brazil Gold'91: An International Symposium on the Geology of Gold, Belo Horizonte, 1991, A. A. Balkema, Proceedings, p. 11-30.
- Leao de Sá, E., and Andrade, L. P., 1990, A experiência da CVRD na lavra seletiva de minério aurífero nos itabiritos [abs.]: Int. Gold Symposium, 6<sup>th</sup>, Rio de Janeiro, August 13-14, Abstracts with program, p. 2.
- Leao de Sá, E., and Borges, N. R. A., 1991, Gold mineralization in Cauê and Conceição iron ore mines - Itabira- MG: Field and Mine trip to Quadrilátero Ferrífero, Minas Gerais, Brazil, Field guide book of Brazil Gold'91: An International Symposium on the Geology of Gold, Belo Horizonte, p. 74-85.

- Machado, N., Noce, C. M., Ladeira, E. A., Belo de Oliveira, O., 1992, U-Pb Geochronology of Archean magmatism and Proterozoic metamorphism in the Quadrilátero Ferrífero, southern São Francisco craton, Brazil: Geological Society of America Bulletin, v. 104, p. 1221-1227.
- Melo, M. T. V., Borba, R. R., and Coelho, W. A., 1986, O Distrito ferrífero de Itabira, Minas do Cauê, Conceição, Dois Córregos, Periquito, Onça, Chacrinha e Esmeril: Principais Depósitos Minerais do Brasil, Departamento Nacional de Produção Mineral, Brasília, v. 2, p. 7-28.
- Muller, G., Schuster, A., and Hoefs, J., 1982, Oxygen isotope variations in polymetamorphic iron ores from the Quadrilátero Ferrífero, Brazil: Revista Brasileira Geociências, v. 12, p. 348-355.
- Olivo, G. R., Gauthier, M., Bardoux, M., 1994, Palladian gold from the Cauê iron mine, Itabira District, Minas Gerais, Brazil: Mineralogical Magazine (in press).
- Olivo, G. R., Gauthier, M., Bardoux, M., Leao de Sá, E., Fonseca, J. T., and Santana, F. C. (in preparation) Palladium-bearing gold deposit hosted by Proterozoic Lake Superior-type iron-formation at Cauê iron mine, Itabira District, Southern São Francisco Craton, Brazil: Geologic and structural controls.
- Rosière, C. A., 1981, Strukturelle und texturelle Untersuchungen in der Eisenerzlagerstätte Pico de Itabira bei Itabirito, Minas Gerais, Brasilien: Unpub. Ph.D. thesis, Univ. Clausthal, 303 p.
- Schorscher, H. D., 1975, Entwicklung des polymetamorphen präkambrischen raumes Itabira, Minas Gerais, Brasilien: Umpub. Ph.D. thesis, University of Heidelberg, 302p.
- Schorscher, H. D., Santana, F. C., Polônia, J. C., and Moreira, J. M. P., 1982, Rio das Velhas Greenstone Belt and Proterozoic rocks, Quadrilátero Ferrífero, Minas Gerais State: International Symposium on Archaean and Early Proterozoic Geological Evolution and Metallogenesis, Sociedade Brasileira de Geologia, Salvador, September 3-11, Excursion annex p. 1-25.
- Souza Filho, C. R., Rodrigues, L. C. R., Chemale, F., Jr., and Alkimim, F. F., 1989, Aspectos deformacionais e relações litoestratigráficas na Mina de Conceição, Distrito Ferrífero de Itabira, Minas Gerais: Simpósio de Geologia, 5<sup>th</sup>, Núcleo Minas Gerais, Simpósio de Geologia, 1, Núcleo Brasília. Sociedade Brasileira de Geologia, Belo Horizonte, Proceedings, p. 16-20.
- Yardley, B. W., 1989, An introduction to metamorphic petrology, John Wiley & Sons, Inc., New York, 248 p.

## CONCLUSIONS AND RECOMMENDATIONS

The peculiar characteristics of the Cauê and Conceição orebodies warrant a new type of gold-palladium deposit entitled in this thesis "Palladium-bearing gold deposit hosted by highly-sheared, metamorphosed Lake Superior-type iron-formation". The main characteristics of this type of gold-palladium deposit are:

- (1) Gold and palladium are hosted in the jacutinga rock-type of a Lake Superior-type iron-formation. Jacutinga is interpreted as a hydrothermally altered Lake Superior-type carbonate-bearing oxide-facies iron-formation (dolomitic itabirite);
- (2) The main palladium-bearing gold veins are parallel to S1-mylonitic foliation and stretched along of the elongation lineation directions. This feature along with textural studies suggest that the main gold mineralization event was synchronous with D1-deformation, coeval with thrust faulting and probably with peak of thermal metamorphism;

- (3) The hydrothermal alterations associated with the gold-palladium mineralizing event are characterized by the formation of talc, phlogopite and tourmaline, as well as hematite and quartz veins;
- (4) The ore mineralogy is peculiar, characterized by palladium-bearing gold, palladium, palladium-oxide, palladseite and arsenopalladinite;
- (5) The whole rock geochemistry of jacutinga reveals anomalous contents in Fe<sub>tot</sub>, Ni, Cr, V, and As when compared with the average values of these metals in other oxide-facies iron-formations reported in the literature. In addition, the gold grades are very high (may attain up to 7000 g/t), restricted to veins, and heterogeneously distributed;
- (6) The age of the mineralizing event is c.a. 1.9 Ga, as determined by Pb-Pb isotope techniques. This age is in agreement with the metamorphic age of the Minas Supergroup and corresponds to the Transamazonian orogenesis in the southern São Francisco craton.

Other deposits in the southern São Francisco craton (e.g. Congo Soco, Maquiné, and Pitangui) have some similarities with the Cauê and Conceição deposits: a) they are hosted by jacutinga; b) they are structurally controlled by the approximately east-trending elongation lineation; c) they are palladium-bearing, and d) they are proximal to the thrust faulted contact between the Minas Supergroup and the underlying units. The similarities suggest that all these gold and palladium concentrations may have formed by the same processes during the same deformational event.

The proposed genetic model for this type of palladium-bearing deposit is integrated with the tectonic evolution of the southern São Francisco craton and may be summarized as follows. During late Archean-Early Proterozoic (c.a 2.6 to 2.4 Ga), a large basin opened, providing favourable conditions for the deposition of the extensive shelf sediments of the Minas Supergroup (Fig. 1; Teixeira and Figueiredo, 1991; Babinski et al., 1993). The basement and source area for the Minas basin sediments were the Archean Granite-gneiss Complex and the Rio das Velhas Supergroup.

During Transamazonian orogenesis (2.2 to 1.9 Ga), there was horizontal shortening of the previously attenuated continental crust causing basin closure and folding, metamorphism and westward thrusting of the Minas sedimentary rocks (Fig. 1, Teixeira and Figueiredo, 1991). During the tectonic transport coeval with D1-deformation, the Minas sequence detached from the underlying surfaces in the eastern edge of the craton. The basal unit of Minas Supergroup (Caraça Group) composed of conglomerates and graphitic phyllites may have served as a décollement surface which may explain its absence in the study area. During this deformational event, the hydrothermal fluids percolated through the most permeable units and structures, leaching gold and palladium.

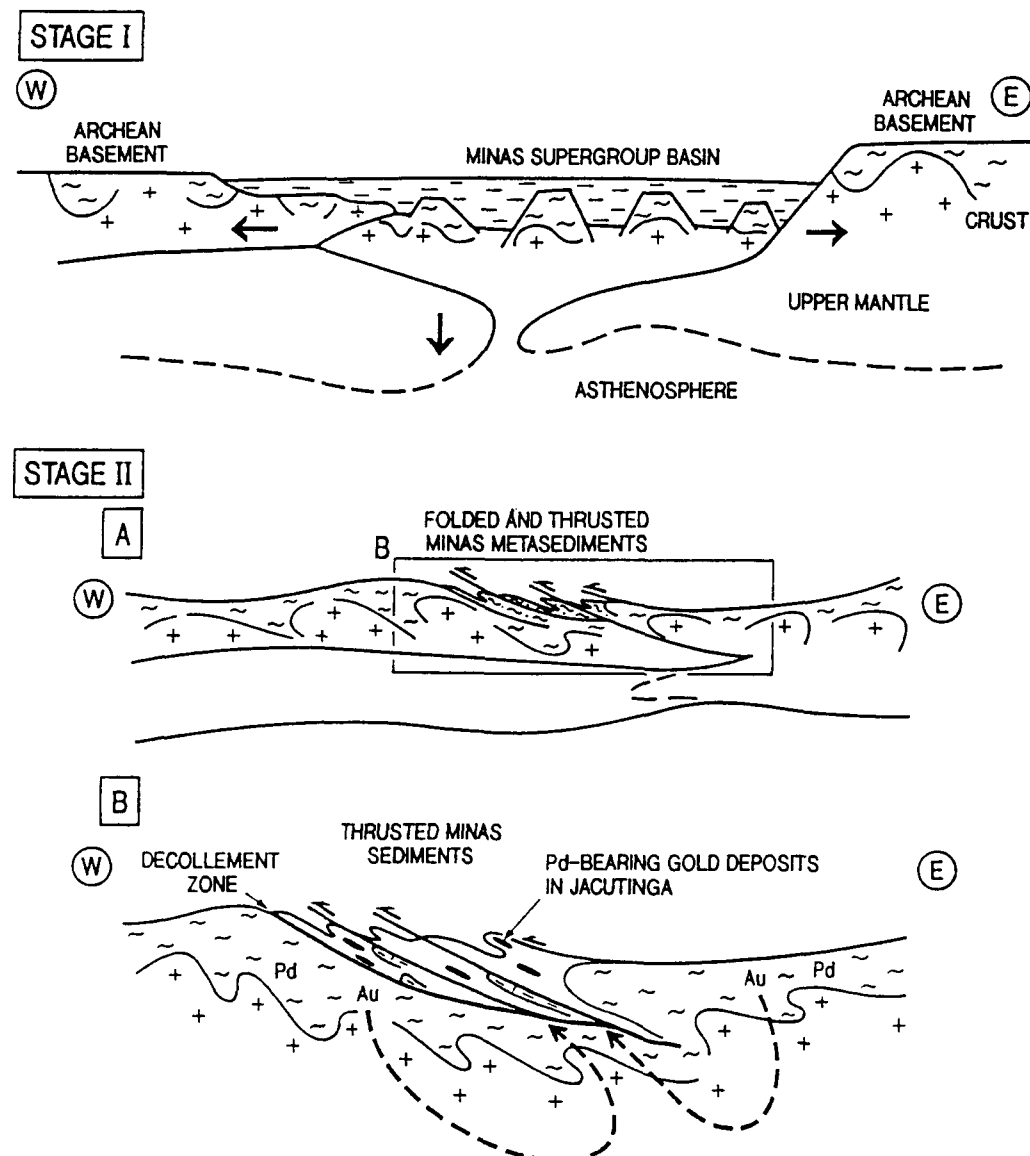


Figure 1. Proposed evolutionary model for the Minas Supergroup (adapted from Teixeira and Figueiredo, 1991). Stage I= opening of the Minas basin (2.4-2.6 Ga, Babinski et al., 1993); Stage II A= basin closure following by folding, metamorphosim and thrusting of the Minas sequence (1.9- 2.2 Ga, Teixeira et al., 1991); B= detail of A, showing hydrothermal circulation during the basin closure.

The physico-chemical conditions of the hydrothermal fluids, characterized by high-temperature and high-oxygen fugacity as suggested by hydrothermal mineral assemblage, were favorable to transport gold and palladium as chloride complexes. Gold and palladium deposition may have occurred due to a change in pH as the fluids reached the dolomitic itabirite layer, forming talc and phlogopite bearing iron formation (jacutinga rock-type). Continuous deformation of the iron-formation unit during the tectonic transport rotated and stretched the palladium-gold orebodies subparallel to the direction of transport. The syn-D1 orebodies (e.g. Corpo Y, Corpo X, Central, Aba Leste, and Conceição) were then folded during the D2 progressive deformation and syn-D2 orebodies were formed and boudinaged (e.g. Aba Norte).

The gold deposits described in this thesis and their proposed genetic hypothesis favor the epigenetic model for gold concentration in iron-formations. Supporting arguments are:

- (1) The strong structural controls of the palladium-bearing gold orebodies;
- (2) The evidence of hydrothermal alteration of the auriferous iron-formation synchronous with D1-deformation;
- (3) The younger Pb-Pb age of the palladian gold and hydrothermal minerals than the age of Minas Supergroup sedimentation, and the agreement of this age with the age of the Transamazonian orogenesis; and

(4) The low background values of Au and Pd (lower than 1 ppb) in the iron-formation unit outside of the mineralized sites, precluding the syn-sedimentary concentration of these noble metals. The most probable source of palladium and gold may be the Archean Rio das Velhas mafic to ultramafic rocks and massive sulfides which has high concentrations of these precious metals (Roesner et al., 1993).

The characteristics of the Itabira District palladium-bearing gold deposits and the genetic model proposed in this thesis have direct implications for the exploration of this type of deposit either on a regional and on a local scale.

On a regional scale, an iron-formation unit, metamorphosed to amphibolite facies, and in thrust-faulted contact with the underlying Archean volcano-sedimentary sequence or granite-gneiss complex is a primary target. The best exploration method for gold concentrations would then be mapping of the iron-formation, looking for hydrothermal alteration on jacutinga indicated by widespread formation of white phyllosilicates (talc and/or phlogopite), commonly weathered to kaolin. This feature, associated with an enrichment in hematite, resulted in a pattern of black with white spots, resembling the plumage colors of the Brazilian bird, the Pipile jacutinga. This characteristic texture of the jacutinga rock-type has been used as a guide for gold prospecting in the southern São Francisco craton since the 18<sup>th</sup> century. Geochemical methods are not recommended on a regional scale because the auriferous veins are commonly modest and discontinuous and the halo of anomalous

Pd and Au contents is confined to only a few centimeters around the mineralized veins.

On a local scale, the occurrence of quartz and hematite veins contemporaneous with the thrusting and shearing events and the presence of tourmaline around the veins are diagnostic of mineralized sites.

This thesis is one of the first scientific effort to understand the palladium-bearing gold deposits hosted by jacutinga. During the course of this research project, several questions were raised about various geological and metallogenetic aspects of the Itabira District. The following list, which is by no means complete, consists of several recommendations for continued research on different topics that could advance our understanding of the Itabira District, its tectonic evolution and ore deposits.

### Structure

A structural analysis of the Itabira District should be done to complement the preliminary work of Chemale and Quade (1986) and integrate the local structural analysis discussed in this thesis and in Souza Filho et al. (1989).

In addition, the deformation of the Minas Supergroup in the Quadrilátero Ferrífero is poorly understood and ambiguous, needing a systematic investigation. The integration of Itabira and Quadrilátero Ferrífero structural geology is critical to understanding the tectonic evolution of the Early Proterozoic units in this sector of the São Francisco craton and, therefore, the regional controls of the palladium-bearing gold deposits.

### Geochemistry

The three dimensional distribution of gold and PGE content in the different units of the Itabira District could be useful in identifying new mineralized zones and the most probable source of these precious metals.

### Metamorphic petrology

A systematic metamorphic petrology study should be carried out throughout of the Itabira District. There is some discrepancies related to the metamorphic grade of the Itabira rocks reported in the scientific literature. The study of metamorphism in jacutinga could be useful in understading the timing of gold mineralization (Is the mineralizing event previous our synchronous to the peak of metamorphism?).

### Geochronology

The Itabira District lacks geochronological data. The Volcano Sedimentary Sequence, iron-formation unit, quartzite unit and intrusive rocks and tectonic imbricated slices should all be dated to clarify the district's correlation with the Quadrilátero Ferrífero sequences. In addition, the hydrothermal minerals of the Conceição gold orebody should be dated by Pb-Pb methods, for comparison to the results obtained in this thesis for the Cauê syn-D1 gold orebody and monazite in jacutinga should be dated by U-Pb methods.

### Metallogeny

The origin of the hydrothermal fluids involved in the Itabira palladium-bearing gold deposits is poorly constrained, and through further mineralogical and isotope studies, the nature of these fluids should be better defined. The study of tourmaline compositions (mineral chemistry and boron isotope compositions) in the gold orebodies of the Itabira District is one example of an investigation that may be critical to understanding the origin of the hydrothermal fluids.

The Congo Soco iron mine in the Quadrilátero Ferrífero has been recently reactivated. The study of their palladium-bearing gold orebodies and their comparison with those described in this thesis would be of utmost importance.

## REFERENCES

- Babinski, M. Chemale, F., Jr., and Schmus, W. R., 1993, A idade das formações ferríferas bandadas do Supergrupo Minas e sua correlação com aquelas da África do Sul e Austrália: Simpósio do Craton do São Francisco, 2<sup>nd</sup>, Salvador, Brazil, August 23-26, 1993, Proceedings, p. 152-153.
- Roesner, H., Schurmann, K., Tobschall, H-J, and Jord-Evangelista, H., 1993, Palladium in the Quadrilátero Ferrífero, Minas Gerais, Brazil: Brazilian Meeting on Platinum-Group Element, 1<sup>st</sup>, Brasília, 1993, Extended Abstract volume, p. 52-54.
- Teixeira, W., and Figueiredo, M. C. H., 1991, an outline of Early proterozoic crustal evolution in the São Francisco craton, Brazil: a review: Precambrian Research, v. 53, p. 1-22.

## **APPENDIX 1**

### **SAO FRANCISCO CRATON: TECTONIC EVOLUTION AND ORE DEPOSITS**

## **SAO FRANCISCO CRATON**

The following section presents a summary of the tectonic evolution of the Sao Francisco Craton and its main ore deposits. The study area is located in the southern sector of Sao Francisco Craton.

### **Tectonic Evolution**

The Sao Francisco Craton of eastern Brazil is part of the South American Platform as defined by Almeida et al. (1981). The Sao Francisco Craton comprises Archean to Proterozoic terranes that were stabilized since 1.8 Ga and are bordered by Brasiliano mobile belts (700-450 Ma) and covered by platformal sequences of Late Proterozoic age (Fig. 1, Teixeira and Figueiredo, 1991).

Several Archean granite-greenstone and medium- to high-grade metamorphic terranes are present in the Sao Francisco craton (Fig. 2, Teixeira and Figueiredo, 1991). In the northern sector, the Jequié-Matuipe granulitic terrane gave Rb-Sr, Pb-

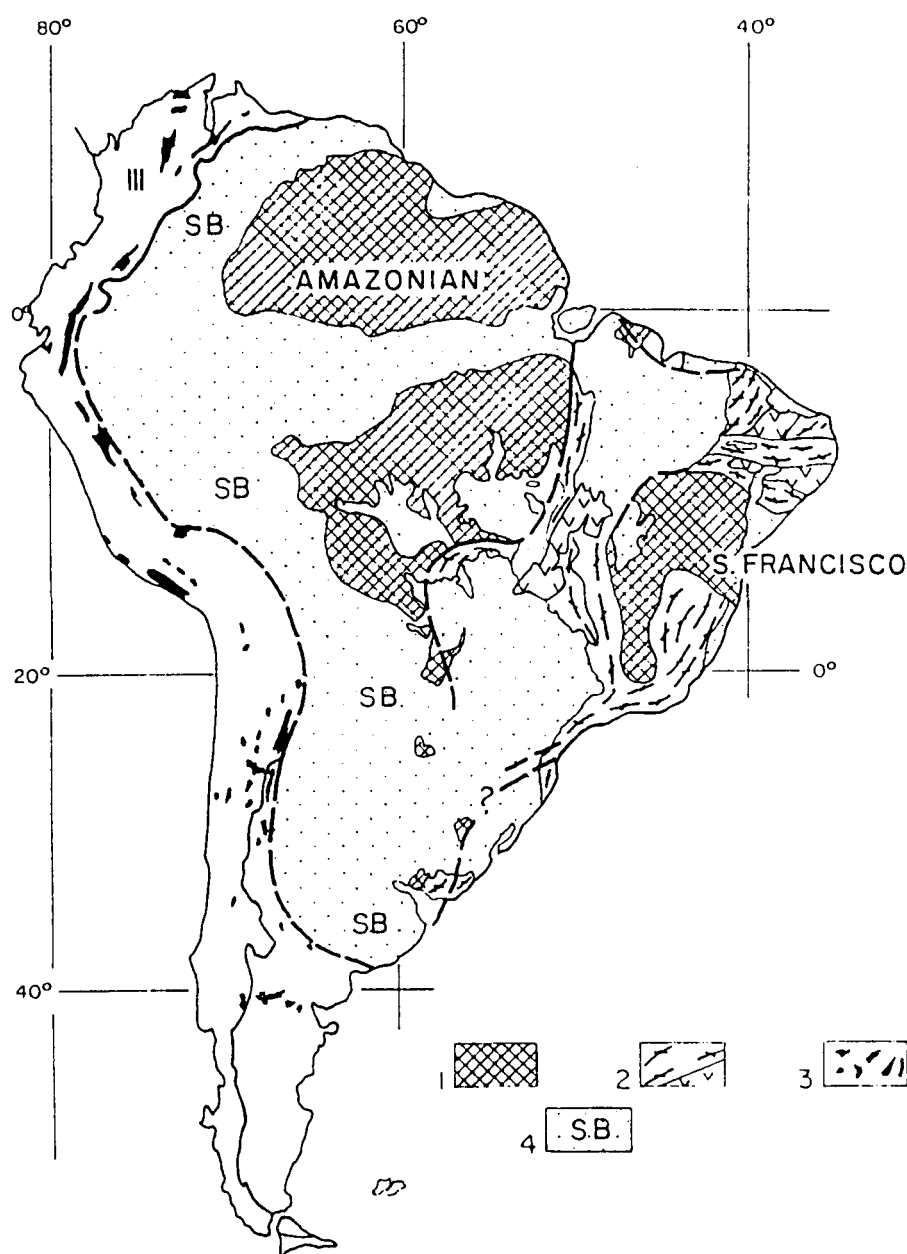


Figure 1. Simplified geotectonic map of South America: 1= Archean to Proterozoic cratons and correlated fragments; 2= Late Proterozoic mobile belts with interior massifs; 3= Andean Chain, including main remobilized Precambrian massifs; 4= Sub-Andean (SB) and Phanerozoic intracratonic basins. (After Teixeira and Figueiredo, 1991).

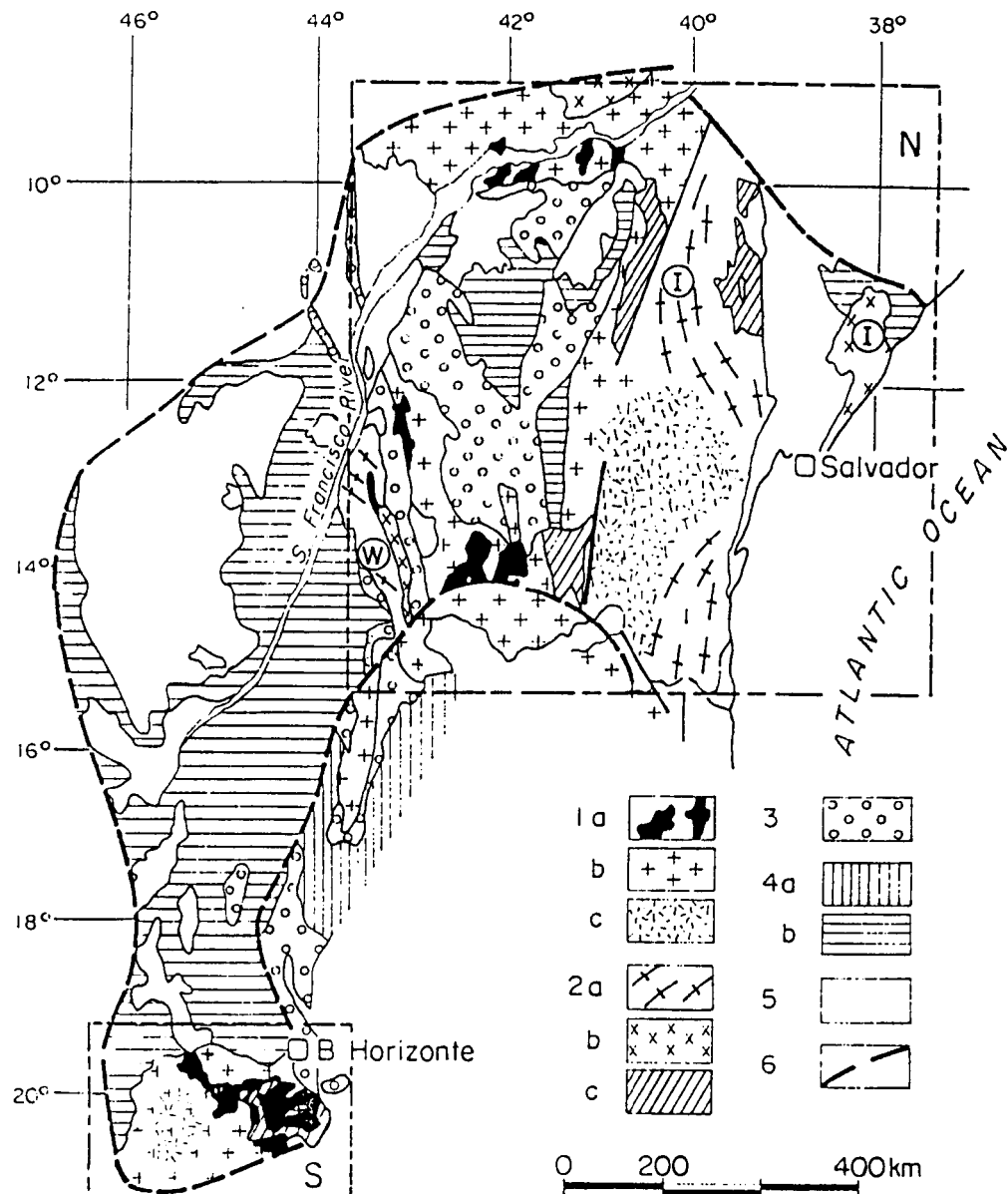


Figure 2. Simplified geological map of the São Francisco Craton adapted from Teixeira and Figueiredo (1991). 1= Archean; a= greenstone belts; b= granitic-gneissic-migmatitic terranes (in part Early Proterozoic); c= main cratonic fragments within the Early Proterozoic belts. 2= Early Proterozoic; I= Itabuna belt; W= western belt; a= high-grade terranes; b= granitic-gneissic migmatitic terranes; c= supracrustal belts. 3= Middle Proterozoic: Espinhaço folded system and associated sedimentary cover. 4= Upper Proterozoic; a,b,c are parts of São Francisco Supergroup. 5= Phanerozoic. 6= Approximate limits of the craton during Late Proterozoic marginal evolution. Cratonic sectors: N= northern; S= southern.

Pb and Sm-Nd ages as old as 3.3 Ga, and its border was partially rejuvenated during 2.4 to 2.2 Ga (Cordani and Brito Neves, 1982). In the southern sector, the Archean basement constitutes a nucleus of about 10 000 Km<sup>2</sup>, that is predominantly composed of medium-grade rocks with Rb-Sr and Pb-Pb ages up to 3.1 Ga (Teixeira and Figueiredo, 1991). These rocks were partially affected by Early Proterozoic isotopic rejuvenation (Teixeira and Figueiredo, 1991). The southern sector also comprises an Archean greenstone belt, referred to as the Rio das Velhas Supergroup, which yields U-Pb ages in zircon of 2776 +23/-10 Ma and 2772 +/-6 Ma (Machado et al., 1992). The greenstone sequence is exposed in the Quadrilátero Ferrífero, in the Itabira District, in the western part of Belo Horizonte, and also crops out toward the southwestern part of the Quadrilátero Ferrífero. The granitoid rocks spatially associated with this greenstone belt were dated at 2772 +7/-6 Ma and 2721 +/- 3 Ma and have been interpreted as contemporaneous with the Rio das Velhas volcanism (Machado et al., 1992). The younger granitoid intrusion (2721 +/- 3 Ma) marks the stabilization of the shield during the Late Archean time as proposed by Machado et al. (1992).

The Early Proterozoic domains defined in Teixeira and Figueiredo (1991) consist of a central high-grade portion of gneiss and migmatites metamorphosed to amphibolite or granulite facies and subjected to an extensive granitization at 2.15-1.9 Ga (Cordani and Brito Neves, 1982). These high-grade terranes are overlain and

bordered by supracrustal rocks of greenschist to amphibolite facies and intruded by granites or alkaline and mafic dyke swarms. In the northern sector, some of the supracrustal rocks are considered to be greenstone belts (Cordani and Brito Neves, 1982). One of the classic examples is the 2.1 Ga Serrinha-Itapecuru belt which overlies a 2.9 Ga sialic basement (Teixeira and Figueiredo, 1991). Other Early Proterozoic supracrustal rocks have been interpreted as platformal sedimentary sequences, such as the 2.3 Ga Jacobina sequence (northern sector, Teixeira and Figueiredo, 1991) and the 2.6 to 2.4 Ga Minas Supergroup (southern sector, Babinski et al., 1993). The Minas supergroup hosts the palladium-bearing gold deposits discussed in this thesis.

Intrusive rocks cut the Early Proterozoic domains and the Archean terranes mainly in the northern sector. They vary from granitic to syenitic and mafic compositions. The late-to post-tectonic granitoids are calc-alkaline suites with Rb-Sr, Pb-Pb and U-Pb zircon ages from 2.1 to 1.9 Ga (Teixeira and Figueiredo, 1991). In the southern sector, only a few intrusive granites, alkaline rocks, and pegmatoids have been identified, revealing isotopic ages of about 2.2-1.9 Ga (Teixeira and Figueiredo, 1991). Metamorphosed and unmetamorphosed mafic dykes have been mapped in the northern and southern sectors of the São Francisco Craton but their chronology of emplacement is not yet well established.

According to Teixeira and Figueiredo (1991) the Early Proterozoic evolution involved crustal rifting and the formation of intracratonic and marginal basins (e.g. the Jacobina sequence and the Minas Supergroup respectively) and back-arc basins (e.g. the Serrinha-Itapicuru greenstone belts). These authors postulated that large amounts of continental and oceanic materials were aggregated into Early Proterozoic belts accompanied by regional metamorphism and crustal reworking at 2.5-2.2 Ga. According to the same authors, the most important of the Early Proterozoic events was the Transamazonian tectono-metamorphic event (2.2-2.0 Ga), after which the region was cratonized. During a Middle Proterozoic extensional event, which was initiated between 1.75 to 1.7 Ga, the Espinhaço supergroup sediments were deposited in an intracontinental rift (Machado et al., 1989; Dossin et al., 1993).

During the Brasiliano orogeny, the São Francisco craton acted as foreland for the development and tectonic evolution of a series of collisional mobile belts (Brito Neves and Cordani, 1991). In the western portion of the craton, a Late Proterozoic platform cover (the São Francisco Group) was deposited and affected by tectonic movements during the last events of the Brasiliano orogeny.

In Table 1, a summary of the important tectonothermal events in the São Francisco Craton is shown, according to Teixeira and Figueiredo (1991), Machado et al., (1992), and Babinski et al., (1993).

	AGE (Ga)		EVENTS
PROTEROZOIC	0.57	///	Rb-Sr, K-Ar (Min)
	0.8	++	Ar-Ar (dykes)
	1.0	H H	
	1.2	==	
	1.4	====	K-Ar, Rb-Sr (Min., clays)
	1.7	==	Pb-Pb (WR)
	1.8	== v v	Rb-Sr (WR)
	1.9	==	U-Pb (zircon)
	2.0	///	Rb-Sr (WR)
	2.1	///	U-Pb (zircon)
	2.2	+ - - +	K-Ar (dykes)
	2.4	H H	
	2.6	==	Pb-Pb (WR)
	3.4	----	
ARCHEAN			- Regional isotopic rejuvenationn of the basement due to marginal belts to the craton ( mainly detected in south)
			- Alkaline intrusives
			- Marine and carbonate clastic deposition and continental glaciation (Sao Francisco Supergroup)
			- Subordinated isotopic rejuvenation related to the espinhaço fold belt; mafic dykes
			- Platformal deposits
			- Granitic plutonism and crustal reworking
			- Continental rifting, volcanism and beginning of the Espinhaço sedimentation
			- Regional cooling of the Craton
			- Intrusive granites, alkaline rocks and mafic dyke skarns
			- Tranzamazonian event (regional metamorphism). Crustal reworking (south) and mantle accretion (north) Serrinha-Itapecuru belt
			- Mafic dyke skarn
			- Intraplate rifting (Jacobine Sequence) and marginal sedimentation (Minas Supergroup)
			- Crustal reworking: migmatites, granitoids and regional metamorphism
			- Granite-greensnstone terranes (e.g. Rio das Velhas Supergroup)
			- Mainly mantle-derivation: successive collisions of the accreted microcontinentes (Jequié- Mauipé sequences)

Table 1.: Summary of important tectonothermal events in the Sao Francisco craton (After Teixeira and Figueiredo, 1991; Machado et al., 1992 and Babinski et al., 1993).

## Ore Deposits

The Sao Francisco craton is an important metallogenic province and includes the Bahia, Minas Gerais and Goias states. The mineral production in these states represents 24% of the total mineral production of Brazil and they have 32% of the proven Brazilian reserves of metallic ores (Misi et al., 1993). The Sao Francisco Craton has large reserves of gold, iron, manganese, magnesite, niobium, diamond, and chromium, as well as small deposits of base metals, all of which are summarized in Table 2 (DNPM, 1986; DNPM, 1988; DNPM, 1991; Misi et al., 1993).

ORE	LOCALITY	GEOLOGICAL SETTING	HOST ROCK	RESERVES and / or PRODUCTION	EXAMPLES
GOLD	Quadrilátero Ferrífero, Minas Gerais state	Archean Rio das Velhas Supergroup (greenstone belt)	Algoma-type banded iron-formation	Reserves: 8 X 10 <sup>6</sup> t of ore at 9 to 12 g/t Au	Morro Velho, Farias, Raposos, Bicalho, and São Bento mines
	Bahia State	Early Proterozoic Serrinha Itapecuru Volcano-Sedimentary Sequence	volcanic rocks and chemical sediments	Reserves: 100 t of gold; average grade of 7.74 g/t Au	Fazenda Brasileiro and Maria Preta mines
	Bahia State	Early Proterozoic Jacobina Group	fluvial braided conglomerate	Reserves: 88 t Au	Jacobina deposit
	Quadrilátero Ferrífero; Minas Gerais State	Early Proterozoic Minas Supergroup	Moeda conglomerate (braided streams) basal unit		Moeda deposit
	Quadrilatero Ferrífero; Minas Gerais State	Early Proterozoic Minas Supergroup	tourmalinite	Total production: 60t Au	Passagem mine
	Quadrilátero Ferrífero and Itabira District; Minas Gerais State	Early Proterozoic Minas Supergroup	Lake Superior-type iron-formation (jacutin-ga)	Production: 6.87 t Au	Cauê and Conceição mines, (studied in this thesis) and Congo Soco mine

Table 2: Summary of the principal ore deposits of the São Francisco Craton

ORE	LOCALITY	GEOLOGICAL SETTING	HOST ROCK	RESERVES and / or PRODUCTION	EXAMPLES
IRON	Quadrilá-tero Ferrífero and Itabira District; Minas Gerais State	Early Proterozoic Minas Supergroup	Lake Superior-type iron-formation	Reserves: $29 \times 10^9$ t of iron ore	Capanema, Timbopeba, Alegria, Cauê, Conceição, Chacrinha mines
MANGAN-ESE	Minas Gerais	Archean greenstone belt	calco-silicates	Reserves: $5.7 \times 10^9$ t of Mn ore at 25% Mn	Morro da Mina, Lafaiete mine
	Quadrilá-tero Ferrífero; Mina Gerais State	Early Proterozoic Minas Supergroup	Lake Superior-type iron-formation	Reserves: $8.3 \times 10^6$ t of Mn ore at 24% Mn	Miguel Congo mine
CHROME	Minas Gerais State	Archean Greenstone Belt	ultramafic rocks	Reserves: $10^5$ t of Cr ore at 30-40% of Cr <sub>2</sub> O <sub>3</sub>	Piui
	Minas Gerais State	Archean Layered mafic-ultramafic intrusion	ultramafic rocks	Reserves: $1.2 \times 10^6$ t at 10-40% of Cr <sub>2</sub> O <sub>3</sub>	Serro
	Bahia State	Early Proterozoic Layered mafic-ultramafic intrusion	ultramafic rocks	Reserves: $10 \times 10^6$ t; at 10-40% of Cr <sub>2</sub> O <sub>3</sub>	Campo Formoso
NICKEL	Minas Gerais State	Archean greenstone belt	mafic ultramafic rocks	Reserves: $6.6 \times 10^6$ t of ore at 2.2% Ni, 0.4% Cu, 0.55% Co, 1.2 ppm Au+PGE	Fortaleza de Minas deposit

Table 2. Summary of the principal ore deposits of the São Francisco Craton (cont..)

ORE	LOCALITY	GEOLOGICAL SETTING	HOST ROCK	RESERVES and / or PRODUCTION	EXAMPLES
TITANIUM VANA-DIUM	Bahia State	layered mafic intrusions	gabbro-anorthosite	Reserves: 10 <sup>6</sup> t at 20% TiO <sub>2</sub> , 0.71% V2O <sub>5</sub>	Campo Alegre de Lourdes deposit
TITANIUM	Bahia State	layered mafic-ultramafic complex	pyroxenite and magnetitite	Reserves: 7x10 <sup>5</sup> t at 0.6-6.0% V2O <sub>5</sub>	Fazenda Gulçari deposit
EMERALD	Minas Gerais State	Archean Rio das Velhas Supergroup (greenstone belt)	metamorphosed ultramafic rocks	Reserves: 12 t of high quality emerald	Itabira deposit
DIAMOND	Minas Gerais State	Middle Proterozoic Espinhaço Supergroup	metaconglomerates	Reserves: 1 X 10 <sup>4</sup> ct	Campo Sampaio mine

Table 2. Summary of the principal ore deposits of the Sao Francisco Craton (end)

## REFERENCES

- Almeida, F. F. M., Hasui, Y., Brito Neves, B. B. de, and Fuck, R. A., 1981, Brazilian structural provinces: An introduction: *Earth Science Reviews*, v. 17, p. 1-29.
- Babinski, M., Chemale, F., Jr, and Schmus, W. R., 1993, A idade das formações ferríferas bandadas do supergroup Minas e sua correlação com aquelas da África do Sul e Austrália: Simpósio do Cráton do São Francisco, 2<sup>nd</sup>, Salvador, Brazil, August 23-26, 1993, Proceedings, p. 152-153.
- Brito Neves, B. B., and Cordani, U.G., 1991, Tectonic evolution of South America during the Late Proterozoic: *Precambrian Research*, v. 55, p. 23-40.
- Cordani, U. G. and Brito Neves, B. B de, 1982, The geologic evolution of South America during the Archean and Early Proterozoic. *Revista Brasileira de Geociências*, v. 12, p. 78-88.
- DNPM, 1991, Principais Depósitos Minerais do Brasil, v. 4, 461 p.
- DNPM, 1988, Principais Depósitos Minerais do Brasil, v. 3, 670 p.
- DNPM, 1986, Principais Depósitos Minerais do Brasil, v. 2, 501 p.
- Dossin, I. A., Dossin, T. M., Charvet, J., Cocherie, a., Rossi, P., 1993, Single-zircon dating by step-wise Pb-evaporation of Middle Proterozoic magmatism in the Espinhaço range, Southern São Francisco Craton (Minas Gerais, Brazil): Simpósio do Cráton São Francisco, 2<sup>nd</sup>, Salvador, Brazil, August 23-26, 1993, Proceedings, p. 39-42.
- Machado, N., Noce, C. M., Ladeira, E. A., Belo de Oliveira, O., 1992, U-Pb geochronology of Archean magmatism and Proterozoic metamorphism in the Quadrilátero Ferrífero, southern São Francisco craton, Brazil: *Geological Society of America Bulletin*, v. 104, p. 1221-1227.
- Machado, N., Noce, C. M., Belo de Oliveira, O. A., and Ladeira., E. A., 1989, Evolução geológica do Quadrilátero Ferrífero no Arqueano e Proterozóico Inferior com base em geocronologia U-Pb. Simpósio de geologia - Núcleo Minas Gerais, 5<sup>th</sup> / Simpósio de Geologia- Núcleo Brasília, 1<sup>st</sup>, SBG Bol. V. 10, p. 1-5.
- Misi, A., Sá, P. V. S. V., Lobato, L. M., Pedrosa-Soares, A. C., 1993, Os depósitos minerais do Cráton do São Francisco e seu contexto geotectônico. O Cráton do São Francisco, SBG., p. 187-215.

Teixeira, W. and Figueiredo, M. C. H., 1991, An outline of Early Proterozoic crustal evolution in the Sao Francisco craton, Brazil: a review: *Precambrian Research*, v. 53, p. 1-22.